MONTE CARLO CALCULATION OF THREE-BODY SCATTERING

thesis by

Narayan K. Mahale

In Partial Fulfilment of the Requirements

For the Degree of

Doctor of Philosophy

California Institute of Technology

Pasadena, California

1985

(Submitted: October 12, 1984)

Acknowledgements

With Dr. Abhijit Saha, now at Kit Peak Observatory, I had fruitful discussion on the sampling method using the Fourier spectrum. To Dr.Tom Eddy of AT&T Bell Laboratories Chicago, I am thankful for pointing out the theorem on sampling using the Fourier spectrum. I am also thankful to Dr. Roy Williams for help with the computer system. For many helpful general discussions I thank Mr. Steve Anlage and Dr. A. Vijayaraghavan. I am indebted to Dr. Karlheinz Langanke for explaining to me a version of a computer program for the Path Integral Monte Carlo. Discussions with Professor Steven Koonin and his guidance and comments during the work of this thesis, I can not over appreciate. Above all I thank Professors Charles Barnes and Ward Whaling for the most important help.

Abstract

We construct an eigenvalue problem by confining many-body system to a bounded domain with the boundary condition that the wave function vanishes. By changing the boundary, however, the eigenvalues of the energy can be varied continuously. The D-matrix is defined for a series of bounded problems with the same value for the ground state energy. The D-matrix is related to the S-matrix, enabling us to calculate the the S-matrix at a given energy. The Schrodinger equation for the system is transformed to a diffusion equation by regarding time as imaginary. Initial ensemble, representing an approximate wave function, is evolved, through Monte Carlo simulation of random walks and branching, to the ground state ensemble. The limitations of investigation are: 1. Ingoing and outgoing channels have two fragments. 2. The interaction between the fragments is negligible outside the boundary mentioned above. 3. The particles are bosons or we know the zeros of the wave function.

First we consider the scattering of a particle by a potential, which is equivalent to the two-body problem, in one dimension. Here we use the Poschl-Teller potential for which the exact solution is known. We use this case to investigate a new sampling method and study of various parameters. Next we consider three particles in one dimension. Here we take interaction to be a potential well, where at least one of the interactions is attractive so that a two-body bound state is possible.

Contents

1. Introduction

As the number of particles in a system increases, the exact solution - by which we mean some analytical scheme for exact calculations - of the Schrodinger equation of the system is no longer possible and we have to resort to approximate analytical methods or numerical calculations. If the number of particles is very large we can resort to the methods of statistical physics. In the physics of nuclei, as well as atomic and molecular physics - rather, chemistry - we have to deal with few-body problems, where the number of particles is too large to deal with analytically but not large enough to consider the methods of statistical physics. Solution to the quantum mechanical three-body problem has been given by Fadeev (Fa61, Fa65) and this scheme has been used for calculations (Pa80, Pa81, Pa84). The four-body problem has been cast into a scheme closely analogous to Fadeev's scheme for three particles (Gr67, Ya67). But this is complicated enough and as yet no attempt has been made to use this for calculations. Systems with still more particles are difficult to handle analytically.

Thus we have to resort to numerical methods such as numerical variational calculus, finite difference schemes and Monte Carlo methods. In variational methods one has to evaluate $3N$ dimensional integrals, N being the number of particles in the system. Here, if the integrals are evaluated by finite difference, the computation time increases as n^{3N} where n is number of divisions along each of the coordinates. We can evaluate these integrals by a Monte Carlo technique but this we consider

as a Monte Carlo method. Finite difference relaxation schemes, in addition to the above scaling factor of computation time, need to be relaxed. Since a finer spatial grid requires a still finer iterative step (Is66), which scales as the inverse square of the spatial division, the number of steps for relaxation scales as n^2. The computation time in Monte Carlo methods, however, scales as $3NN_e$ where N_e is the size of the ensemble. Thus Monte Carlo methods are particularly efficient as the number of particles increases. This efficiency is due to the natural ability, through importance sampling, of Monte Carlo methods to give importance to the regions where the wave function is large.

Monte Carlo methods in statistical physics have been investigated extensively and have yielded many new results (Bi79, Bi84). Even in classical statistical physics new results have come to light. For example, a new phase with a short range order in simple classical solids - rather, glass - has been discovered (Ab80). The method has also been used in bound state problems in atomic (An75, An76, An80, An81, Re82) and nuclear physics. Investigations of Monte Carlo methods in scattering problems, however, are virtually nonexistent. The difficulty in a scattering problem is that we have to deal with the complex amplitudes and the unbounded space. This problem, however, has been solved, for the scattering in two-fragment channels and short range potentials, by Koonin and Alhassid (Al84), by connecting the scattering matrix (S-matrix) to the D-matrix, which is obtained by solving a series of artificially created eigenvalue problems. The problem of scattering of a particle by a potential, which is equivalent to the two-body problem, has been analyzed in the above work. Here we consider application of the formalism developed in (Al84) to the three-body problem. The motivation behind this,

however, has been to solve the problems with larger number of particles.

The general problem of calculating the S-matrix for a many-body system is not a possible task. Here we define the problem under consideration by summarizing the limitations on the investigation. Though we will not be dealing with more than three particles we shall talk in general terms so that the motivation behind the investigation is constantly in mind.

Fragments : If there are attractive potentials a many-body system can compose itself into many fragments. Here we consider channels, ingoing as well as outgoing, with two fragments. However, these fragments could exchange some of the particles; *i.e*, we consider rearrangement processes. In each of the channels α, the Hamiltonian for the system can then be decomposed as follows :

$$H = h_\alpha + \frac{p_\alpha^2}{2\mu_\alpha} + V_\alpha \qquad 1.1$$

where h_α is the internal Hamiltonian leading to the bound state of the fragments, the second term is the kinetic energy due to relative motion, with the reduced mass μ_α, of the fragments, and V_α is the potential between the fragments. The internal wave functions of the fragments will be assumed to be known. However, in practice we may use approximate eigenfunctions.

Interactions : Firstly, we consider only two-body potentials. Next, we shall assume that if the fragments are at a distance greater than d_α the interaction V_α between them is negligible. This is a reasonable approximation if the potential decays fast. Since the nuclear potentials decay exponentially with a characteristic length of the order of a fermi,

this is a good approximation in nuclear physics. Comparatively we may not be as well off with regard to the physics of atoms and molecules. If the screening of the long range potential (viz. coulomb potential) is adequate, that is, the bonds are covalent rather than ionic, the accuracy will be good.

Boson/Fermion : As discussed in Chapter-3 the method of solution is not straight forward unless we know the zeros of the wave function. We will be limiting ourselves to the cases where we know the zeros. Though we may be able to deal with some fermion problems, especially if the spatial wave function is totally symmetric, we will generally be limited to the bosonic systems.

Angular Momentum : Computationally we will be dealing with one-dimensional cases; the formalism, however, is applicable to three dimensions as well. In the one-dimensional case we have no angular momentum to deal with. The three-dimensional problem is complicated by the angular momentum. The eigenfunctions of the angular momentum are the Legendre's polynomials. So we know the zeros of the wave function and, in principle, we have no problem; however, it is cumbersome in practice and we shall restrict ourselves to s-wave scattering.

First, a brief description of the method. As mentioned above, first we have to reduce the problem to a finite region. This is accomplished, following Koonin and Alhassid (Al84), by the method analogous to Wigner and Eisenbud formalism (Wi47). If the fragments are far apart, then we can consider them to be free and we can solve the problem in the exterior region. The region where V_α is important may be enclosed by a finite region, the interior region. If we prescribe a boundary condition on the interior region, then the problem in the interior region transforms to an

eigenvalue problem. With various choices of the interior region but always enclosing the interaction region, and boundary conditions, we can change the eigenvalue of the Hamiltonian for the interior problem. Next we define a matrix, the D-matrix, which is calculated from the solution to the interior region. Since we know the boundary condition we can match the interior solution to the exterior solution and obtain the relation between the S-matrix and the D-matrix and thereby calculate the S-matrix.

Next we have to choose a method of solution to the interior problem. We use PIMC, the Path Integral Monte Carlo (Ko84). For a review of various other Monte Carlo methods see Binder (Bi79). As will be observed later, in analyzing the scattering phenomenon, we not only need accurate value of the energy but need accurate information about the wave function itself. The variational methods, and therefore variational Monte Carlo, though they give good results for the energy of the eigenvalue problem, are not adequate in giving the information about the wave function. Therefore, it is probably essential that we choose PIMC or GFMC (Green's Function Monte Carlo). These two methods are very similar and without further justification we choose PIMC.

Next we give a brief description of the contents of the chapters to follow.

In Chapter-2 we define the D-matrix, which is to be calculated from the eigenvalue problem, confined to the interior region, and give the relation between the S-matrix and the D-matrix. In Sections-2.1 to 2.3 we follow Koonin and Alhassid; we, however, derive the expressions for the one-dimensional case while Koonin and Alhassid consider the three-dimensional case. Section-2.1 defines the scattering matrix through its

relation to the solution in the asymptotic region, which we call the exterior, where the interaction is assumed to be negligible or absent. To obtain the S-matrix we must relate the solution in the exterior region to the solution in the interior to be computed by the Monte Carlo simulation. Section-2.2 defines the D-matrix for a given interior region with a prescribed boundary condition; herein we relate the S-matrix with the D-matrix. In Section-2.3 we derive the integral expressions, which can be readily evaluated with the Monte Carlo, for the elements of the D-matrix.

While in Chapter-2 we considered the theoretical aspects leading to the formulation of the problem amenable to the Monte Carlo technique, in Chapter-3 we discuss the algorithms for the computation. Section-3.1 discusses the Path Integral Monte Carlo method to obtain the ground state of the Schrodinger equation. Here, the transformation of the Schrodinger equation to a diffusion equation, simulation of the resultant diffusion equation by random walks and branching, and the importance sampling method due to Kalos, are discussed. In Section-3.2 we give a brief outline of the computational procedure and in subsequent sections, give details of some of the algorithms. To simulate the diffusion equation we need an ensemble of points representing the wave function. To begin with we have to have an approximate ensemble which is evolved to obtain a more accurate ensemble. In Section-3.3 we describe an algorithm used to initialize the approximate ensemble. This ensemble is then evolved through the diffusion equation by simulation via random walks and branching. While propagating the ensemble we must take care of the local balance, the algorithm for which is the topic of Section-3.4. As the ensemble propagates in time, the size of the ensemble drifts due to the branching process. It is necessary to keep the size of the ensemble

relatively stable. In Section-3.5 we describe the procedure to restore the ensemble.

Chapter-4 considers various parameters in the algorithm and investigates the possibility of optimization and use of these parameters. In Section-4.1, for the benefit of the reader who skipped Chapter-3, we recapitulate the procedure described in detail in Chapter-3; this recapitulates various parameters to be investigated. The evolution of the ensemble gives rise to a sequence of ensembles which are correlated. Therefore, we have to account for this correlation in estimating the error. In Section-4.2 we describe the procedure followed to account for the correlation. To account for the correlation we need to calculate the correlation length such that if we sample the ensemble at this interval the sampled ensembles will be independent. In Appendix-3 we give a new method to calculate the correlation length. This method is based on a computer experiment and therefore is empirical. Since the initial ensemble is approximate it takes some time for the system to relax and we should discard the ensembles during the relaxation time. Appendix-3 also presents a method to find the relaxation time. The procedures developed in Appendix-3 are illustrated in Section-4.3 through an example. In Sections-4.3 and 4.4 we consider the scattering of a particle by a potential which has been treated in (Al84). In Section-4.4 we examine the effects of various parameters on the error and thereby conclude the optimum values and uses of these parameters.

In Chapter-5 we analyze the three-body problem, with two-body interaction potential, in one dimension. There are three characteristically different cases depending on the type of interaction between different pairs. Section-5.1 discusses some general features of the

problem. In Section-5.2 we consider the case where one pair (say particle 1 and 3) has attractive potential while interaction between the other two pairs is repulsive. This has only one two-fragment mode and two channels are possible. We restrict our analysis to the antisymmetric channel. The second possibility is that interaction between one pair (again particle 1 and 3) is repulsive while the other two pairs interact through an attractive potential and we have two two-fragment modes. We consider this case in Sections-5.3 and 5.4. Once again in Section-5.3 we restrict the analysis to the antisymmetric combination. Sections-5.2 and 5.3 solve only half the problem and for full solution one has to solve symmetric combination. We can, however, solve the full problem in a single simulation. This is presented in Section-5.4. Analysis of the case where all three pairs of interaction are attractive, giving three two-fragment modes, is similar and we do not consider this case. [1]

Lastly, in Chapter-6 we give a summary and make some concluding remarks.

In the appendices at the end of the thesis we give some of the details of side issues. Appendix-1 gives explicit expressions for the three-body problem. In Appendix-2 we list the algorithms for random number generators used in the simulation. Appendix-3 discusses the methods we use to determine the correlation time and the equilibration time. In Appendix-4 we give a test of the program by comparing the Monte Carlo results with the results from a finite difference relaxation scheme.

---

1 Of course, the case with all pairs of particles with repulsive interaction is not within the limitation of the two-fragment channels since here it is impossible to form a two-body bound state.

Appendix: Units

We shall use two sets of conventions with regard to the units, one for the analytical expressions and another in the numerical calculations. First, for the analytical part, predominantly used in Chapters-2 and 3, we use,

$$\hbar = 1.0 \ ; \text{and } m = 1.0. \qquad 1.2$$

We may, however, keep $\hbar$ and m explicitly in some of the expressions if this clarifies the physical significance.

Next the computations are performed in the following units. [2]

Length	Fermi(fm)
Energy	MeV
Time	10^{-23}Sec.
Phase	Radians(Rad)

In these units we have

$$\hbar = 0.65822 \ ; \text{ and } \hbar^2/m_p = 41.47 \qquad 1.3$$

where m_p is the mass of the proton. Since mass, m, of the particle and $\hbar$ enter the Schrodinger equation in the combination of $\hbar^2/m$ we may express the mass in terms of the proton mass and use the second expression in Eq.-1.3 for normalization.

---

2. These are the units usually used in nuclear physics. For further details see Se82.

2. The D-Matrix and Its Relation to the S-Matrix

2.1 The Scattering Matrix

Although we will be restricting ourselves, as far as the numerical calculations are concerned, to the three-body problem, the computer program has many general features necessary for the many-body case. Therefore, the notation followed below is general. Appendix-1 gives some details of the three-body case explicitly. Here we follow the one-dimensional case. The formulae for the three-dimensional case are available elsewhere (Al84). The development below and subsequent sections follow Alhassid and Koonin (Al84).

We consider, as already mentioned, the case where outgoing as well as ingoing channels have two composite fragments. Therefore, we decompose the Hamiltonian into various components as,

$$H = h_\alpha + \frac{p_\alpha^2}{2\mu_\alpha} + V_\alpha, \qquad 2.1.1$$

where $h_\alpha = h_\alpha^1 + h_\alpha^2$ is the internal Hamiltonian for the channel α, and h_α^A, $A=1, 2$ are the internal Hamiltonian of each of the fragments. p_α is the momentum due to the relative motion of the fragments with the reduced mass μ_α. Since we may disregard the motion of the center of mass of the system, we have, with the notation $\sum_A$ for the sum over the particles belonging to the fragment A and $\sum_{\bar{A}}$ for the sum over the particles not belonging to the fragment A,

$$h_\alpha^A = \sum_A \frac{p_i^2}{2m_i} + \frac{1}{2}\sum_A V_{i,j} \qquad 2.1.2$$

$$p_\alpha = \sum_1 p_i - \sum_2 p_j \qquad 2.1.3$$

$$\mu_\alpha = \frac{(\sum_1 m_i)(\sum_2 m_i)}{\sum_1 m_i + \sum_2 m_i} \qquad 2.1.4$$

$$V_\alpha = \frac{1}{2}\sum_{\bar{1}}\sum_{\bar{2}} V_{i,j} \qquad 2.1.5$$

where we have considered only two-body forces $V_{i,j}$, between the particle i and j.

Let us now examine the contribution to the energy and the wave function due to different components of the Hamiltonian. Let Ψ^α be the solution corresponding to the ingoing channel α, with energy E. Then by definition we have

$$H\Psi^\alpha(x,t) = E\Psi^\alpha(x,t). \qquad 2.1.6$$

The internal energy e_α^A and the eigenfunction η_α^A for each fragments is given by

$$h_\alpha^A \eta_\alpha^A = e_\alpha^A \eta_\alpha^A, \qquad 2.1.7$$

while the total internal energy $e_\alpha = e_\alpha^1 + e_\alpha^2$ and the internal eigenfunction $\eta_\alpha = \eta_\alpha^1 \eta_\alpha^2$ satisfy

$$h_\alpha \eta_\alpha = e_\alpha \eta_\alpha. \qquad 2.1.8$$

In the asymptotic region, if the channel potential V_α vanishes for $r_\alpha > d_\alpha$, the solution for the relative motion of the fragments will be a plane wave with the wave number k_α given by,

$$k_\alpha = [2\mu_\alpha(E-e_\alpha)]^{half.} \qquad 2.1.9$$

For an ingoing channel α there will be outgoing components in channel α, as well as in channels $\beta \neq \alpha$. These asymptotic states are given by,

$$\underset{r_\alpha \to \infty}{Lim}\Psi^\alpha = \frac{i}{2}[exp(-ik_\alpha r_\alpha) - S_{\alpha\alpha} exp(ik_\alpha r_\alpha)]\eta_\alpha \qquad 2.1.10$$

for the channel α and for $\beta \neq \alpha$,

$$\underset{r_\beta \to \infty}{Lim}\Psi^\alpha = \frac{-i}{2}[k_\alpha / k_\beta]^{1/2} S_{\beta\alpha} exp(ik_\beta r_\beta)\eta_{beta.} \qquad 2.1.11$$

Next we define the wave functions ψ_β^α in the asymptotic regions as,

$$\underset{r_\beta \to \infty}{Lim}\Psi^\alpha = \psi_\beta^\alpha(r_\beta)\eta_\beta \qquad 2.1.12$$

where,

$$\psi_\beta^\alpha(r) = \frac{i}{2}[\delta_{\alpha\beta} exp(-ik_\alpha r) - [k_\alpha / k_\beta]^{1/2} S_{\beta\alpha} exp(ik_\beta r)]. \qquad 2.1.13$$

The coefficients $S_{\alpha\beta}$ in the above formula define the S-matrix. Next we define the diagonal matrices,

$$[exp(i\hat{k}r)]_{\alpha\beta} = \delta_{\alpha\beta} exp(ik_\alpha r); \text{ and } [\hat{k}^{1/2}]_{\alpha\beta} = \delta_{\alpha\beta} k_\alpha^{half.} \qquad 2.1.14$$

Now the scattering solution can be written as,

$$\hat{\Psi} = \frac{i}{2}[exp(-i\hat{k}r) - exp(i\hat{k}r)\hat{k}^{-1/2} S \hat{k}^{1/2}] \qquad 2.1.15$$

where ψ_α^β is the element of $\hat{\Psi}$ in row α and column β. In three dimensions we have angular momentum and hence must consider the spin indices. We could, however, interpret α,β as general indices including the spin and

therefore no generality is lost. We shall, however, confine ourselves to the zero angular momentum case with spinless bosons.

2.2 The D-Matrix and Its relation to the S-Matrix

As will be discussed in Section-3.1, in Path Integral Monte Carlo the wave function is interpreted as the probability density, and the Schrodinger equation is simulated by propagating an ensemble representative of the wave function. If we wish to simulate the diffusion by random walks and branching of the ensemble, it is necessary that the domain be small for an efficient numerical calculation. The scattering states Ψ^{α}, however, are complex and, in addition, they cover an infinite domain. Therefore, straightforward application of the method is not possible. Following Koonin and Alhassid (Al84), however, we can define another matrix, the D-matrix, which is computable by Monte Carlo and is related to the S-matrix. In this section we define the D-matrix and establish the relation between the D-matrix and the S-matrix. In the next section integral expressions for the elements of the D-matrix, convenient in Monte Carlo calculations, will be given.

First we make an assumption that in each channel α, for $r_{\alpha}>d_{\alpha}$, the potential V_{α} between the two fragments vanishes. In practice, however, we will have to analyze the cases where V_{α} is negligible for $r_{\alpha}>d_{\alpha}$. Next, at $R_{\alpha}>d_{\alpha}$, we impose a boundary condition,

$$\varphi_{\alpha}/\varphi_{\alpha}'|_{r_{\alpha}=R_{\alpha}} = f_{\alpha} \qquad 2.2.1$$

where φ_{α} are the solutions to the problem with the above boundary condition. Now the solutions to the Schrodinger equation have a discrete set of eigenvalues E_n; *i.e.*,

$$H\varphi_\alpha^n = E_n \varphi_\alpha^n. \qquad 2.2.2$$

Though the spectrum of the E_n is discrete, they are functions of f_α and R_α. By varying the values of f_α and R_α we can vary E_n continuously. Solution to the ground state of the above discrete eigenvalue problem can be readily calculated by the method of Section-3.1. Since we will be restricting ourselves to the wavefunctions without any nodes and to the cases $R_\alpha > d_\alpha$, we will be confined to the values of energy below an upper bound. In principle we will not be restricted by a lower bound on the energy. However, if we wish to have an efficient method we have to confine ourselves to smaller values of R_α by varying the value of f_α. Here we restrict ourselves to the boundary condition $\varphi_\alpha=0$. This will put a practical limit on the lowest energy we can handle efficiently.

To see how the above solution in the interior region is related to the scattering solution, consider the Schrodinger equation,

$$H\Phi^\alpha = E\Phi^\alpha \qquad 2.2.3$$

with the condition that Φ^α vanishes at $r_\beta=R_\beta^0$ in all the channels $\beta\neq\alpha$, α being the incoming channel. That is, if φ_β^α are the asymptotic wavefunctions of the relative motion, then

$$\varphi_\beta^\alpha(r_\beta=R_\beta^0) = 0\,; \text{ for } \beta\neq\alpha. \qquad 2.2.4$$

This defines the problem uniquely if we fix the energy to be E. If we impose a boundary condition on channel α the energy spectrum will become discrete. However, we can adjust the value of $R_\alpha=R_\alpha^1$ such that the ground state energy is E.

Next we define the D-matrix through the asymptotic form of φ_β^α as

follows,

$$\varphi_\alpha^\alpha = \frac{1}{k_\alpha}\cos k_\alpha(r_\alpha - R_\alpha^0) + D_{\alpha\alpha}\sin k_\alpha(r_\alpha - R_\alpha^0) \qquad 2.2.5$$

and

$$\varphi_\beta^\alpha = D_{\beta\alpha}\sin k_\beta(r_\beta - R_\beta^0)\ ; \quad \beta \neq \alpha \qquad 2.2.6$$

or in a matrix form, analogous to the case of scattering states $\hat{\psi}$,

$$\hat{\varphi} = \hat{k}^{-1}\cos\hat{k}(r - R^0) + D\sin\hat{k}(r - R^0). \qquad 2.2.7$$

The elements $D_{\beta\alpha}$ depend on the response of the interior region to the incoming wave. The elements of the D-matrix are to be calculated by a Monte Carlo method through the integral expression for them to be given in the next section. Now for a given energy E, and therefore k_α, φ_α^α can be made to vanish at $R_\alpha^1 \neq R_\alpha^0$ where R_α^0 is the point at which we make φ_α^β corresponding to an incoming channel β vanish. From the above asymptotic formulae we obtain for the elements of D-matrix,

$$D_{\alpha\alpha} = \frac{-1}{k_\alpha}\cot k_\alpha(R_\alpha^1 - R_\alpha^0) \qquad 2.2.8$$

$$D_{\beta\alpha} = \frac{1}{k_\beta}\frac{\partial\varphi_\beta^\alpha}{\partial r_\beta}\Big|_{r_\beta = R_\beta^0}\ ; \quad \beta \neq \alpha. \qquad 2.2.9$$

For a given energy E there are N independent solutions corresponding to each incoming channel α. These independent eigenfunctions φ_β^α form a complete set of eigenfunctions at this energy. Therefore, we can obtain the scattering solutions ψ_β^α by superposition of φ_β^α. In matrix notation we have,

$$\hat{\psi} = \hat{\varphi}B \qquad 2.2.10$$

where the matrix B is to be found by comparison of asymptotic forms of $\hat{\psi}$ and $\hat{\varphi}$. This also establishes the relation between the D-matrix and the S-matrix. These relations are (Al84),

$$B = (-i\hat{k}^{-1}+D)^{-1}exp\,(-i\hat{k}R^0) \qquad 2.2.11$$

and,

$$S = -exp\,(-i\hat{k}R^0)\,\frac{1-i\hat{k}^{\frac{1}{2}}D\hat{k}^{\frac{1}{2}}}{1+i\hat{k}^{\frac{1}{2}}D\hat{k}^{\frac{1}{2}}}exp\,(-i\hat{k}R^0). \qquad 2.2.12$$

The S-matrix is unitary. From this it follows that the D-matrix is real and symmetric and has N(N + 1)/2 independent elements. As described in the next section, these can be calculated by Monte Carlo simulation in the interior region defined by $r_\alpha \leq R_\alpha^1$ and $r_\beta \leq R_\beta^0$, the wavefunction vanishing on the boundary.

2.3 Integral Expressions for the D-Matrix

First we state an integral identity proved by Alhassid and Koonin (Al84). As already mentioned before, here we follow the one-dimensional case, while in (Al84) a three-dimensional case is considered. In the appendix, at the end of the section, we point out the changes necessary to convert the formulae to the three-dimensional case. Let Φ and χ be translationally invariant many-body wavefunctions. Asymptotic forms of these in all channels β are,

$$\chi \rightarrow \chi_\beta(r_\beta)\eta_\beta \qquad 2.3.1$$

$$\Phi \rightarrow \varphi_\beta(r_\beta)\eta_\beta. \qquad 2.3.2$$

Let K be the total kinetic energy operator and l be the range of motion of

the center of mass. Then,

$$\int [\chi^* K\Phi - \Phi K\chi^*] dl = -l\sum_\beta \frac{\hbar^2}{2\mu_\beta}[\chi_\beta^* \frac{\partial \varphi_\beta}{\partial r_\beta} - \varphi_\beta \frac{\partial \chi_\beta^*}{\partial r_\beta}]_{r_\beta = R_\beta} \qquad 2.3.3$$

where the integration is over the domain $r_\alpha \leq R_\alpha$. Below we use this identity to get the integral expressions for the elements of the D-matrix.

First consider the diagonal elements $D_{\alpha\alpha}$. The Eq-2.2.8 shows that we can calculate $D_{\alpha\alpha}$ once we have the value of the energy. We impose the boundary condition that the solution vanish on $r_\alpha = R_\alpha^1$ and $r_\beta = R_\beta^0$ with $\beta \neq \alpha$. Let Φ be the eigenfunction of the complete Hamiltonian $H=K+V$ with energy E; *i.e.*,

$$H\Phi = E\Phi. \qquad 2.3.4$$

Let χ be the eigenfunction of the partial hamiltonian $H_0=K+V_0$ with energy E_0 which is soluble. That is,

$$H_0\chi = E_0\chi. \qquad 2.3.5$$

Now the right hand side of the identity (2.3.3) is zero and we can readily obtain,

$$\Delta E = E - E_0 = \frac{\int \chi(V-V_0)\Phi dl}{\int \chi\Phi dl}. \qquad 2.3.6$$

We can use χ for the importance sampling and readily obtain the value of the energy by Monte Carlo. We can therefore calculate k_α for the relative motion to obtain $D_{\alpha\alpha}$ given by,

$$D_{\alpha\alpha} = -\frac{1}{k_\alpha} cotk_\alpha (R_\alpha^1 - R_\alpha^0). \qquad 2.3.7$$

Next we take up the off-diagonal elements $D_{\beta\alpha}$. Here we take $\Phi=\Phi^{\alpha}$, the solution corresponding to incoming channel α. We choose χ to consist of only the asymptotic component in channel β given by,

$$\chi^{\beta} = \chi_{\beta}\eta_{\beta} \qquad 2.3.8$$

where, χ_{β} are arbitrary functions of r_{β}. Here the integration region is given by $r_{\beta}\leq R_{\beta}^{0}$ for $\beta\neq\alpha$ and $r_{\alpha}<R_{\alpha}^{1}$. Since Φ^{α} vanishes on the boundary we get, for $\beta\neq\alpha$,

$$\int[\chi^{\beta}K\Phi^{\alpha}-\Phi^{\alpha}K\chi^{\beta}]dl = -\frac{\hbar^2}{2\mu_{\beta}}lk_{\beta}D_{\beta\alpha}\chi_{\beta}^{*}(R_{\beta}^{0}) \qquad 2.3.9$$

and for $\beta = \alpha$,

$$\int[\chi^{\alpha}K\Phi^{\alpha}-\Phi^{\alpha}K\chi^{\alpha}]dl = \frac{\hbar^2}{2\mu_{\alpha}\sin k_{\alpha}(R_{\alpha}^{1}-R_{\alpha}^{0})}l\chi_{\alpha}^{*}(R_{\alpha}^{1}). \qquad 2.3.10$$

We also have,

$$K\Phi^{\alpha} = (E-V)\Phi^{\alpha}; \qquad 2.3.11$$

and,

$$K\chi^{\beta} = [(e_{\beta}-V+V_{\beta})+K_{\beta}]\chi^{\beta} \qquad 2.3.12$$

where K_{β} is kinetic energy due to the relative motion in the channel β. Now dividing the expression for $\beta\neq\alpha$ by the expression for $\beta=\alpha$ we get the integral expression for the off -diagonal elements to be,

$$D_{\beta\alpha}=-\frac{\mu_{\beta}}{\mu_{\alpha}k_{\beta}\sin k_{\alpha}(R_{\alpha}^{1}-R_{\alpha}^{0})}\frac{\chi_{\alpha}(R_{\alpha}^{1})}{\chi_{\beta}(R_{\beta}^{0})}\frac{<(E-e_{\beta}-V_{\beta}-K_{\beta})\chi_{\beta}\eta_{\beta}>}{<(E-e_{\alpha}-V_{\alpha}-K_{\alpha})\chi_{\alpha}\eta_{\alpha}>} \qquad 2.3.13$$

where <...> indicates average over the distribution Φ^{α}. Here we have

assumed that the internal wavefunction for the fragments are known. In practice, however, we may have to use approximate solutions. Now these integral expressions can be evaluated by Monte Carlo. The three dimensional expression for $D_{\beta\alpha}$, derived in (Al84) is the same as above if we take the form of χ^{β} as $\frac{\chi_{\beta}\eta_{\beta}}{r_{\beta}}$. Next we have to choose the functions χ_{β}. This choice is governed by the particular problem at hand. Below we consider some cases of interest.

First consider the problem of scattering of a particle by a potential V(x). Here we have two channels: 1. The particle on the left hand side of the potential, 2. The particle on the right hand side of the potential. The problem is equivalent to the two-body problem and the internal wave functions can be dispensed with. We introduce the nodes at $x=a$ and $x=b$. We consider the particle impinging from the left. We choose $\chi_1=x-b$ and $\chi_2=x-a$ and recover the result of (Al84).[1]

$$D_{21}=\frac{1}{k\sin k}\frac{<(E-V)(x-a)>}{<(E-V)(x-b)>} \qquad 2.3.14$$

In each channel we will have waves coming from the left or from the right. We can superpose these solutions to get symmetric or antisymmetric combinations. The wavefunctions for the symmetric and antisymmetric combinations are orthogonal to each other and do not mix since the Hamiltonian does not have a parity mixing term. We may therefore solve the complete problem by solving the symmetric and antisymmetric cases separately. Here we impose nodes at $|r_{\alpha}|=R_{\alpha}^{1}$ for the channel α and at $|r_{\beta}|=R_{\beta}^{0}$ in all other channels. Of course, for antisymmetric

1. The treatment of this case in (Al84) is somewhat different, however, but one can cast this in terms of the D-matrix formalism and compare the results.

combinations there will be an additional node at r_α=0. Here we choose χ_β=*constant* in all the channels. This gives,

$$D_{\beta\alpha}=-\frac{\mu_\beta}{\mu_\alpha k_\beta \sin k_\alpha (R_\alpha^1-R_\alpha^0)}\frac{<(E-e_\beta-V_\beta)\eta_\beta>}{<(E-e_\alpha-V_\alpha)\eta_\alpha>}. \qquad 2.3.15$$

Lastly, for all β we consider $r_\beta<0$ and $r_\beta>0$ as two separate channels analogous to the first case considered above. Here we choose nodes at R_α^1 and $-R_\alpha^0$ along r_α, and at $\pm R_\beta^0$ along r_β. To calculate $D_{\beta\alpha}$ we choose the functions χ_β and χ_α to be,

$$\chi_\alpha=(r_\alpha+R_\alpha^0) \qquad 2.3.16$$

$$\chi_\beta=(r_\beta+R_\beta^0).$$

Then the expression for $D_{\beta\alpha}$ is given by,

$$D_{\beta\alpha}=-\frac{\mu_\beta}{\mu_\alpha k_\beta \sin k_\alpha (R_\alpha^1+R_\alpha^0)}\frac{(R_\alpha^1+R_\alpha^0)}{2R_\beta^0}\frac{<(E-e_\beta-V_\beta)(r_\beta+R_\beta^0)\eta_\beta>}{<(E-e_\alpha-V_\alpha)(r_\alpha+R_\alpha^0)\eta_\alpha>}. \qquad 2.3.17$$

3. Path Integral Monte Carlo (PIMC)

3.1 Monte Carlo Solution of the Schrodinger Equation

There are several ways of applying Monte Carlo methods (Ce79) to estimate the expectation values of operators for many-body quantum mechanical systems. First, consider the Variational Monte Carlo. The Schrodinger equation for a stationary state is an eigenvalue problem. We can recast this as a problem of minimizing the expectation value of the Hamiltonian with subsidiary conditions. As is well known, the subsidiary conditions are orthonormality conditions for the eigenfunctions. Here we construct an ansatz for the wave functions with unknown parameters and determine the parameters which minimize the energy. A Monte Carlo technique is then used to estimate the integrals involved. This method, however, gives an approximate result irrespective of the statistics. Moreover, the variational techniques are not particularly good in obtaining the accurate wavefunction.

Another approach is the Green's Function Monte Carlo (GFMC). Here the iterative process of obtaining the ground state wave function from an initial approximate wave function is cast as an integral equation involving the Green's function of the time independent Schrodinger equation. Therefore, in principle, we need to know the exact Green's function of the system. We may, however, approximate the Green's function and from successively better approximations extrapolate to the exact Green's function.

Here we follow yet another method (Re82). The Schrodinger equation is transformed into a diffusion equation, which henceforth will be referred to as the Schrodinger-diffusion equation, by regarding time as imaginary. Then the path of the ensemble representing an approximate wave function is calculated to obtain the representative ensemble of the ground state wave function through Monte Carlo solution of the diffusion equation. Here the estimator for the energy is unbiased and the errors are due to limitations on computer time, and truncation of the space and the potential, if the potential range is infinite, these errors being common with the methods mentioned above. We now describe this method in a greater detail.

Let $E_0, E_1, E_2 \ldots\ldots$ be the eigenvalues of the Hamiltonian and $U_0, U_1, U_2 \ldots\ldots$ be the respective eigenfunctions. Then any function, in particular the initial approximate wave function, satisfying the boundary conditions of the system can be decomposed into these eigenfunctions as,

$$\Psi(t=0,x) = \sum_{n=0}^{\infty} a_n U_n(x). \qquad 3.1.1$$

At any other time t the initial wave function evolves to,

$$\Psi(t,x) = \sum_{n=0}^{\infty} a_n U_n(x) exp(-iE_n t). \qquad 3.1.2$$

Here and elsewhere, in equations, we set $\hbar=1$. Now if we shift the energy levels by E_0 and consider the equation in the imaginary time $\tau=-it$ we get,

$$\Psi(\tau,x) = \sum_{n=0}^{\infty} a_n U_n(x) exp[-\tau(E_n - E_0)]. \qquad 3.1.3$$

We see that the components corresponding to all the energy levels except the ground state are damped and, if the initial wave function is not in the space normal to the ground state, we have,

$$\lim_{\tau\to\infty}\Psi(\tau,x) = a_0 U_0(x). \qquad 3.1.4$$

Thus the evolution of the wave function in imaginary time domain leads to the ground state wave function.[1] This is the basis of the Path Integral Monte Carlo (PIMC) or Diffusion Monte Carlo.

To see how the evolution is to be simulated by Monte Carlo, consider the Schrodinger-diffusion equation for a many body system.

$$\frac{\partial\Psi(x,\tau)}{\partial\tau} = [\frac{\hbar^2}{2m}\nabla^2 + E_T - V(x)]\Psi(x,\tau) \qquad 3.1.5$$

Here x represents all the coordinates and $V(x)$ is the potential. Further, we have shifted the energy by an arbitrary value of E_T. E_0 is the value we want to determine and therefore we must use a trial value which should be updated as the calculations proceed. This does not change the possible accuracy of the method since, for large values of τ, components other than ground state will be damped. But an energy shift other than E_0 will contribute to the drift of the ensemble size. This can be remedied by updating the ensemble if the drift is undesirable. If the term $E_T - V(x)$ were to be absent, Eq-3.1.5 is simply a diffusion equation in a hyperspace with a diffusion constant $D = \frac{\hbar^2}{2m}$. As is well known (Ch43, Wa54), this can

1. If we chose the initial wave function orthogonal to the ground state we reach the first excited state in the limit. This suggests a method to deal with higher energy levels. In treatment via Monte Carlo, however, we must ensure that the representative ensemble does not have any component of the ground state at each iteration step.

be simulated by a random walk of an ensemble of "particles" in the hyperspace. The $E_T - V(x)$ term gives rise to rate of change in the population of the ensemble, as can be seen if this were to be the only term on the right-hand side of Eq-3.1.5. A population of N after an interval of $\delta\tau$ changes by $\delta N = (E_T - V) N \delta\tau$. This can be simulated by branching, that is, creating a replica or destroying the old member with probability $(E_T - V)\delta\tau$, creating if the term is positive and destroying if the term is negative.

In quantum mechanics the wave function is the amplitude and the square of the amplitude gives the probability density. The value of the amplitude, therefore, can be either positive or negative. As a matter of fact, it could be complex, though there is no loss of generality in assuming the eigenfunctions of stationary states to be real valued. The Monte Carlo simulation of the diffusion equation by random walks treats the wave function as a probability function and must therefore be positive. If the wave function has regions of negative values, however, we can simulate this by changing the sign of the whole wave function which is equivalent to changing the phase of the amplitude by a constant. This allows us to solve the equation separately in positive and negative regions. If we know the zeros of the wave function this would be straight forward, but the problem is we generally do not know the zeros. Though one can do this by trial and error, an elegant solution to this is not known. This gives rise to a serious problem in treatment of the fermions since the wave function must be antisymmetric on exchange of two identical fermions. If the antisymmetry is forced on the spatial part of the wave function, there will be regions of negative amplitudes. As already mentioned in the introduction, we here consider the cases in which the

amplitude is positive throughout or we know the zeros from other considerations such as symmetry of the problem.

Next consider the ground state expectation value of the operator A in coordinate representation,

$$<A> = \frac{\int U_0(x)A(x)U_0(x)dx}{\int |U_0(x)|^2 dx} \qquad 3.1.6$$

which has an unbiased estimator,

$$\bar{A} = \underset{N\to\infty}{Lim}\frac{1}{N}\sum_{i=1}^{N} U_0(x_i)A(x_i)U_0(x_i) \qquad 3.1.7$$

where x_i are chosen from the uniform distribution in the range of integration and $U_0(x)$ is normalized to,

$$\int |U_0(x)|^2 dx = 1. \qquad 3.1.8$$

It may be observed, however, that the contribution to the integral is not of equal importance over the range of integral. For example, if $U_0(x)$ is zero at some point, sampling at this point does not contribute at all. Thus sampling according to the importance of the contribution to the integrals may have to be resorted to. This suggests that it may be possible to choose x_i from a weighted distribution to improve the efficiency. To investigate this we may recast the expression 3.1.6 for the expectation value as follows.

$$<A> = \frac{\int |U_T(x)|^2 \frac{U_0(x)}{|U_T(x)|^2} A(x)U_0(x)dx}{\int |U_0(x)|^2 dx} \qquad 3.1.9$$

Now if we sample x_i with weight $U_T^2(x)$, we will have higher contribution

from the points where the value of $U_T(x)$ is higher. We may now be able to adjust $U_T(x)$ such that efficiency is maximized; *i.e.*, the variance is minimized. However the function which minimizes the variance - actually the variance becomes zero - turns out to be $U_0(x)$. But this is a Catch-22 situation, since this is exactly what we want to solve for. All is not lost, however. We learn that if we sample x_i from a distribution nearer to the actual distribution we will improve the efficiency significantly. We may use for $U_T(x)$ an approximate solution to the problem which is obtainable analytically or otherwise. At least we can make some guess from the qualitative analysis of the system. This procedure is called Importance Sampling, where sampling is weighted so that the points of greater importance are sampled more frequently. This is the procedure followed in Variational Monte Carlo where $U_0(x)$ is also approximated by $U_T(x)$. The unbiased estimator in that case is,

$$\bar{A} = \underset{N\to\infty}{Lim} \frac{1}{N} \sum_{i=1}^{N} U_T^{-1}(x_i) A(x_i) U_T(x_i). \qquad 3.1.10$$

While the above method of importance sampling is applicable in calculating integrals by Monte Carlo, we want to use importance sampling to solve a differential equation. The solution to the Schrodinger-diffusion equation gives the distribution of ensemble with density $U_0(x)$. But we wish to have the distribution according to $|U_0(x)|^2$. This suggests that we may be able to improve the efficiency if we were to find a distribution closer to $|U_0(x)|^2$. So, following Kalos (Ka74), we consider the function $\Phi(x,\tau)$ defined by,

$$\Phi(x,\tau) = U_T(x)\Psi(x,\tau). \qquad 3.1.11$$

The equation for the evolution of $\Phi(x,\tau)$ is,

$$\frac{\partial\Phi(x,\tau)}{\partial\tau} = D\nabla^2\Phi(x,\tau) - [E_L(x)-E_T]\Phi(x,\tau) - D\nabla\cdot[\Phi(x,\tau)F_q(x)] \quad 3.1.12$$

where,

$$E_L(x) = \frac{HU_T(x)}{U_T(x)}, \quad 3.1.13$$

and

$$F_q(x) = \frac{2\nabla U_T(x)}{U_T(x)}. \quad 3.1.14$$

Here we make several observations :

Comparing with the equation for the Brownian motion (Ch43, Wa54) in the presence of a drift, we see that $F_q(x)$ is the quantum analog of the classical force responsible for the drift. In the regions of small value of U_T this force is large. This drives away the ensemble members from this region, thereby hastening the approach to equilibrium. Thus, while in calculation of the integrals the efficiency is increased by sampling the points of importance more often; here the efficiency is improved by accelerating the equilibration process.

$E_L(x)$ is the energy calculated using the trial function U_T. We may here observe that the branching now depends on E_L-E_T rather than on $E_T-V(x)$. This is rather convenient since, even if the potential is singular at points, we can get rid of the singularity in the E_L by an appropriate choice of the trial function and, as a matter of fact, for true wave function, this is just a constant, E_0, everywhere. This will reduce the drift in the ensemble size. The asymptotic solution for $\Phi(x,\tau)$ is,

$$\lim_{\tau\to\infty}\Phi(x,\tau) = U_T(x)U_0(x)exp[-\tau(E_0-E_T)]. \qquad 3.1.15$$

This suggests that we may take the value of the E_T as the ground state energy once the ensemble stabilizes. A good estimate of the stability of the ensemble requires a large ensemble. Further, it is also necessary that the value of E_T be the same over many iterations. For the above reasons the method is not particularly efficient. However, the average value of the E_L is also an unbiased estimate of E_0.

Finally some comments on the choice of the trial function. The best trial function is $U_0(x)$. So we should choose trial function from the best analytic approximation we can make. We should incorporate all the qualitative features such as symmetry property, curvature, cusp behavior and boundary conditions. If the potential is singular we can analyze the local behavior of the Schrodinger equation and remove this singularity from the E_L. This then can be continued in the far region appropriately. Choice of $U_T(x)$ should be such that the E_L has smooth behavior. [2]

3.2 An Outline of the Procedure

In this section we give a broad outline of the computational procedure and in subsequent sections we give the details of important algorithms. A reader not interested in the details of the algorithms should be able to jump, we hope without loss of continuity, to Chapter-4 at the end of this section.

---

2. If we were to disregard the evolution of $\Psi(x,\tau)$ and assume $U_T(x)$ as the wave function we recover the variational Monte Carlo. This indicates that PIMC is an improvement over the variational Monte Carlo.

a. Fix the values of R_β^0 for all open channels such that the interaction between the fragments is negligible for $r_\beta \geq R_\beta^0$.

b. Next we choose a particular channel α. Choose a value for $R_\alpha^1 \geq R_\alpha^0$. The Monte Carlo calculations are to be performed inside the region $r_\beta \leq R_\beta$, where $R_\alpha = R_\alpha^1$ for channel α, and $R_\beta = R_\beta^0$ for $\beta \neq \alpha$. The boundary condition is that the wave function has a node at the boundary.

c. Next choose the trial wave function U_T. Further, we should know the internal wave functions η_β and internal energy e_β for all the values of β. If we do not know the internal wave function we may construct an ansatz with some parameters and determine these parameters such that the energy is minimized. Thus we also obtain the internal energy.

d. We now initialize the ensemble. This ensemble must be as good a representative of the true wave function as possible. Here we have two different alternatives. Firstly, we may have no information other than the approximate wave function U_T. Here we initialize the ensemble which is representative of U_T. Section-3.3 gives the details of the algorithm for this case. We will also have an opportunity to determine the effects of various parameters. When we vary the parameters, the ensemble with previous parameters could be a better representative of true wave function in contrast to the one generated by using U_T, if the change in the parameters is small. Here we will use the ensemble from the previous run, thereby reducing the relaxation time.

e. Now consider the mth (the value of m is set to 1 at the beginning) configuration of the ensemble. We propagate the configuration by simulation of the diffusion equation by the random walks in the presence of the quantum force F_q. That is, we find the position of the particles in the configuration at $\tau+\delta\tau$ given their position at τ. However, we cannot

accept the motion every time for the following reason. The probability for a configuration at x to move to x' is to be properly balanced by the probability to move from x' to x. To accomplish this we need to know the exact Green's function for the Schrodinger-diffusion equation. Since we do not know the exact Green's function we are forced to use an approximate Green's function, which is exact as $\delta\tau$ approaches zero. Due to inaccuracy in the Green's function the proper balance of motion between x and x' is not maintained. The algorithm to evolve the position of the member and the method to ensure the detailed balance are described in Section-3.4.

f. Next we consider the branching. As described in Section-3.1, in addition to the random walks, we need to take into account the change in population of the ensemble. This change in the population, however, could be fractional. The fractional part of the change is treated as the probability to generate a new member; this is known as branching. In addition to branching we must also discard the configuration if it reaches outside the region defined by $r_\alpha \leq R_\beta$. In Section-3.5 we give the algorithm for the above.

g. We now increase the value of the m by unity and the steps e and f are repeated for all the configurations. Thus we obtain the ensemble at a time $\tau+\delta\tau$ from the ensemble at τ. Once we obtain the new position of the configurations; we can calculate the contribution to the expectation values of the energy, numerators and denominators of the D-matrix elements and thereby obtain an estimate of the D-matrix elements at a particular time. It may be noted, however, that we are calculating the elements $D_{\beta\alpha}$ with α fixed; *i.e.*, we get a row α of the D-matrix. We have to choose a different value of α in step-b to calculate another row.

h. As the ensemble evolves the size of the ensemble drifts. We must take care that the ensemble does not become too large or too small. Therefore, we must restore the size of the ensemble to a desirable value. We prescribe the upper limit, N_U, and the lower limit, N_L, and randomly destroy required number of members or create new members, as required, through random selection from the existing ensemble. In Section-3.5 we discuss the details of the algorithm for restoring the ensemble size.

i. Now we go back to the step-e and repeat the steps-$e \rightarrow h$ and thus integrate the diffusion equation with an integration step $\delta\tau$.

j. The value of the energy depends on the choice of the value of R_α^1. By varying the value of R_α^1 we obtain the D-matrix elements at different energy. If, however, we wish to obtain the D-matrix at a particular energy, we must iterate steps-$b \rightarrow i$. Our aim being general investigation we calculate the D-matrix at different energies and store the information.

k. As mentioned before the steps-$b \rightarrow j$ give a particular row of the D-matrix. To calculate other rows of the D-matrix we must repeat the steps $b \rightarrow j$ with all the possible choices of α. To calculate the S-matrix at a particular energy we need the D-matrix at that energy. In general, choice of R_α^1 in different channels to give the same energy is to be done by trial, but if we store the D-matrix for many closely spaced energies we can approximate the D-matrix for intermediate energies by interpolation. Once we obtain the D-matrix the calculation of the S-matrix, using the equation-2.3.12, is simple.

The above calculation gives us a sequence of values of the D-matrix element with an interval of $\delta\tau$. Taking an average over this sequence is equivalent to summing over many ensembles. However, we have to pay

attention to two aspects in estimating the values. Firstly, since we may be initializing the ensemble approximately we should not sample the calculation at the beginning. We must disregard some initial integration steps so that the system has approximately reached the equilibrium. Secondly, the sequence of ensembles obtained during the evolution is correlated. We, however, must average over uncorrelated ensembles. These two aspects are considered in Chapter-4.

3.3 Initialization of the Ensemble

Here we explain the procedure to initialize the ensemble which is representative of the trial function U_T. The probability density, corresponding to the wave wave function U_T, is given by $|U_T|^2$. There are several methods of constructing an ensemble with a given distribution (Ha64). Below we describe the algorithm used in the calculations herein.

We choose the first configuration arbitrarily, although it is advantageous to choose this such that the probability density for the configuration is significant. Now suppose that we have chosen m configurations. We denote the coordinates of the configuration by $x^{(m)}$. Choose the trial coordinates for the $(m+1)th$ configuration from the uniform distribution in the region. The relative probability for the acceptance of $(m+1)th$ configuration in comparison to mth configuration is given by,

$$P_r = \frac{|U_T(x^{(m+1)})|^2}{|U_T(x^{(m)})|^2}. \qquad 3.3.1$$

P_r is the conditional probability for choosing the trial configuration given that mth has been chosen. Thus we should accept the trial

coordinates for the $(m+1)th$ configuration with the probability P_r. Hence, if $P_r>1.0$ we should accept the coordinates. If $P_r<1.0$, however, we generate a random number R, with the uniform distribution in the range (0,1.0) and accept the coordinates if $P_r \leq R$. If $P_r>R$ we choose a new set of coordinates and repeat the test for the acceptance. Sometimes it may happen that the number of trials required is too large. We restrict ourselves to a maximum number of trials, after which we accept the coordinates even if the test fails. There is not much lost in the above restriction since this is not the ensemble we ultimately want but only the initialization, and it will be evolved to the desired ensemble. We choose the maximum number of trials as five. The adequacy of this number can be seen from the average number of trials required to generate a configuration, which was about three.

3.4 The Detailed Balance and Evolution of the Ensemble

The Eq.-3.1.12, the Schrodinger-diffusion equation, determines how $\Phi(x,\tau)$, defined in 3.1.11 evolves. If $G(x',x)$, the Green's function, is the solution to Eq.3.2.12 with the boundary condition $G(x',x)=\delta(x-x')$, then we can write the solution to $\Phi(x,\tau)$ in integral form as,

$$\Phi(x',\tau+\delta\tau) = \int G(x',x,\delta\tau)dx\,\Phi(x,\tau). \qquad 3.4.1$$

$G(x',x)$ gives the transition probability for the particle at x to move to x' in time $\delta\tau$. In general, the exact solution to $G(x',x,\delta\tau)$ is not known, however, and therefore we must resort to an approximate solution. If the local energy $E_L(x)$ and quantum force F_q are assumed constant during the integration time $\delta\tau$, we get an approximate solution to G as,

$$G(x,x') = N_g \exp\left([-(x'-x-DF_q\,\delta\tau)^2]/4D\delta\tau\right) \qquad 3.4.2$$

where,

$$N_g = (4\pi D\delta\tau)^{-Nd/2}\exp\left(-\delta\tau[E_L(x)+E_L(x')]/2-E_T\right) \qquad 3.4.3$$

where, N is the number of configurations in the ensemble and d is the dimensionality of the space. The above approximation becomes exact in the limit $\delta\tau\to 0$. The Green's function above constitutes two parts, the Gaussian part and the normalization constant, N_g. The normalization constant is different than the regular normalization for the Gaussian. The extra factor in N_g accounts for the change in the population of the ensemble. This part is to be used for the branching, *i.e.*, creation and annihilation of the member as it is moved.

The Gaussian part of the Green's function shows that the particle j, of the configuration m, moves from x to x' given by,

$$x'^{(m)}_j = x^{(m)}_j + D(F_q)_j\,\delta\tau + \chi. \qquad 3.4.4$$

The second term above is the drift due to the quantum force F_q and χ is Gaussian random number with zero mean and variance $2D\delta\tau$. We must, however, pay attention to the detailed balance before accepting the movement. That is, we should compare the transition from $x\to x'$ with the transition $x'\to x$. For this purpose we define,

$$W(x',x) = \frac{U_T^2(x')G(x'\to x)}{U_T^2(x)G(x\to x')}. \qquad 3.4.5$$

If the Green's functions in the above expression are exact, the value W(x',x) is unity. But the Green's function we use in the computation is approximate due to the finite integration step. Therefore, we need to

modify the Green's function such that it restores the detailed balance. If we replace the Green's function in the Eq.3.4.5 by $A(x,x')G(x,x')$, where

$$A(x',x) = min(1.0, W(x',x)), \qquad 3.4.6$$

then the effective $W(x',x)$ is unity. This is incorporated in the calculation by accepting the movement of the configuration with probability $A(x',x)$. That is, if the value of $W(x',x) \geq 1.0$, we accept the move. If $W(x',x) < 1.0$ then we generate a random number between 0 and 1.0 and accept the move if the random number is less than $W(x',x)$.

3.5 Branching and Restoration of the Ensemble

The part of the normalization factor N_g, of the equation 3.4.2, is the usual normalization of the Gaussian distribution. The remaining factor gives the multiplicity of the configuration. The multiplicity part of N_g is,

$$M = exp[-\delta\tau([E_L(x)+E_L(x')]/2-E_T)]. \qquad 3.5.1$$

After the evolution of the configuration we have to retain M copies. However, M has an integer part M_{in} and a fractional part M_{fr}. First consider the case $M > 1.0$. The integral part is handled by creating $M_{in}-1$ new copies. The fractional part is treated as the probability of creating a new copy. This is accomplished by generating a random number between 0.0 and 1.0 and creating a new copy if the random number is less than M_{fr}. If $M < 1.0$, however, we treat this as the probability of survival of the configuration. Once again we generate a random number between 0.0 and 1.0 and destroy the configuration if the random number is greater than M.

If the size of the ensemble, N_e, drifts too far, we restore N_e to the desired value, N_0. If the ensemble crosses a prescribed upper bound, N_U, extra configurations are deleted by random selection as follows.

Algorithm-A

A1. Generate a random number r_1 in range 0 to 1.0. Define $S=$ integer part of $(1+r_1 N_e)$.

A2. Generate a random number r_2. Define $I=$ integer part of $(1+r_2 N_e)$.

A3. Redefine $S=(S+I)_{mod.N_e}$.

A4. Delete the configuration S by repacking the ensemble by setting all the configurations $i>S$ to $(i-1)th$ configuration. Set $N_e=N_e-1$.

A5. Repeat steps A3 and A4 until $N_e=N_0$

If the ensemble crosses the lower bound, N_L, then we create a required number of configurations by randomly selecting from the existing ensemble as below.

Algorithm-B

B1. Generate a random number r_1 in range 0 to 1.0. Define $S=$ integer part of $(1+r_1 N_e)$.

B2. Generate a random number r_2. Define $I=$ integer part of $(1+r_2 N_e)$.

B3. Check whether I is a prime relative to N_e, i.e., $(N_e)_{mod.I}=0$. If the check fails go back to the step B2. Otherwise proceed to B4.

B4. Redefine $S=(S+I)_{modN_e}$.

B5. Create a new configuration by copying the Sth configuration and adding it to the end of the list.

B6. Repeat steps B4 and B5 to create N_0-N_e new configurations.

B7. Now set $N_e=N_0$

In steps A1, A2, B1 and B2, presence of unity in expressions for S and I is to ensure that they are not zero. Here we may remark that, while random destruction of the configurations, beside changing the size, does not change the distribution of the ensemble, the creation of new configurations essentially upsets the distribution. In algorithm B it is important to check that I is relative prime with respect to N_e. If this is disregarded then there is possibility of repetitions among the newly created configurations. This will create, as was observed, imbalance in the distribution of the ensemble.

4. Error Estimation and Computational Parameters of the Algorithm

4.1 Parameters Artificial to the Algorithm

First let us recapitulate the procedure:

We initialize an ensemble of size N_e, either from a previous run or generating anew a representative of initial wave function U_T, the function for importance sampling.

We also initialize E_T, the shift in the energy. The value of E_T can be obtained either from a previous Monte Carlo calculation of an approximately similar system, a variational estimate, or an analytic approximation. In any case we can set this to be zero if any guess is difficult. An inaccurate value of E_T, however, will require a longer relaxation time. The energy shift E_T is updated at an interval of N_T steps.[1]

Now the evolution of the ensemble is calculated with an integration step $\delta\tau$. The energy, which is the expectation value of the Hamiltonian of the system, is calculated for this ensemble. The expectation values of other operators necessary to calculte $D_{\beta\alpha}$ are also calculated.

As the ensemble evolves, N_e drifts. If the ensemble reaches the upper limit N_U or the lower limit N_L, it is updated to N_0, as described in Section-3.5, by destroying the configurations selected at random or creating new members through a random selection from the existing

1. The new value of E_T is taken to be half of the old value, plus half of the mean of the expectation value of the Hamiltonian during N_T iterations.

ensemble.

The inegration is carried out for an adequate number of steps and expectation values at each of the iteration are calculated. Initial N_R iterations are discarded to allow the the system to relax from the initial condition. How this number is determined is discussed in Appendix-3. The average over the rest of iterations is taken as the estimate.

To calculate the error we calculate the second moment about the average. The consecutive ensembles during the evolution are correlated and in estimating the error they cannot be treated as independent. We have to take into account the correlation "length" N_S at which the ensembles become uncorrelated. This is discussed in greater detail in Section-4.2

In addition to the above, the problem in an infinite domain is reduced to a finite domain which gives rise to truncation of the potential if the range is infinite. The error due to the truncation of the potential can not be dealt within the Monte Carlo method, however, and we have to resort to analytical methods for an estimate of this error. The error due to the finite time step can be reduced by extrapolating to infinitesimal time step from the results at several different time steps. We will not deal with the truncation aspect mentioned above. We will, however, for some illustrative cases, extrapolate to the infinitesimal time step through a linear least square fit.

In subsequent sections of this chapter we study other parameters viz: N_R and N_S, N_T and E_T, N_U, N_0 and N_L in a greater detail. N_R and N_S are parameters characteristic of the system. $N_R\delta\tau$ is the time required for the system to relax to the ground state from the initial condition and will depend on how well we can initialize the ensemble and how much the ensemble gets destabilized by updates while restoring the size. $N_S\delta\tau$ is

the time required for the random walk part of the diffusion to wash out the effects of the quantum force F_q. All the other parameters listed above are artificial to the algorithm. These parameters do not affect the theoretical possibility of improving the accuracy, which is only limited by the computer time available. Nevertheless we can investigate whether they can be optimized or used to obtain other information about the system. This is the subject matter of this chapter. We propose to use the information, experimentally found here for a simple soluble example, in subsequent cases where we seek to solve the problems which are otherwise difficult or impossible to solve.

4.2 Error Estimation

An accurate estimate of the expectation value of an operator requires a large ensemble. Alternately we may increase the accuracy by averaging over many independent ensembles which together form a large ensemble. These ensembles can be obtained from the iterations in Diffusion Monte Carlo after the system has relaxed. While we need independent ensembles for the purpose, the series of ensembles obtained in the Diffusion Monte Carlo are correlated. Therefore we cannot estimate the error on the basis of the ensembles considered as independent. This can be readily seen from the fact that by reducing the integration step we increase the number of ensembles and if we estimate on the basis of all the ensembles we artificially reduce the standard error without averaging over many independent ensembles.

If the ensembles are sampled at a sufficient interval, N_S, they will be uncorrelated. We can then find the error based on the ensembles sampled at an interval N_S. One way to determine N_S is to examine the

correlation of the energy, assuming that the uncorrelated energy implies uncorrelated ensembles. The correlation coefficient, $C_{N,n}$, is calculated by shifting the series by n units and calculating the correlation between the overlapping $N-n$ points. That is, we define $C_{N,n}$ as,

$$C_{N,n} = \frac{\sum_{i=1}^{N-n} e_i e_{i+n}}{[\sum_{i=n}^{N} |e_i|^2]^{1/2}[\sum_{i=1}^{N-n} |e_i|^2]^{1/2}} \qquad 4.2.1$$

where $e_i = E_i - \overline{E}$. Now, for example, consider Figure-3. Notice that at $n=56$ $C_{N,n}$ has first minimum. We then take N_S to be 56. Blindly taking N_S as n at the first minimum of $C_{N,n}$, however, could lead to an erroneous result. For example, consider the series of points obtained from $sin(\omega\tau)$. Therefore, it is necessary to make sure that $C_{N,n}$ remains low and oscillates about zero randomly.

In Appendix-3 we give a new method, based on computer experiments, to define N_S. The method is based on comparison between random- rather, pseudo-random - numbers and the series of energy sampled at an interval. Though a theoretical analysis is lacking we hope that this method does not have some of the drawbacks of the previous method. In Appendix-3 we have argued that the new method is useful in determining the relaxation time and analyzing metastable cases. In the next section we illustrate the method through an example. First we make some remarks on how we use the sampling interval.

By shifting the starting point for the sampling we can get N_S different samples. They are all equivalent; i.e., we may start sampling at any point after the equilibration point. Therefore we may take the mean over all the values; we may not, however, treat them as independent in

determining the standard error. We could follow one of the following three schemes.

1. Out of N_S samples we get by shifting the starting point, we may just consider one of the samples and find the average and the standard error based on this one sample. Here much information is lost.

2. We may quote the mean value based on all the iterations and also average the standard error over all N_S samples.

3. We could find the mean and standard error based on all the iterations and renormalize the standard error for the correlation between the consecutive ensembles by multiplying it by $(N_S)^{\frac{1}{2}}$.

We shall follow the the third scheme.

4.3 Example: Scattering of a Particle by a Potential

In this section we illustrate, through an example, the methods of Appendix-3. Here we give a detailed account which will be suppressed in the later description, where we give only the results of a similar analysis. Below, we analyze the calculation of the phase shift for the scattering of a particle, of mass m, by a potential $V(x)$. As is well known, this is equivalent to the two-body scattering if we replace the mass m and coordinate x of the particle by the reduced mass and relative coordinate for the two-body system. Of course, the interaction between the particle is the same as the potential. This example will also be used to investigate the effect of various parameters, listed in Section-4.1, in subsequent sections of this chapter.

We choose the potential to be Poschl-Teller (Po33); that is,

$$V = \frac{V_0}{[\cosh(x/x_0)]^2}. \qquad 4.3.1$$

We confine the particle to the region $|x| \leq a$ and calculate the energy. The wave function is forced to have a node at the boundary $|x| = a$. A trial wave function appropriate for this case is,

$$U_T = \sin(\pi x / a). \qquad 4.3.2$$

The relation between the energy E and the wave number k in the asymptotic region is,

$$k = (2mE/\hbar^2)^{1/2}. \qquad 4.3.3$$

The phase shift is then given by,

$$\delta_{ph} = \pi - ak \ . \qquad 4.3.4$$

This problem is analyzed in Koonin and Alhassid (Al84). There the problem is interpreted as solution to the radial Schrodinger equation for zero angular momentum state in three dimensions. We may also interpret this as the antisymmetric combination of incoming waves from both the directions in one dimension. From the above investigation, Table-4 is reproduced, wherein, along with the Monte Carlo results, exact values of the phase shift (Ca67) and these values corrected for the truncation are listed.

We choose the following values of the physical parameters, [1]

$$x_0 = 2.0\text{fm}, \quad V_0 = -8.0\text{MeV}, \quad m = m_p \quad \text{and} \quad a = 5.0\text{fm}. \qquad 4.3.5$$

A choice of other parameters for the computation is,

---

1 For the units used in the computation see the appendix at the end of Chapter-1. m_p is the proton mass.

$$E_T = 0\ ,\ \delta\tau = 0.001 \times 10^{-23} sec\ ,$$

$$N_0 = 100;\ N_U = 110;\ N_L = 90\ . \qquad 4.3.6$$

Though calculations were carried out for 7,000 iterations, in the following we consider a window of 5,000 iterations; the purpose of this will be clear by the end of this section. First we discuss two other methods, which we wish to compare with the method of Section-4.2, of finding the sampling interval

First let us consider the method followed in Koonin and Alhassid (Al84) or other similar Monte Carlo works. We examine the correlation coefficient $C_{N,n}$, defined by the Eq.-4.2.1. We determine the value of n such that the correlation coefficient, $C_{N,n}$, approaches zero or has a minimum in the neighborhood of zero. We take this value of n as the sampling interval. Figure-3 shows a plot for $C_{N,n}$, where first 700 iterations, corresponding to relaxation time, were discarded and next 5,000 iterations were used. The number 700 above has been used from the analysis to follow later. From Figure-3 we find that $N_S = 56$. Similarly we determine the sampling interval, N_S, by disregarding 0, 800, 900 and 1000 initial iterations. The table below gives the results.

Iterations Discarded	Sampling Interval	
0	65	
700	56	
800	58	
900	59	(53)
1000	59	(53)

For the first three cases we find that the correlation coefficient

approaches zero but does not cross zero for a long time. The value of $C_{N,n}$, however, remains low. Therefore, we choose the value of n at the first minimum of $C_{N,n}$. However, for the last two cases $C_{N,n}$ crosses zero before reaching the minimum. Here we give, within the brackets, the value of n at the zero crossing. Clearly, for a consistency we should determine the sampling interval on the basis of the first minimum. We also note the decrease in the sampling interval after the system has relaxed.

Another method we tried, before the discovery of the method of Appendix-3, was to examine the Fourier power spectrum, defined in Appendix-3, of the series. Figure-4 shows the power spectrum for the series, 5000 iterations long, starting at iteration 700. Once again we normalize such that the range for τ is unity. We observe that the amplitude is negligible beyond a certain frequency f_{max}. To calculate the sampling interval note that the power spectrum (Fig-1) for the random numbers, the sampling interval for which is obviously one, becomes negligible at a frequency of about 0.5N, and we can obtain the sampling interval, $N_s \approx N/2f_{max}$. Therefore, we take $5000/2f_{max}$ as the sampling interval for the energy series. The rationale behind this is that if we take the sampling interval less than the above, there will be no frequencies with significant amplitude to change the value from one sampling point to the next. [2] When f_{max}=2500, the case of random series, we get the sampling interval of 1, which we should expect. Similarly to the first method we determine the sampling interval for various cases tabulated below.

---

2. For a stationary continuous signal of finite duration the best estimate of the average is obtained by sampling at twice the maximum frequency (Ba66).

Iterations Discarded	f_{max}	Sampling Interval
0	66	38
700	66	38
800	66	38
900	66	38
1000	66	38

The Figure-4 and Figure-1 show some uncertainity in determining the value of f_{max}. We also note firstly, the value of N_S is lower compared to the first method and secondly, there is no effect due iterations discarded.

Next we consider the method of Section-4.2 which we propose to use in future. First we disregard the relaxation time, to which we shall come back later, and consider the first 5,000 iterations. For convenience we define,

$$\vartheta = \overline{m}_1 / N \qquad 4.3.7$$

where $\overline{m}_1$ is defined in Appendix-3.[3] Instead of doing a binary search, which we describe later, in Figure-5a we plot the value of ϑ for the sampling interval of 10 through 60. We have, for reference, drawn a horizontal line at ϑ =0.60. For N_s>42 we see that ϑ>0.60 most of the time and fluctuates between 0.6 and 0.66. This fluctuation will depend on the length of the sample. Here we note that the standard error for ϑ is about 0.01 and therefore expect this fluctuation. Below N_s<40 we notice that ϑ,

3. For a given seriese of length N, m_1 is defined such that,

$$\sum_{n=1}^{m_1} C_{N,n}^2 = 1.0$$

and $\overline{m}_1$ is the average of m_1 over the N_S series, obtained by sampling at an interval N_S, by shifting the starting point. For more details refer to Appendix-3.

on the average, increases. We also see that the fluctuation is smaller for smaller N_S. This is because the sampled series is correlated. Therefore, we conclude that the sampling interval should be 42±2.

It is not necessary to calculate for a large range of N_S. We may systematically search for a good candidate for N_S. This may proceed as a binary search as follows. We start with N_S=64 or 128 and search until we encounter $\overline{m}_1/N$ about 0.60 (this number depends on the standard error and we take this three times the standard error away from 0.63). Due to fluctuations in ϑ we may not reach the correct value of N_S every time. For example, from Figure-5a we see that we may end up at N_S=31. We examine the neighborhood of this value of N_S and find that the value of ϑ does not remain high for N_S>31. Therefore, we conclude that the large value of ϑ at N_S=31 is due to fluctuation and we therefore reject this value. On the other hand suppose we come across $N_s \approx 40$ and examine the neighborhood. We find that below N_S=40 ϑ increases as N_S increases, and above N_S=40 ϑ remains high, albeit with some fluctuation. From this local analysis we conclude that the sampling interval is approximately 42±2.

So far we have disregarded the fact that initial iterations are during the relaxation period of the system. Now we apply the method of Appendix-3 to determine the relaxation time. To determine the relaxation time we examine Table-5 where we list the iterations at which the ensemble is updated. We notice that the interval between the updates is increasing in the beginning. After iteration 824, however, this interval fluctuates. We also observe that beyond this the ensemble drifts towards both the limits. From this we guess that the relaxation time is somewhere between 215 and 824 iterations. Although we could start sampling

at iteration 824, which may be rather prudent, we wish to check this further and if possible improve the guess. Table-6 lists the sampling interval against the iterations discarded. The sampling interval decreases as the starting point is moved up until 700, after which it remains constant. As exemplified by the Figures-5b & 5c, which correspond to discards of 700 and 1000, the precision is better compared to Figure-5a for which no iterations have been discarded. For a finer look at the case of Figure-5b we give the Table-7 where values of ϑ and the standard error are tabulated against the sampling interval. The fluctuation in the value of the ϑ beyond N_S=31 is clear. The fluctuation is due to lack of correlation in the sampled series. This fluctuation by itself is a good indicator of the right sampling interval and is independent of the distribution of energy. Figures 5a, 5b and 5c show that the precision with which we can determine N_S improves beyond the relaxation point. The improvement of the precision beyond relaxation seems to be true in general. Thus we arrive at the result N_R=700 and N_S=31.

Now let us compare the three methods described above. We see that the first two methods are conservative in comparison to the third. In the first case the reason is that due to finiteness of the series we should expect the correlation to be nonzero even for a good representative of a random series. Therefore, probably we should not wait until the correlation approaches a minimum or zero. We should rather be satisfied if the correlation comes to the level of maximas at the far right of Figure-3. The method definitely fails if we consider a time series $E(t)=sin(wt)$ which has a correlation function, $C(T)=cos(wT)$. Thus in addition to the correlation approaching zero we have to make sure that the correlation remains small throughout and has some fluctuation. The proposed

method, however, does not have any trouble handling a general situation.

The examination of Figure-4 shows that, besides some ambiguity in locating the point beyond which we consider the amplitude negligible, we also see that the amplitude persists, albeit small. These two factors make the Fourier spectrum method conservative. We may note, however, that the relaxation time has no effect on the sampling interval. This is due to the fact that we rely on the high frequency behavior to determine f_{max}. The relaxation time, however, is large and affects only the low frequency behavior.

In the third method we take care of the detailed behavior of the correlation and use all the information we have. Therefore, we should expect, besides the error due to the finiteness of the series which is common to other two methods, to get a more precise answer. The method is more sensitive to the relaxation time. We can make it more sensitive to the relaxation time by considering a smaller window; this will, of course, increase the error due to the finiteness of the series, which will further enhance the effects of the relaxation.

We may yet have a reservation about the method we propose since we are comparing the average over a set of uncorrelated series with that of a set of series which are correlated. That is, the corresponding members of two series obtained from a single shift are correlated. In Table-8a we give the values of m_1 we get for different starting points with the sampling interval of 120, the first 700 iterations being discarded. In Table-9 we compare the distribution of m_1 for this case with the case of random series given in Table-1, along with the Gaussian distribution. In Table-8b we summarize the properties of m_1 for the above two cases. These two distributions are the same within the expected error for the finite size

sample. The point is that, if we were to find m_1 for many samples obtained by restarting the problem with different seeds for the random number generators, their distribution would be the same as that of the samples obtained from shifting the starting point and therefore we conclude that either average is useful in determining the value of $\overline{m}_1$.

4.4 Effects of Various Parameters

Now we wish to examine the effects of various parameters on the accuracy of the Monte Carlo calculations. The physical problem we consider is the same as in Section-4.3. The relation between the energy and the phase shift, given by the Eq.-4.3.4, is straightforward; therefore, we quote only the value of the energy. The value of the energy is to be compared with its value in Table-4 for the appropriate value of the parameter a which is 5.0 fm. In Table-10a we list the results of Monte Carlo simulations with different values of the parameters with the same integration step $\delta\tau=0.001\text{x}10^{-23}sec$. Table-10b gives the results of the Monte Carlo simulation, for one of the cases from the Table-10a, with various integration steps. Now we discuss these results.

Parameters N_U, N_0 and N_L

We remind the reader that N_L and N_U are lower and upper bounds on the ensemble and that the ensemble is restored to N_0 if it goes out of bounds. The table below, extracted from Table-10a, gives the results for the variation of these parameters with all the other parameters fixed. The number of iterations was 7000 with an integration step $\delta\tau=0.001\text{x}10^{-23}sec$.

Table-A

N_0	N_L	N_U	N_R	N_S	E	δE
					MeV	MeV
100	95	105	400	29	5.40205	0.01093
100	90	110	700	32	5.37471	0.01290
100	85	115	1300	35	5.39177	0.01476
100	80	120	inadequate	limits.		

From the above table we observe that the relaxation time, sampling interval and the standard error increase as we allow larger deviations. The reason for this is that the ensemble is destabilized every time it is restored and stability needs to be restored. This is especially true when we update it from the lower bound by duplicating some configuration. As we allow larger deviations the destabilization is larger as the table above shows. In the last case the ensemble did not acquire adequate stability and we have discarded this case completely. The values of the N_R in the table above, and quoted in future, are only approximate, say within 100 to 200 iteration steps, the error being on the conservative side. Therefore, any regularity in these values must not be taken too seriously.

Next we change the nominal size, N_0, of the ensemble. Below we extract the relevant data from Table-10a.

Table-B

N_0	N_L	N_U	N_R	N_S	E	δE
					MeV	MeV
200	195	205	800	27	5.37172	0.00873
200	190	210	400	35	5.38246	0.00947
200	180	220	800	36	5.37480	0.00972

Here we observe that the standard error in the energy is reduced. This should be expected since error in calculation should roughly follow the inverse square-root of the ensemble size. Further, we see that the error does not change much as we change the bounds on the ensemble. We also see that the relaxation time has a minimum. The reason for this optimum is as follows. If the bounds are too small we tend to update the ensemble from the unstable one and new members will introduce further instability. That is, if the ensemble is not the equilibrium ensemble, it is better to let it change before we begin updating. If, however, we let the ensemble drift too much, then the updating (especially creating from the existing ensemble) introduces an error in the composition of the ensemble. Further, we see that the relaxation time does not depend on the ensemble size as is clear from comparing the first two cases of Table-A with the last two cases of Table-B above. The time for computation to the relaxation, however, is proportional to the ensemble size. Hence, we can improve the efficiency by starting with a lower number of configuration and doubling this once the relaxation has occurred.

Next consider the detection of the equilibration point. Since with larger deviations the drift of the ensemble to the bounds takes many

iterations it becomes difficult to determine whether the system has relaxed by looking at the intervals between updates of the ensemble. For example, for the last case from Table-A above the first update occurred after 827 iterations. The closer bounds, however, give rise to a different difficulty. Here it was found that the ensemble reaches these bounds quite frequently even after the equilibrium, and the detection of the equilibration point becomes rather difficult.

From the above discussion and observations it seems adequate that the ensemble be allowed to drift about 5% from the nominal value. The nominal size of the ensemble, if lower, will reduce the computation time during the relaxation, and if higher then the standard error is less dependent on the bounds on the ensemble.

Parameters, E_T and N_T

The importance of choosing E_T close to the exact value of the energy is clear. By itself the choice of E_T is not sufficient, however, since this must be accompanied by an accurate representative ensemble. If the ensemble is not a good representative, subsequent updates will introduce inaccuracy in E_T. If the ensemble is a good representative, then the updating will make E_T approach the true value quickly unless the initialization of E_T is really far off. Thus it is important that both the ensemble and E_T be initialized accurately. Instead of initializing from the trial wave function U_T, we may sometimes be able to use the ensemble and E_T from a previous calculation, if the problem is close to the one we already calculated.

Next let us consider N_T, the interval at which the value of E_T is renewed. The expectation value of the Hamiltonian calculated on the

basis of a finite ensemble will fluctuate about the true value of the energy. Therefore, E_T will fluctuate if we were to renew it after every iteration. The inaccurate E_T will give rise to excessive drift in the ensemble. These fluctuations could give rise to instability in the calculation. The fluctuation will reduce if we update it on the basis of an average over several iterations. To investigate the effect of N_T, we calculate with different values of N_T, with all other parameters the same. Table-C, once again extracted from Table-10, shows the results. For the table below we have chosen N_U=105, N_0=100 and N_L=95 according to the prescription given above. To examine the efficiency we must compare the computation of the same duration, which is accomplished by keeping the number of iterations, chosen to be 7000, the same. Once again the integration step $\delta\tau$ is 0.001x10−23*sec*.

Table-C

N_T	N_R	N_S	E	δE
			MeV	MeV
10	400	30	5.38640	0.01254
20	400	29	5.40205	0.01093
25	400	37	5.38762	0.01320
30	400	83	5.38944	0.01995
35	400	65	5.39194	0.01806
40	400	35	5.39882	0.01344

First we observe that the relaxation time N_R does not change significantly. We expect this since N_T is small in comparison to N_R. However, N_S as well as the standard error in E exhibits significant variations.

A part of the change in the standard error is due to the change in the N_S. A part of the change, however, is due to the change in the dynamics due to the variation in N_T.

A question to be answered is whether the reduction in N_S is desirable. A large value of N_S indicates a stronger correlation between consecutive ensembles during the evolution. One reason for the correlation is that the ensemble evolves according to an equation, viz. the Schrodinger-diffusion equation. Too weak a correlation could mean that we are not following the governing equation accurately; i.e., $\delta\tau$ is too large. Therefore, we may conclude that we must choose N_T such that N_S is maximum. Another reason for stronger correlation, however, is using the same value of E_T; i.e., change in the value of E_T introduces some randomness. We want the mean value of E_T to be the same as the real value of the energy. We must choose N_T such that the standard deviation in E_T is minimum. This will lead to minimum standard error in the energy. If we observe the standard error in E we see that the error is minimum for N_T=20. We should be careful before concluding and see how the calculations compare with different seeds for the random number generator. In the table below we compare the N_T=20 case for different seeds for the random number generator.

Table-D

Seed	N_R	N_S	E	δE
			MeV	MeV
2194817532.000	400	29	5.40205	0.01093
456327659848.0	400	29	5.38649	0.01233
639627100293.0	400	31	5.37804	0.01286

From the data above it is difficult to see that there is an optimum value of N_T. We note that N_S has a maximum. However, the maximum for N_S is not yet understood. Nevertheless, we must be cautious in selecting N_T.

Integration Step $\delta\tau$

The computations are done with a finite integration step. Therefore, we must verify that the change in the integration step does not alter the result significantly. Table-E, which is same as Table-10b, gives the result of the calculation with various integration steps.

Table-E

$\delta\tau$	L	N_T	N_R	N_S	S	E	δE
$10\text{x}10^{-23}sec$						MeV	MeV
0.00100	7000	20	400	32	175	5.41989	0.01707
0.00100	14000	20	400	38	357	5.38759	0.00937
0.00075	10000	20	400	48	200	5.37993	0.01406
0.00050	10000	30	600	88	107	5.37471	0.01290
0.00050	10000	40	800	87	105	5.40599	0.01829
0.00025	10000	20	800	49	195	5.37981	0.01231

$\delta\tau$=0.001 and 0.0005 cases have been calculated with different seeds. The second case has been calculated for a longer run. Next we find the value E in the limit $\delta\tau\rightarrow 0.0$ by a linear least square fit (Be69); i.e., we do a least-square fit to the equation $E(\delta\tau)=A+B\delta\tau$. From this extrapolation we get $E(0)$=5.37403±0.0061 MeV. This is in good agreement with the exact value, E=5.3732MeV, and the Monte Carlo result, E=5.3752±0.0054 MeV, from (Al84).

5. Three-Body Problem: One-Dimensional Case

5.1 Preliminary Remarks

In this chapter we consider the scattering of a three-body system in one dimension with a two-body interaction.[1] We choose all the three particles to be of mass m and the potential between particles i and j, $V(i,j)$, to be,

$$V(i,j) = V(j,i) = V_{i,j} f(x_i - x_j) \qquad 5.1.1$$

where,

$$|V_{i,j}| = V_0$$

and,

$$f(x_i - x_j) = 0; \text{ if } |x_i - x_j| > a_{i,j} = a_0$$

$$= 1; \text{ if } |x_i - x_j| \leq a_{i,j}.$$

This is a square well if V_0 is negative, and a square barrier if V_0 is positive.

The formulation of the scheme, as described in Chapter-2, assumes that ingoing and outgoing channels contain two fragments. Therefore, at least one pair of particles should be able to form a bound state. There always exists a bound state for a particle in a potential well. [2] Hence it is

1. Appendix-1 gives notation and some useful information for this system.
2. A standard problem in any text on Quantum Mechanics, for example (La77).

sufficient that one of the $V_{i,j}$ is negative. If the potential well is deep then several bound states exist. We shall, however, confine ourselves to the depths with a single bound state. The two-body binding energy, $e_\alpha = e$, depends on the parameters m, V_0 and a_0. If, however, the dimensionless number $Q = \frac{m V_0 a_0^2}{\hbar^2}$ is invariant,[3] then the solutions for various cases can be obtained by appropriate scaling of a single solution.

The wave function for the ground state, which is to be used for the internal wave function, $\eta_\alpha = \eta$, is given by,

$$\eta = A\cos(k_1 x);\ x \le a_0 \qquad 5.1.2$$

$$= B\exp(-k_2|x|);\ x \ge a_0$$

where,

$$k_1 = |2M(e+V_0)/\hbar^2|^{1/2} \text{ and } k_2 = |2Me/\hbar^2|^{1/2},$$

where x is the relative coordinate of the pair and M is the reduced mass; i.e., $M = m/2$. From the continuity of the wave function and its slope at $x = a_0$, we can express B in terms of A and determine the binding energy e. The constant A can be determined by normalization of the wave function.

Next we need to estimate the range, $d_\alpha = d$, of interaction between two fragments. We may define the effective potential, $V(R)$, between the fragments at a distance R apart, by convoluting the interaction between the constituents with the square of the internal wave function.[4] Fig-7

3. $\hbar$ in the dimensionless number, Q, is a universal constant. Variation of the integration step, however, can be construed as a variation in $\hbar$ and we may estimate the appropriate integration step $\delta\tau$ by replacing $\hbar$ by $V_0\delta\tau$.
4. The mathematical expression, Eq.-5.2.1, is given in Section-5.2.

shows the effective potential for one of the cases. The concept of effective potential, though inadequate at short distances, is quite appropriate for the purpose of defining d, since here we need only the long distance behavior. Presently, let us define d as the distance at which the effective potential reduces to $0.01\,V_0$. [5] Table-11 gives the binding energy e and the range d for the various values of the parameters m, V_0 and a_0. As to be expected, d increases as a_0 increases, and decreases as m and V_0 increase.

Now, depending on the nature of forces we have three cases defined below.

Case-1: $V_{1,3}$ negative; $V_{2,3}$ and $V_{2,1}$ positive. Here we have one two-fragment mode.

Case-2: $V_{1,3}$ positive; $V_{2,3}$ and $V_{2,1}$ negative. Now we have two two-fragment modes.

Case-3: All $V_{i,j}$ negative with three two-fragment modes.

For each two-fragment mode we have two channels depending on the sign of r_β. Figure-8 shows this explicitly for Case-2 above. However, we may superpose these channels to give symmetric or antisymmetric combinations. As discussed in Section-2.3, due to absence of parity mixing term in the Hamiltonian the above two combinations do not mix. Therefore, the symmetric and antisymmetric combinations can then be regarded as two channels and can be solved independently. To solve the problem completely we have to solve both symmetric and antisymmetric cases

5. We must keep in mind, however, that the general criterion for the definition of d is, that the effective potential should be small in comparison to the kinetic energy. If the kinetic energy turns out to be low then we must redefine d and choose new values of R^0_α.

independently and this could be inefficient. However, two methods of solving the problem can be used for program verification.

In subsequent sections we will consider the following three cases.

Case-I: Case-1, Antisymmetric Channel.

Case-II: Case-2, Antisymmetric Channel.

Case-III: Case-2, Two Channels in Each Mode.

Finally, we note that the program was checked for bugs as well as for accuracy by comparing the Monte Carlo calculations with the results of a finite difference relaxation scheme for a three-body system. We give the details in Appendix-4. Tables 12a and 12b summarize the results of these calculations.

5.2 Case-I: Case-1, Antisymmetric Channel

Here only the pair 1 and 3 can form a bound state. Now if the total energy, E, is negative the only possible mode is 2.[1] If, however, E is positive the disintegration channel (channel 4) is also a possibility.[2] But for the positive energies close to zero, we expect the likelihood of disintegration to be negligible. Therefore, we may be able to extend the analysis, based on the two-fragment assumption, into continuum without serious error. This aspect will be examined.

For low energy scattering we may disregard the internal structure of the composite fragment and make an approximation that the two fragments interact through an effective potential defined below. Let us

1. We have chosen the signs of $V_{i,j}$ purely for computational convenience. With the above choice, if the particle indices add to an even number, then the interaction is negative. Channels are named after the unbound particle (see Appendix-1).
2. However, we can always assume that the ingoing channel is two-fragment.

define the relative coordinate $r=x_1-x_3$ and the channel coordinate $R=x_2-(x_1+x_3)/2$. Let the eigenfunction for the bound fragment be $\eta(r)$. Then we define the effective potential as,

$$V(R)=\int[V(2,3)+V(2,1)]\,|\eta(r)|^2 dr. \qquad 5.2.1$$

To integrate the above we impose the condition, $x_1+x_2+x_3=0$, which is equivalent to choosing the reference frame in which the center of mass is at rest. Of course, R and r can be taken as the generalized coordinates. Fig-7 shows the effective potential for a sample case. This effective potential gives us an idea of the range of interaction between the fragments.

First we analyze the problem as an approximate two-body problem with interaction V(R). Then we simulate the three-body problem and compare the results. We choose the parameters as follows, [3]

$$a_0=2.0\text{fm},\ m=3.0m_p,\ \text{and}\ V_0=8.0\text{MeV}. \qquad 5.2.2.$$

Referring to Table-11, we confirm that there is only one two-body bound state, and note

$$e=-5.06995\text{MeV}\ \text{ and }\ d\approx 4.34\text{fm}.$$

---

3. We will, as mentioned above, generally restrict ourselves to the values of V_0 to give only one two-body bound state. However, we shall examine one case with two two-body bound states for the energy near the second level. For this we take $V_0=20$MeV with other parameters unchanged.

A. Two-Body Approximation

We further reduce the system to the problem of scattering of a particle by a potential. The mass of the fragments are m and $2m$; hence, the reduced mass is $2m/3$. Thus we consider the problem, similar to the problem in Chapter-4, of scattering of a particle of mass $\mu=2m/3$ by the potential $V(R)$. As in Chapter-4, we calculate the phase shift.

The nodes are set at $|R|=a$ and the system is simulated, inside the region $|R|\leq a$, by the Monte Carlo. Once again, as in Section-4.3, the trial function U_T is taken as,

$$U_T = sin(\frac{\pi R}{a}). \qquad 5.2.3$$

Clearly the energy we calculate is the channel kinetic energy E_k; and the total energy E, to be compared with the three-body Monte Carlo calculation, is given by $E=E_k+e$. The phase shift, for the kinetic energy E_k, is,

$$\delta_{ph}=\pi-ka \ ; \ where \ k=|\frac{2\mu E_k}{\hbar^2}|^{\frac{1}{2}}. \qquad 5.2.4$$

Table-13 gives the results of the present approximation for various values of the parameter a. With $N_U=105$, $N_0=100$ and $N_L=105$, all the runs were for 7000 iterations. For a particular case of $a=10.0$fm, the low energy case where the results are likely to be accurate, we have calculated with various integration steps. Here we extrapolate the results, by the linear least square fit, to the infinitesimal integration step. Within the two-body approximation, with the results of the last chapter and (Al84) in mind, the results are likely to be accurate. However, these results are to be compared with the three-body Monte Carlo. Therefore,

presently we defer the discussion of the results and describe the three-body Monte Carlo.

B. The Three-Body Monte Carlo

We have to choose an appropriate trial wave function. As already mentioned, only one two-fragment channel is possible. We have to force a node on the channel coordinate, R, and keep the boundary conditions along the other coordinate open. However, the internal eigenfunction $\eta(r)$ is negligible for large values of r. Hence we may introduce a cut-off along this coordinate. That is, we impose a node at $r=r_0$. We choose r_0=10.0fm and note that $\frac{\eta(10)}{\eta(0)}$=0.0046. Since $\eta(r)$ is an even function of r, the trial wave function must also be an even function of r. The trial function appropriate for the analysis of the phase shift is, [4]

$$U_T = sin(\frac{\pi R}{a})cos(\frac{\pi r}{r_0}). \qquad 5.2.5$$

The energy calculated here is the total energy E and the kinetic energy is given by, $E_k=E-e$. The phase shift can then be calculated using the equation 5.2.4. Table-14 lists the results of Monte Carlo calculations for various values of a. Once again we take N_U=105,N_0=100 and N_L=95 and the number of iterations is 7000.

As mentioned above we also analyze a case with two two-body bound states. Here we take V_0=20MeV with all other parameters unchanged. All

4. A better trial function would have been,

$$U_T=sin(\frac{\pi R}{a})\eta(r).$$

Then the wave function does not vanish at finite r which actually is the case. Therefore we have some systematic error, giving higher value for the energy.

of the above is valid for this case as well. In Table-16 we list the results.

Discussion

Table-13 gives the results of the two-body approximation for various values of a. For a=10.0fm the results with various integration steps are given. For a=7.0fm three simulations with different seeds are listed. Since the three-body Monte Carlo results are not going to be accurate for the disintegration channel and moreover the two-body approximation is likely to be inaccurate for large E, it is not useful to consider a lower than 6.0 fm.

Table-14 gives the results of the three-body Monte Carlo simulation. As the parameter a reduces it was found, as should be expected, that a smaller integration step was necessary. For three more cases with a = 4.5, 5.0, 5.5 fm and $\delta\tau$=0.0005 x10^{-23} Sec the instability was found and therefore we have not listed the results.[5] But examination of the table shows that the energy for the last two cases could very well be positive. For the positive energy there is possibility of disintegration. Though it may be reasonable to expect good results, if the probability for the disintegration is low, it is to be noted that dimensionality of the phase space is increased when we go from the two-fragment region to the three-fragment region. This may be the reason for the instability, though we cannot make a definitive conclusion without a closer examination near the transition region.

5. The instability can be detected, as described in Section-4.2, by observing the frequency of updating the ensemble. Moreover, since the ensemble has difficulty in reaching the equilibrium, the ensemble crosses only one of the bounds.

In Table-15 we have summarized the comparison between the two-body approximation and the three-body Monte Carlo calculation. In this table E_2 and δ_{ph2} refer to the two-body approximation and E_3 and δ_{ph3} refer to the three-body Monte Carlo.

First consider the behavior of the energy. We notice that for a given value of a, $E_2 > E_3$. This is to be expected. The two-body approximation is equivalent to assuming part of the wave function (e.g., two-body bound state eigenfunction η) and then find the best solution to the Schrodinger equation. As is well known, solving the Schrodinger equation is equivalent to a variational problem where the energy is minimized. Therefore, we will get lower energies for the simulation of the exact case as compared to the simulation of the two-body approximation. As we reduce a the inaccuracy of the two-body approximation increases which is to be expected. For a=10.0 fm we have extrapolated the results to $\delta\tau$=0 for both the methods. Here we have,

$$E_2 = -3.50774 \pm 0.00838 \text{MeV and } E_3 = -3.6614 \pm 0.02365 \text{MeV}.$$

As far as the energy is concerned, keeping in mind the error in the estimates, the results can be considered satisfactory.

Though, for a large a, two-body approximation gives reasonably good results for E, we are, however, interested in the calculation of the phase shift at a given energy rather than energy at given a. Therefore, we should determine a for a given energy. The two-body approximation will give larger a for given E. From the equation for the phase shift we conclude that the two-body approximation will give a lower phase shift. Next, we note, in contrast to the two-body scattering, what is important in the calculation of the phase shift is kinetic energy rather than the total

energy. Moreover, we find the phase shift as a difference from π rather than from zero. Therefore, we need a much more accurate estimate of E to calculate the phase shift. Thus, a small error in the total energy gives rise to a large error in the phase shift as can be seen from Table-15. For example,

$$at\ E \approx -3.50\ \text{MeV},\ \delta_{ph2} \approx -0.75\ radians \text{ and } \delta_{ph3} \approx -.54 radians\ .$$

Hence we conclude that, though the two-body approximation determines, for a large a, the value of energy for a given a reasonably well, the estimate of the phase shift at a given energy is not adequate.

Table-16 gives the results where we have two two-body bound states. As the energy approaches the bound state value we find that the algorithm becomes unstable. Though we have attempted to examine the results with smaller integration, it is of course possible that we should use a still smaller integration step. We, however, found that for the values of a less than 5fm it was difficult to get a reasonable sampling interval. Even for a=4.9 fm, which differs from 5 very slightly, we find the instability, while for a=5.0fm the convergence is clear. Since this raised some doubt about the run at a=5.0fm, another run, though only for 3000 iterations long, was made with a different seed for the random number generator. The result is satisfactory as can be seen from Table-16. Therefore, we conclude that the calculations probably do break down as the energy approaches the higher bound state from below.

5.3 Case-II: Case-2, Antisymmetric Channels

Here the particle 2 could form a two-body bound fragment either with particle 1 or 3. This does not, however, necessarily lead to two modess. We may consider two cases. Firstly, we have the situation where the particles 1 and 3 are identical. Now we cannot distinguish between the two modes and therefore we have only one mode. Next, we may consider the particles to be distinguishable. In this case we have two modes. On one hand, the first case may be analyzed directly to give the phase shift. We may, however, superpose the scattering states of the latter case to get the solution for the indistinguishable case. The extent of agreement between the two alternative ways of treating the case of identical particles will give some indication of the accuracy of the method.

Once again if the total energy is negative, the only possibility is the two-fragment channels. We may, however, find that $E<e$, from which we may conclude occurrence of the three-body bound state. We choose the parameters to be,

$$a_0=2.0\text{fm},\ m=2m_p \text{ and } V_0=10.0\text{MeV}. \qquad 5.3.1$$

With the above parameters there is only one two-body bound state with

$$e=-5.96385\text{MeV};\ \mu=4m_p/3. \qquad 5.3.2$$

If we define the range of interaction between the fragment on the basis of effective potential defined in Section-5.2, however, we would be making a mistake. The effective potential so defined is zero. If we examine the physical situation more carefully, we see that in reality the unbound particle will polarize the composite fragment. For example, the particle 1 in the vicinity of the fragment (2,3) will attract the particle 2 and repel the

particle 3.[1] Therefore, we define the range on the basis of Table-12, calculated on the basis of situation in Case-1, and for the above choice of parameters $d \approx 4.50$ fm.

C. Particles 1 and 3 Identical

First consider channel coordinates r_1 and r_3 as the generalized coordinates. The wave function must be symmetric in both the coordinates and must vanish on the boundary at $r_1=a$ and $r_3=a$. The trial function U_T must satisfy the above criterion and, in addition asymptotically be in appropriate channels. We choose U_T as,

$$U_T = \sin(\pi r_1/a)\sin(\pi r_3/a). \qquad 5.3.3$$

We see that the first two criteria are satisfied. To see the asymptotic behavior clearly we write U_T as a function of the generalized coordinates r_1 and r^1. Then we have,

$$U_T = \sin(\pi r_1/a)\sin(\pi r_1/2a)\cos(3\pi r^1/4a) \qquad 5.3.4$$

$$+\sin(\pi r_1/a)\cos(\pi r_1/2a)\sin(3\pi r^1/4a).$$

Channel-1 is characterized by large values of r_1 and small values of r^1. For such a situation we see that the trial function has characteristics similar to the characteristic of the wave function if the interaction between the fragments is zero. The phase shift is now given by,

$$\delta_{ph} = \pi - ka \qquad 5.3.5$$

---

1. The polarization is not possible for Case-1 and Case-3 since the particles of the two-body fragment are symmetric with respect to the unbound particle.

where

$$k = | \frac{2\mu E_k}{\hbar^2} |^{1/2}; \text{ and } E_k = E - e.$$

Table-17 gives the results. We defer the discussion of the results to a later time..

D. Particles 1 and 3 Distinguishable

As mentioned above, we have two possible channels. Instead of calculating S-matrix for a spectrum of energy it would be more interesting to calculate the S-matrix at a given energy and calculate the phase shift for the Case-C above by superposing the solutions for different channels, regarding these channels to be indistinguishable.

Next we need to find the expression for the phase shift in terms of the elements of S-matrix. First consider the one channel case. Here if the incoming wave function is given by ψ, then the scattering solution is,

$$\psi_{sct} = \psi - S_{1,1}\psi^* . \qquad 5.3.6$$

Then the relation between the phase shift, δ_{ph} and the S-matrix [2] is given by,

$$S_{1,1} = exp(2i\delta_{ph}). \qquad 5.3.7$$

We, however, have two channels if the particles are distinguishable. If the incoming wave function in Channel-1 is ψ_1 then the scattering solution is

$$\psi_{sct} = \psi_1 - S_{1,1}\psi_1^* - S_{2,1}\psi_2^* . \qquad 5.3.8$$

2. Here the matrix is one-dimensional.

But we cannot distinguish between the two channels and therefore we consider the superposition of ψ_2 and ψ_1. Then we can write,

$$\psi_{sct} = \psi - (S_{1,1} + S_{1,2})\psi^* \qquad 5.3.9$$

where,

$$\psi = \frac{1}{\sqrt{2}}(\psi_1 + \psi_2).$$

Now comparing with equation 5.3.7 we get,

$$S_{1,1} + S_{1,2} = exp\,(2i\,\delta_{ph}). \qquad 5.3.10$$

This has an obvious generalization to many channels which are indistinguishable if appropriate particles are considered identical.

Next we must choose the trial function such that it has nodes in both the channels. We will consider the incoming channel to be 1. Now we take the trial function as

$$U_T = sin\,(\pi r_1 / a)\,cos\,(\pi r_3 / 2b). \qquad 5.3.11$$

Here $R_3^0 = b$ and $R_1^1 = a$ and we have nodes at $r_1 = a$ and $r_3 = b$. The expression for $D_{2,1}$ relevant for this case is given by Eq-2.3.15. Though we must choose a and b less than d, we may vary both the parameters. Rewriting U_T above as a function of r_1 and r^1 we can see that it has desired properties in Channel-1.

At low energy we expect the error to be large compared to the kinetic energy. At energies above zero the approximation is likely to be inadequate. Therefore, we simulate for three different cases: one at low energy, one at high energy and one at medium energy. Table-18 gives the results of the calculation.

Discussion

As mentioned above Table-17 gives the results for the indistinguishable case, *i.e.*, the case C above. All the runs are for 7000 iterations. The parameters for ensemble size are, N_U=105, N_0=100, and N_L=95. As the parameters a and b are reduced it is necessary to reduce the integration step. A larger error in the estimate of the energy as a gets larger is due to the same size of the ensemble representing the wavefunction over larger space. Though the error in the estimation of energy does not vary by much, the error in the phase shift increases as the energy reduces. As repeated frequently, this is due to the fact that the error with respect to the kinetic energy gets larger.

Table-18 gives the results for the case with distinguishable channels. Evaluation of the expression for $D_{1,2}$, Eq.-2.3.15, needs the value of the energy. Hence it is convenient to evaluate $<\eta_\alpha>$ and $<V\eta_\alpha>$ for all α and calculate the D-matrix elements at the end using the average value of E. Another procedure is to calculate the part of D-matrix elements involving $<\eta_\alpha>$ and $<V\eta_\alpha>$ at each iteration. The latter method is less accurate. In estimating the error, however, it is difficult to determine the error in D-matrix from the error in $<\eta_\alpha>$ and $<V\eta_\alpha>$ since these estimates are correlated.[3] The error estimates are based on the calculation via the second method. We see that the errors are larger at a lower energy. A part of this is due to the higher relative error in the kinetic energy. But there is also some contribution due to the larger error in the estimates $<\eta>$ and $<V\eta>$. A close look at the derivation shows that off-diagonal D-matrix elements are based on the derivatives of the wave function at the

3. Two methods give the results within this error estimate. However, it is clear that the first method will give better estimates of D-matrix elements.

boundary between the interior and exterior regions. As the region gets larger the estimate of parameters at the boundary becomes less accurate. This is clearly shown by the error in the off-diagonal elements.

Instead of giving the S-matrix elements we have listed the phase shift, obtained by superposition, for the indistinguishable case. These phase shifts are to be compared with the ones given in Table-17. The fifth case from Table-17, E=−3.64872 MeV, and the third case from Table-18, E=−3.47844 Mev, are very close in energy and within the error estimates could be regarded as identical. The phase shifts for these two cases are marginally consistent with the error estimate. We, however, need much better statistics to make a final conclusion. Though we have to take into account the extrapolation to the infinitesimal time step, we note that the integration steps for above two cases are identical. The interior region, however, is different and extrapolation to $\delta\tau$=0 could be different.

5.4 Case-III: Case-2, Two Channels in Each Mode

Possible fragmentation modes are same as for Case-II. Similarly, as in Case-II, we can consider the particles 1 and 3 either to be identical or distinguishable. For the distiguishable case we have four channels which are depicted graphically in Figure-8. If the particles are identical we cannot distinguish between channels 1 ($\overline{1}$) and 3 ($\overline{3}$). As in Case-II, we can obtain the solution to the identical particle case by superposing the channels 1 ($\overline{1}$) and 3 ($\overline{3}$). This gives relation between the S-Matrix elements for these two cases. Once again the extent of agreement between the two alternative ways of treating the case of identical particles will give some indication of the accuracy of the method and verification of the algorithm.

Once again, if the total energy is negative, the only possibility is the two-fragment modes and, if $E<e$, we may conclude that a three-body bound state can be formed. We choose the parameters the same as in Case-II; i.e.,

$$a_0=2.0\text{fm},\ m=2m_p \text{ and } V_0=10.0\text{MeV}. \qquad 5.4.1$$

With the above parameters there is only one two-particle bound state with

$$e=-5.96385\text{MeV},\ \mu=4m_p/3 \text{ and } d\approx 4.53\text{fm}. \qquad 5.4.2$$

E. Particles 1 and 3 Identical

Here we have two channels designated by 1 and $\bar{1}$. The scattering solution is of the form,

$$\psi_1^1=exp(ir_1)-S_{1,1}exp(-ir_1) \ + \ r_1\rightarrow r_3 \qquad 5.4.3$$

and

$$\psi_{\bar{1}}^1=-S_{\bar{1},1}exp(-ir_1) \ + \ r_1\rightarrow r_3.$$

We set the nodes at $r_1=a$, $r_1=b$, $r_3=a$ and $r_3=b$. We take the trial wave function U_T to be,

$$U_T=sin[\frac{\pi(r_1-b)}{(a-b)}]sin[\frac{\pi(r_3-b)}{(a-b)}]. \qquad 5.4.4$$

The above nodes define the parameters R_α, for the interior region and we have,

$$R_1^1=a \text{ and } R_1^0=-b.$$

The off-diagonal element of the D-Matrix, $D_{\bar{1},1}$, is given by the Eq.-2.3.16. Therefore, two elements of the D-Matrix to be calculated are given by,

$$D_{1,1}=-\frac{1}{k}cotk(a-b), \qquad 5.4.5$$

and,

$$D_{\bar{1},1}=\frac{1}{ksink(a-b)}\frac{<(E-e-V_1)(r_1-a)\eta_1>}{<(E-e-V_1)(r_1-b)\eta_1>}.$$

Table-19 gives the results of the calculation. The number of iterations for all the cases is 7500 of which initial 500 were discarded. Once again we choose N_U=105, N_0=100 and N_L=100. The integration step is $0.0002\text{x}10^{-23}Sec$ for all the cases.

F. Particles 1 and 3 Distinguishable

As already mentioned we have four channels shown in Figure-8. Without loss of generality we take the incoming wave to be $exp(ir_1)$. The four channels are: back scattering,

$$\psi_1^1=exp(ikr_1-S_{1,1}exp(-ikr_1), \qquad 5.4.6$$

transmission,

$$\psi_{\bar{1}}^1=-S_{\bar{1},1}exp(ir_1) \qquad 5.4.7$$

rearrangement back scattering,

$$\psi_3^1=-S_{3,1}exp(-ir_3) \qquad 5.4.8$$

and rearrangement transmission,

$$\psi_{\bar{3}}^1=-S_{\bar{3},1}exp(ir_3). \qquad 5.4.9$$

As mentioned above we can obtain the results for the identical particles case by superposition. This gives the following two identities,

$$(S_{1,1})_{idnt.}=(S_{1,1}+S_{3,1})_{dist.} \qquad 5.4.10$$

$$(S_{\bar{1},1})_{idnt.}=(S_{\bar{1},1}+S_{\bar{3},1})_{dist.} \qquad 5.4.11$$

where the subscripts *idnt.* and *dist.* refer to Case-E and Case-F, respectively.

We set the nodes, at $r_1=a$, $r_1=b$, $r_3=b$ and $r_3=-b$, defining the interior region. The trial wave function is taken to be,

$$U_T=sin[\frac{\pi(r_1-b)}{(a-b)}]sin[\frac{\pi(r_3-b)}{2b}]. \qquad 5.4.12$$

The nodes define the parameters R_β as, $R_1^1=a$, $R_1^0=-b$, $R_{\bar{1}}^0=b$, $R_3^0=-b$ and $R_{\bar{3}}^0=b$. From this we obtain the D-Matrix elements using the exression 2.3.16 as,

$$D_{1,1}=-\frac{1}{k}cotk(a-b), \qquad 5.4.13$$

and,

$$D_{\bar{1},1}=\frac{1}{k\sin k(a-b)}\frac{<(E-e-V_1)(r_1-a)\eta_1>}{<(E-e-V_1)(r_1-b)\eta_1>}.$$

$$D_{3,1}=D_{\bar{3},1}=\frac{1}{k\sin k(a-b)}\frac{(a-b)}{2b}\frac{<(E-e-V_3)(r_3-b)\eta_3>}{<(E-e-V_1)(r_1-b)\eta_1>}.$$

Table-20 gives the results of computation for one case. The nodes for this case are chosen such that the value of the energy is in the range covered by the indistinguishable particle case so that we can examine the identities 5.4.10 and 5.4.11 by interpolation if necessary. The integration step

is $0.0002 \times 10^{-23} sec$. The ensemble size parameters are N_U=105, N_0=100 and N_L=95. 14000 iterations were carried out, of which the initial 500 were discarded.

Discussion

Table-19 gives the results for Case-E above. We note that the estimates for the energy are close to the internal energy for the two-body bound state. Thus the kinetic energy is low and the error estimates for the energy are significant. We also note that the lower the energy the higher the error in the estimate. The error in the real imaginary parts of the scattering amplitudes is also quite large. The errors for the last case in Table-19 are quite large and therefore the results may be completely disregarded.

Table-20 gives the results for Case-F where particles are considered distinguishable. Once again the errors are large. The value of the energy for this case is very close to the energy for the second case in Table-19. In fact, considering the magnitude of the error, we may regard the energy to be identical and compare the identities 5.4.10 and 5.4.11. Below we give the various terms of these identities.

$$(S_{1,1}+S_{3,1)_{dist}} = -0.24187 - i\,0.11920 \qquad 5.4.10a$$

$$(S_{2,1}+S_{4,1)_{dist}} = 0.42568 - i\,0.86376 \qquad 5.4.11a$$

$$(S_{1,1)_{idnt}} = -(0.17553 \pm 0663) - i(0.11457 \pm 0.0493) \qquad 5.4.10b$$

$$(S_{2,1)_{idnt}} = (0.53445 \pm 0.0865) - i(0.81880 \pm 0.0964) \qquad 5.4.11b$$

The sources of error are numerous. Firstly, we have considered that the second case in Table-19 and the case in Table-20 are at the same energy. This may not be the case considering the error in the estimates of the energy. The quantities in 5.4.10a and 5.4.11a are sums of two quantities with considerable error. These two quantities, however, are not independent and estimate of the error in the sum is difficult and therefore we have not quoted any error. But the error, however, is at least of the order of error in one of the quantities summed. The magnitude of this error is of the order of the error for the quantities in 5.4.10b and 5.4.11b. With all these errors in mind we may regard that the identities 5.4.10 and 5.4.11 are satisfied. For a definite conclusion, however, considerable amount of computation will be necessary. The identities 5.4.10 and 5.4.11 should be valid in principle and any discripancy will be a comment on the computer program [1] and the accuracy of the Monte Carlo results.

Contrasting the values of energy for the cases in Section-4.3 with the cases in Section-4.4 we notice that we have low energies for the latter. Here, the way we get information about the antisymmetric channel is by by distorting the symmetric channel slightly. Another way would be to distort the node structure of the antisymmetric channel, keeping the three nodes to get the information about the symmetric channel. For a completely antisymmetric case we know the location of the nodes. However, the relative location of three nodes for a distorted case is not known

1. We could assume that these two cases are at an identical energy. Then we could consider the two results as independent and average the quantities in 5.4.10a-b, and, 5.4.11a-b and compare these quantities with the average. Then we can consider the results as more satisfactory. In a computer work, however, one has a tendency to stop when the results are satisfactory and one must guard against such a tendency.

a priori. But, if we could solve the problem of location of nodes elegantly, then we could treat the situations with higher energy by distorting the antisymmetric case. This would be useful in calculating the scattering matrix at higher energy. If the middle node falls outside the range of interaction, then we need to consider the region between the two nodes covering the interaction (which amounts to the distorted symmetric case) since in the other region we can consider the fragments as free.

6. Summary and Conclusions

Our main purpose was to calculate the scattering matrix for a many-body system, restricted to two-fragment channels, by Monte Carlo simulation. We use the Path Integral Monte Carlo (PIMC) or the Diffusion Monte Carlo. We have confined the investigation to a three-body system, with a two-body interaction, in one dimension. The interaction between a pair is either a square well or a square barrier. The parameters of the square well have been chosen, except for one case, such that there is only one two-body bound state. Depending on the nature of the interactions, one, two, or all three pairs of particles can form a two-body bound state, thus giving three different cases.

In each of the disintegration modes we have two channels corresponding to the unbound particle on the left and on the right of the bound fragment. These two channels can be superposed to get a symmetric and an antisymmetric wave function. The symmetric and antisymmetric wave functions can be construed as an alternative definition of channels. However, the decomposition into symmetric and antisymmetric channels are indepedent if the Hamiltonian does not have a parity mixing term. The complete problem can now be solved by simulating the symmetric and the antisymmetric channels separately. Here the nodes are symmetric about r_α=0. We can, however, solve the complete problem in one simulation by choosing the asymmetric node structure. Though the first method is inefficient in comparison to the latter method, we have two ways of solving the same problem by Monte Carlo.

This can be used as the program verification tool. We have not done this in this work, however, but we have used another method of verification to be discussed later.

If only one pair of particles can form a two-body bound state we have only one two-fragment mode. In this case we have studied the problem in two different ways: 1) Two-body Monte Carlo approximation, where the composite and a free particle are considered to interact through an effective potential and 2) Three-body Monte Carlo. Here we have restricted ourselves to the antisymmetric channel. The two-body approximation, as to be expected, is in good agreement with the three-body Monte Carlo at low energies. Though the value of the energy calculated with the same boundary condition, that is, the node at a point along the channel coordinate, is in good agreement, the phase shift does not agree as well. This is not paradoxical if we remember that we should compare the error with the kinetic energy. We also investigated the situation with total positive energy, which corresponds to the opening of the disintegration channel (i.e., the three-fragment channel). If the energy is low we should expect the small amplitudes for scattering into the disintegration channel. Here, it seems plausible that we should be able to disregard the three-fragment channel. We, however, find that the Monte Carlo calculations do not give good results and, if the simulation can be continued into the continuum at all, it is in a narrow region. We have also analyzed the case with two two-body bound states. The aim was to find how well the calculations proceed as the energy reaches the value near the second bound state. Once again we find that, if we go near the second energy level, the calculations break down. Though the evidence is not overwhelming, it seems that possibility of another energy level as well as

the continuum of energy level is detrimental to the calculation if the energy is larger than these levels.

Next we choose the interaction such that the two pairs of particles can form a two-body bound state. Once again we restrict ourselves to the antisymmetric channel. We may, however, choose the distinguishability of the particles. Thus, if the particles are considered distinguishable, we have the possibility of two channels. However, if the particles are identical (we confine ourselves to the bosons) then we have one channel. We can, however, obtain the solution to the indistinguishable cases by superposing the solutions to the distinguishable cases. Thus we can simulate the one-channel case in two different ways. We may choose the trial function symmetrical in all the channels and treat the problem as one-channel case, or we may treat it as a multichannel case and superpose the solutions to construct the one-channel case. We have calculated the phase shift for the one-channel case in these two different ways. Though the accuracy of the calculation needs to be improved with better statistics and extrapolation to the infinitesimal integration step, the results are satisfactory within the error. However, the principle is clearly true and provides a good check within the Monte Carlo calculations. This is quite desirable when the problems cannot be treated otherwise. Even for the distinguishable particles this check can be used as another program verification tool.

Next we solve the above problem in full by choosing an antisymmetric node structure. Now if the particles are distinguishable, we have four channels. If the particles are identical, however, we have two channels. As before we can solve the identical particle case in the two ways mentioned above. This gives us the relation between the S-matrix

elements for distinguishable and nondistinguishable cases. We have simulated these two cases and compared the results. Though the statistical error remains to be improved for a definite conclusion, the results are consistent with the error estimates.

Besides the above we have also given (in Appendix-3) a sampling method and studied the effects of various artificial parameters in the algorithm. This is of general interest in solutions of diffusion equations via the Monte Carlo technique. The sampling interval obviously reflects the correlation between consecutive values of the energy, which constitute a time series, during iteration. Since during relaxation the system tends to the ground state, there is a stronger correlation. Therefore, we get a larger sampling interval if we do not exclude the part of the series during relaxation. Moreover, once beyond the relaxation point we have better precision in determining the sampling interval. Hence we can use the behavior of the sampling interval in conjunction with the drift in the ensemble size to detect the equilibration point. The methods given here could be of use in analysis of metastable systems.

As the ensemble drifts it is necessary to restore it to a nominal value. There is an optimum value of allowable drift. For the example we studied this was about 5%. Once established, this has been used throughout. Monitoring the restoration process is useful in detection of the equilibration point as well as the stability with regard to the integration step. Since the initial ensemble is approximate, the drift is large and the restoration frequency is large. Besides, at the beginning the ensemble drifts to only one of the bound since the distribution of the ensemble is skewed. These two characteristics and the behavior of the sampling interval are useful in the detection of the equilibration point.

A smaller integration step obviously gives a large sampling interval. A large sampling interval, however, is not always due to a small integration step. If the integration step is large then the configurations with high local energy are readily destroyed, which reduces the fluctuation in the energy. This, though, gives rise to a large sampling interval, and, however is accompanied by a large drift of the ensemble size, indicated by frequent restoration. Another observable is that the drift is skewed to one of the bounds, usually the lower bound. Thus the sampling interval and the drift of ensemble size are useful in determining the adequacy of the integration step.

Ideal reference energy is the exact energy for the system. Since we do not know the exact energy, we have to use the value based on the simulation itself which needs to be updated at certain intervals. The interval at which we update the reference energy has a definite effect, at least for the example we considered, on the correlation exemplified by the maxima in the sampling interval, the significance of which is not clear. The example we studied does not indicate any instability and the region of the small sampling interval seems adequate and reduces the estimate of the standard error. A large sampling interval sometimes indicated a change in frequency of the update of reference energy. However this was not useful in fixing the parameters in the subsequent cases.

Further study of multichannel scattering may be along the following lines. We have here used the exact eigenfunction for the two-body bound state. For practically interesting cases, however, we will not have this information. Therefore, it would be of interest to investigate the sensitivity of the results to small changes in the two-body eigenfunction. Study of a realistic model would also be of interest. The case of the

Fermion remains to be solved. The fixed node treatment used in calculation of bound state energy, however, is likely to be inaccurate since in scattering calculations the wave function is of importance, while in calculation of bound state energy the exact wave function is not as important. The real problem is to get away from the fixed node treatment. One way to accomplish this is to estimate the "pressure" in each of the regions between the nodes and to determine how they should move. This is possibly an ideal problem for the concurrent processors where each of the regions is analyzed by different processors for some time and the nodes are moved after a large number of iterations. The geometry for more than three particles, however, complicates the matter.

The sampling method we have used is based on an empirical study. One may abstract a mathematical problem from this: Given a finite series of numbers, which is stationary albeit with some correlation, we want to sample this series at a given interval such that the sampled series is the best representative of random number sequence. A theorem giving the estimates of the error will be of use in science and engineering and possibly in economics.

Appendix 1. Three-Body Problem: Notation

The description below is for the one-dimensional case. The extension to three dimensions is straight-forward.

The Hamiltonian.

The Hamiltonian, in each of the channel α, may be written as,

$$H = H_0 + V_\alpha + V^\alpha \qquad \text{A1.1}$$

where H_0 is kinetic energy, V_α is the interaction potential between the fragments and V^α is the internal potential responsible for the binding energy of the fragments.

Convention for numbering the channels.

Fragmentation Mode	Channel Number
0 Three particles dissociated:	0
1 Two fragments;2 and 3 bound:	1 $\overline{1}$
2 Two fragments;1 and 3 bound:	2 $\overline{2}$
3 Two fragments;2 and 1 bound:	3 $\overline{3}$
4 Three particles bound state:	4

A general treatment of the scattering requires that the configurations of positive and negative values of r_α be considered as separate channels. If such is the case we will designate the channel with negative values of r_α by $\overline{\alpha}$. It is also convinient to define $r_{\overline{\alpha}} = -r_\alpha$. Now we give expressions for

some of the parameters for Channel-1. The parameters for Channels-2 and 3 can be obtained by cyclic exchange among indices 1, 2 and 3.

The channel potential V^1 and internal potential V_1 are given by,

$$V_1=V_{1,2}+V_{1,3};\quad V^1=V_{2,3}. \tag{A1.2}$$

Channel coordinate r_1 and corresponding internal coordinate r^1 are given by,

$$r_1=x_1-(m_2x_2+m_3x_3)/(m_2+m_3) \tag{A1.3}$$

$$r^1=x_2-x_3$$

$$\mu_1=(m_1)(m_2+m_3)/(m_1+m_2+m_3). \tag{A1.4}$$

If $m_1=m_2=m_3=m$ the above expressions reduce to,

$$r_1=x_1-(x_2+x_3)/2 \tag{A1.5}$$

and,

$$\mu_1=2m/3. \tag{A1.6}$$

The motion of the center of mass may be excluded with the condition,

$$x_1+x_2+x_3=0. \tag{A1.7}$$

Since we can take r_1 and r^1 as generalized coordinates, it is useful to express the similar coordinates in other channels in terms of r_1 and r^1.

$$r_2=-\frac{1}{2}(r^1+2r_1);\ r^2=-\frac{1}{4}(2r_1-3r^1) \tag{A1.8}$$

$$r_3=-\frac{1}{2}(r^1-2r_1);\ r^3=-\frac{1}{4}(2r_1+3r^1).$$

A useful transformation

Due to condition A1.7 we need two independent coordinates to describe the system. In Appendix-4 we check the Monte Carlo algorithm by comparing with a calculation by a relaxation technique. There, due to the simplicity of the geometry, it is convenient to use the channel coordinate $r_1=X$ and $r_2=Y$ as the independent coordinates. Figure-6 shows the region $r_i \leq a$ in the X-Y coordinate sytem. For the case $m_1=m_2=m_3=m$ we have the coordinates of the particles given by,

$$x_1=\frac{2X}{3},\ x_2=\frac{2Y}{3} \text{and } x_3=-2(X+Y)/3. \qquad \text{A1.9}$$

Then with the two-body potential $V_{i,j}=V(|x_i-x_j|)$ the Hamiltonian transforms to,

$$H= -\frac{\hbar^2}{2}\frac{3}{2m}\left[\frac{\partial^2}{\partial X^2}+\frac{\partial^2}{\partial Y^2}-\frac{\partial^2}{\partial X \partial Y}\right]$$

$$+ V(|2(X-Y)/3|) + V(|4X/3+2Y/3|) + V(|2X/3+4Y/3|). \qquad \text{A1.10}$$

Appendix-2. Random Number Generators

Here we list the random number generators used in the simulation. 16807, 2147483647 and 2147483648 are machine dependent numbers. The computer we used was VAX with 32 bit words. The choice of the above constants is to give maximum cycle for the random number generator (Ha65).

Uniformly Distributed Random Numbers

```
REAL*8 FUNCTION RANDM(dseed)
DOUBLE PRECISION dseed,d2p31p,d2p31
DATA d2p31m,d2p31/2147483647.D0,2147483711.D0/

dseed = DMOD(16807.D0*dseed,d2p31m)
RANDM = dseed/d2p31
END
```

Gaussian Distributed Random Numbers

```
REAL*8 FUNCTION RANDG(dseed)
IMPLICIT REAL*8 (A-H,O-Z)
```

```
      DATA
     sqrt2,d2p31m,d2pn31/1.414214D0,2147483647.D0,2147483648.D0/
      DATA a1,a2,a3/-.5751703D0,-1.896513D0,-.5496261D-1/
      DATA b0,b1,b2,b3/-.113773D0,-3.293474D0,-2.374996D0,-1.187515D0/
      DATA c0,c1,c2,c3/-.1146666D0,-.1314774D0,-.2368201D0,.5073975D-1/
      DATA d0,d1,d2/-44.27977D0,21.98546D0,-7.586103D0/
      DATA e0,e1,e2,e3/-.5668422D-1,.3937021D0,-.3166501D0,.6208963D-1/
      DATA f0,f1,f2/-6.266786D0,4.666263D0,-2.962883D0/
      DATA g0,g1,g2,g3/.1851159D-3,-.2028152D-2,-.1498384D0,.1078639D-1/
      DATA h0,h1,h2/.9952975D-1,.5211733D0,-.6888301D-1/

  100 CONTINUE
      dseed = DMOD(16807.D0*dseed,d2p31m)
      RANDG = dseed/d2pn31
      x = 1.0D0 - 2*RANDG
      IF( .NOT.(x.GT.-1.D0 .AND. x.LT.1.D0)) GO TO 100

      sigma = DSIGN (1.D0,x)
      z = DABS(x)
      IF( z.LE. 0.85D0)GO TO 400

      a = 1.D0 - z
```

```
      b = z
      w = DSQRT(-DLOG(a + a*b))
      IF( w.LT.2.5D0)GO TO 300

      IF( w.LT.4.0D0)GO TO 200

      wi = 1.0D0/w
      sn = (( g3*wi+g2)*wi+g1)*wi
      sd = (( wi+ h2)*wi + h1)*wi +h0
      f  = w + w*(g0 + sn/sd)
      GO TO 500

200   CONTINUE
      sn = ((e3*w + e2)*w + e1)*w
      sd = (( w+ f2)*w + f1)*w + f0
      f  = w + w*(e0 + sn/sd)
      GO TO 500

300   CONTINUE
      sn = ((c3*w + c2)*w + c1)*w
      sn = (( w + d2)*w + d1)*w + d0
      f  = w + w*(c0 + sn/sd)
```

```
      GO TO 500

400   CONTINUE
      z2 = z*z
      f  = z + z*(b0 + a1*z2/(b1+z2+a2/(b2+z2+a3/(b3+z2))))

500   CONTINUE
      y = sigma*f
      RANDG = SQRT2*y

      END
```

Appendix-3. The Sampling Method and Detection of Equilibration Point

The Sampling Method

We have a time series of expectation values of energy and we wish to sample this series at an interval such that we get a random series, i.e., an uncorrelated series. This sampling interval can be defined to be the correlation length. One way to find the sampling interval is to compare the sample against a sample of pseudo random numbers, generated on the computer, of the same size and distribution. Therefore, we want to know the distribution of the energy values. We expect the distribution to be the Gaussian about the mean.[1] This is borne out by the statistical tests of many series of energy and we illustrate one such example in Table-1. The energy series is for the example to be described in Section-4.3

Next we consider a method of comparison between the samples from the time series and the samples of Gaussian distributed random numbers, which will be referred to as the random number samples in here. For this purpose we define a Fourier integral, $F(\omega)$, and a correlation coefficient, $C_{N,n}$, for a finite series of length N. Let E_i be the value of the energy at time τ_i with an average $\overline{E}$. Let $e_i = E_i - \overline{E}$. Then we define a Fourier integral for this as,

$$F(\omega) = \sum_{i=1}^{N-1} \int d\tau (a_i + b_i \tau) exp\,(-i\omega\tau) \qquad \text{A3.1}$$

1. The reason for this is that the energy is mean over large number of configurations.

where,

$$a_i = \frac{e_i\tau_{i+1} - e_{i+1}\tau_i}{\tau_{i+1}-\tau_i} \; ; \; b_i = \frac{e_{i+1}-e_i}{\tau_{i+1}-\tau_i}.$$

The power spectrum of the series is defined as,

$$P(\omega) = |F(\omega)|^2. \qquad \text{A3.2}$$

The correlation coefficient , $C_{N,n}$, is calculated by shifting the series by n units and calculating the correlation between the overlapping $N-n$ points. That is, we define $C_{N,n}$ as,

$$C_{N,n} = \frac{\sum_{i=1}^{N-n} e_i e_{i+n}}{[\sum_{i=n}^{N} |e_i|^2]^{1/2}[\sum_{i=1}^{N-n} |e_i|^2]^{1/2}}. \qquad \text{A3.3}$$

Figure-1 shows the power spectrum and the correlation coefficient, $C_{N,n}$, for a random sample of size 200. Here we remark:

a. The time scale is normalized such that τ_N=1.0.

b. We observe that the power spectrum has significant value to about a frequency of 100, which is half the frequency of the sample points.

c. We can assert that the tail of the correlation coefficient curve is equivalent to the one we will obtain from a smaller sample except for n =0. For n=0, $C_{N,n}$=1.0.

d. As the sample size reduces $C_{N,n}$ becomes significant and varies violently.

From Fig-2 we see that the direct use of the above quantities is difficult due to fluctuations, which are particularly large for small sample size. Secondly, it is not a particular sequence of random number we

should be comparing but rather an average property of such samples. What we need is a measure which is averaged over many random samples. Below we define such a measure.

We consider a random sample of size N , and calculate $C_{N,n}$, as defined by Eq.-4.2.4 by shifting the sample by n. As defined above, $C_{N,n}$ is calculated on the basis of only the overlapping part of the sample. Now we define,

$$Q_{N,m} = \sum_{n=1}^{m} C_{N,n}^2. \qquad \text{A3.4}$$

We find the value $m=m_1$ where the value of $Q_{N,m}$ = 1, interpolating if necessary. [2] Next we wish to average m_1 over an adequate number of samples to get an estimate of $\overline{m}_1$. For this purpose we generated 20,000 Gaussian distributed random numbers and constructed as many samples of a particular size as possible by taking consecutive random numbers, with no intersection between any two samples. For example, for size 50, sample one has 1 through 50 numbers, sample two 51 through 100 numbers..... etc, which give 400 samples. In Table-2 we give the values m_1 for all the samples of size 50.[3] Table-3 summarizes the results for the sizes 50 through 1000 at an interval of 50. From Table-3 we see that the relative standard error depends on N times S, which is approximately 20,000.

Table-3 suggests a linear fit with or without a constant term,

$$\overline{m}_1 = a + bN \qquad \text{A3.5}$$

2. If $Q_{N,m}$ is chosen larger than 1 then $m_1$will be undefined for some samples.
3. We here note that m_1 has Gaussian distribution based on a test detailed in Table-7.

gives,

$$a = 0.5820 \quad \text{and} \quad b = 0.6193,$$

while,

$$\overline{m}_1 = bN; \textit{ gives } \quad b = 0.6220. \qquad \text{A3.6}$$

If we compare the above in light of the standard error it is quite appropriate to assume that the linear relation $\overline{m}_1 = bN$ is adequate.[4]

We find the sampling interval as follows. We guess an approximate sampling interval by observing the correlation coefficient for the time series or we may arbitrarily start with N_S=64. If the sampling interval is inadequate, this will be clear from the fact that the $Q_{N,m}$ quickly approaches unity. Obviously it is not adequate to consider only one sample. However, by changing the starting point for the sampling, we get N_S different samples and average the value of m_1 over these samples. For uncorrelated samples we expect the value of $\overline{m}_1$ between 0.60N an 0.66N if the standard error is about 0.01N, which we expect. It is clear that too large a sampling interval will satisfy the criterion. However, we wish to determine the least value of the sampling interval that will satisfy the criterion. This can be done by a binary search starting from N_S= 128 or 64. Computationally, however, it is efficient to start from a larger value and go down than start from the smaller value and move upwards. Once we approach a candidate for the sampling interval, we check in the

4. In the continuum limit, i.e., $N \to T$ and $n \to t$, if we consider a continuous stationary Gaussian random process of length T, then the correlation, C(T,t) with a shift of t, defined analogous to $C_{N,n}$, is (Pa65),

$$|C(T,t)|^2 = \frac{1}{(T-t)} \text{ and } \overline{m}_1 \approx 0.63235N.$$

neighborhood. If the candidate is right, then below we will see $\overline{m}_1/N$ decreasing and above we find $\overline{m}_1/N$ constant. However, there will be fluctuations and we have to consider this as average behavior. We defer further discussion to Section-4.4 where we illustrate the method through an example.

Detection of the Equilibration Point

Since the initial ensemble is a representative of an approximate wave function, we have to wait for the system to relax before we begin sampling. Hence we need a procedure to find when the system approaches the equilibrium, that is a stationary stochastic process, albeit with some correlation. The time, or iteration number N_R, at which the system has relaxed to the ground state, of course, with some fluctuations, we refer to as the equilibration point. One way to do this is to determine the characteristic time of the the system and thereby guess at the relaxation time. That is, we say that the relaxation time is some multiple of the characteristic time and discard the iteration during this time. Besides the uncertainities involved in such a procedure, it may be that the system has many characteristic times. To estimate the relaxation time one has to evaluate the relative importance of various time scales. Though this may be simple in some cases, it may not be so in general. Some systems may have metastable regions which may give rise to further complications. Therefore, it may be worthwhile to find a method of detecting the relaxation time within the Monte Carlo simulation. Below we describe such a method.

As the iterations proceed, the size of the ensemble N_e drifts due to replication or deletion of the configurations. As discussed in Section-2.1,

if the local energy is larger than the reference energy E_T, then there is a chance that the configuration will be destroyed. If the local energy is smaller than the reference energy; however, new replicas of the configuration are created. This, of course, changes the reference energy for the later iterations and also gives rise to the drift of the ensemble size. In the beginning when the ensemble is representative of the approximate wave function, this drift will be large. If the system is relaxed, however, the reference energy will fluctuate about the ground state energy. Also the probabilities for replication and deletion will become equal. Therefore, the ensemble size will stabilize and the rate of drift will reduce. Therefore, while the ensemble reaches the bounds frequently during relaxation, this frequency will reduce considerably after the relaxation has occurred. Another difference is that, while during relaxation the ensemble will repeatedly reach one of the bounds, for the relaxed system the ensemble will hit both upper (N_U) and lower (N_L) bounds on its size. If we observe the nature of the drift of the ensemble, which can be accomplished by monitoring the frequency of the update and type of bounds crossed, we can get a fair judgement about the relaxation time. Further, with some experience, this monitoring helps to judge the adequacy of the integration step $\delta\tau$ with regard to the stability of the algorithm, since the larger the $\delta\tau$ the faster is the drift.

All the above statements are true only in a statistical sense. Hence although the above procedure is reasonably accurate, there are times when ambiguities are present. There is a chance that the ensemble will hit the same bound repeatedly even after relaxation. Sometimes the update may create new members where they will be readily destroyed. This gives rise to some variation of the frequency of updates.

Nevertheless, we can guess that at certain points the stationary state may have been reached. This can be further verified as described below.

During relaxation there is a stronger correlation between one iteration to another since both of them try to drive the system toward the stationary state; some fluctuations, however, will persist. Now if we were to determine the sampling interval including relaxation time, then the sampling interval will be larger compared to the sampling interval based on the iterations after relaxation. Once the system has reached the stationary point, however, the sampling interval, determined by the method of Section-4.2, will approach a relatively constant value. We can use this in conjunction with the nature and the rate of drift of the ensemble size to judge whether the system has relaxed.

Although we will not have an opportunity for its use, we make a brief remark on the possibility of treating the system with a metastable state. The metastable state is characterized by a very slow drift towards the stable state. The drift could be assumed linear. [5] In the case of a stable state we consider the deviations from the mean. Now we consider the deviations from the assumed linear relation. The correlation will be least when the assumed slope is adequate. Consequently, the sampling interval will be minimum. This requires good precision, and therefore a long run time, in determining the sampling interval.

5. This assumption is not essential and further generalization is straight forward.

Appendix 4. A Test of the Algorithm

Here we use the X-Y coordinate system defined in Appendix-1. To test the alogorithm for the three-particle case we consider the problem below. We consider a system of three identical particles(bosons) in one dimension with two-body interaction potential which we take to be square-wells of depth V_0 and width s. We choose the parameters to be,

$$m=m_p \;;\; V_0=8.0MeV \text{ and } a_0=1.0\text{fm}. \qquad \text{A4.1}$$

We choose the boundaries of the system to be $R_a=a=5.0$. At the boundary the wave function is forced to vanish. We wish to find the lowest energy state with the above conditions.

The Monte Carlo Solution

This problem can readily be solved by the Monte Carlo algorithm used in this work. We choose the trial wave function to be,

$$U_T=\cos(\pi X/2a)\cos(\pi Y/2a)\cos(\pi(X+Y)/2a). \qquad \text{A4.2}$$

We choose a = 5 fm. The Monte Carlo results for various integration steps are given in Table-12b

The Relaxation Solution

We divide the region in a grid of size $\Delta x = \Delta y = 10.0/N_x$. Consider a grid point at i along the X-axis and j along the Y-axis. Let $U_{i,j}(\tau)$ be the value of the wave function at the grid point (i,j) at time τ. A wave function W evolves, regarding the time as imaginary, as,

$$\frac{\partial U}{\partial \tau} = -HU \qquad \text{A4.4}$$

where the Hamiltonian H, is given by equation A1.9. As usual we can incorporate an energy shift E_T through the transformation

$$U \rightarrow exp(-\tau E_T)U. \qquad \text{A4.5}$$

Then the equation for U is,

$$\frac{\partial U}{\partial \tau} = -(H - E_T)U. \qquad \text{A4.6}$$

Integrating the equation-A4.6 by finite difference, with an integration step $\delta\tau$, we get,

$$U(\tau+\delta\tau) \approx (1-(H - E_T)\delta\tau)U(\tau). \qquad \text{A4.7}$$

Using equation A4.7 we can integrate the wave function to give the ground state. We need to define the differential operator in the Hamiltonian as a finite difference operator. The operator corresponding to five-point operator ∇_5 (Da74) we define as,

$$\frac{\partial U_{i,j}}{\partial X^2} = \frac{U_{i+1,j} + U_{i-1,j} - 2U_{i,j}}{\Delta X^2} \qquad \text{A4.8}$$

$$\frac{\partial U_{i,j}}{\partial Y^2} = \frac{U_{i,j+1} + U_{i,j-1} - 2U_{i,j}}{\Delta Y^2}$$

$$\frac{\partial U_{i,j}}{\partial x\,\partial y} = \frac{U_{i+1,j+1} + U_{i-1,j-1} - U_{i+1,j-1} - U_{i-1,j+1}}{4\Delta X \Delta Y}.$$

Here we make the following remarks on the relaxation calculation.

a. We initialize $U_{i,j}$ with U_T given by equation A4.2.

b. For E_T we use the expectation value of the Hamiltonian with current values of the $U_{i,j}$, given by,

$$E_T = \frac{\sum_{i,j} U_{i,j} H_{i,j} U_{i,j}}{\sum_{i,j} | U_{i,j}^2 |}. \qquad \text{A4.9}$$

This will give the value of the energy at the end of the calculation once the ground state is reached.

c. After relaxing the relaxation we renormalize the values of $U_{i,j}$. If this is not done the values of $U_{i,j}$ can drift to low values since E_T is different than the ground state energy.

d. For a given value of ΔX the value of $\delta\tau$ is not arbitrary. The value of $\delta\tau$ must be lower than the critical value and above this the relaxation procedure is not stable. Moreover there is an optimum value of $\delta\tau$ for which the relaxation procedure is fastest. We find this optimum value for a coarse size and then scale this for use for a finer grid by

$$\delta\tau_2 = \delta\tau_1 [\Delta X_1 / \Delta X_2]^2. \qquad \text{A4.10}$$

e. Table-12a gives the results for various grid sizes. We extrapolate to $\delta\tau$=0 through a linear least-square fit.

The Results:

Finite Difference Relaxation:

1. Linear Extrapolation: E = -3.11312 MeV

2. Quadratic Extrapolation: E = -3.09789 MeV

Path Integral Monte Carlo: E = -3.06766 MeV ±0.033

Referring to Table-11 two-body binding energy is: e = -1.23553 MeV. Since E is less than e there is a three-particle bound state.

References

[Ab80] F. F. Abraham, J. Chem. Phys. 72, 359 (1980)

[Al84] Y. Alhassid and S. E. Koonin, Annals of Physics 155, 108 (1984)

[An75] J. B. Anderson, J. Chem. Phys. 63, 1499 (1975)

[An76] J. B. Anderson, J. Chem. Phys. 65, 4121 (1975)

[An80] J. B. Anderson, J. Chem. Phys. 73, 3897 (1980)

[An81] J. B. Anderson, J. Chem. Phys. 74, 6307 (1981)

[Ba66] H. T. Balch, J. C. Dale, T. W. Eddy and R. M. Lauver, The Bell System Technical Journal, XLV No.5, 733 (1966)

[Be69] P. R. Bevington, *Data Reduction and Error Analysis for the Physical Sciences* (McGraw Hill, New York, 1969)

[Bi79] K. Binder, Ed., *Monte Carlo Methods in Statistical Physics* (Springer-Verlag, Berlin, 1979)

[Bi84] K. Binder, Ed., *Applications of the Monte Carlo Method in Statistical Physics* (Springer-Verlag, Berlin, 1984)

[Ca67] F. Calogero, *The Variable Phase Approach to Potential Scattering* (Academic Press, N.Y. 1967)

[Ce79] D. M. Ceperly and M. H. Kalos, in *Monte Carlo Methods in Statistical Physics*, Ed. K. Binder (Springer-Verlag, Berlin, 1979), pp. 145-197

[Ch43] S. Chandrasekhar, Reviews of Modern Physcs, 15, 3 (1943)

[Da74] G. Dahlquist and A. Abjorck, Trans. N. Anderson, *Numerical Methods* (Prentice-Hall,1974) PP320-321

[Fa61] L. D. Fadeev, Sov. Phys. JETP12, 1014 (1961)

[Fa65] L. D. Fadeev, *Mathematical Aspects of the Three- Body Problem in Quantum Scattering Theory* (Davey, New York, 1965)

[Gl83] W. Glockle, *The Quantum Mechanical Few- Body Problem* (Springer-Verlag Berlin, 1983)

[Gr67] P. Grassberger, W. Sandhas, Nucl. Phys. B2, 181 (1967)

[Ha64] J. M. Hammersley and D. C. Handscomb, *Monte Carlo Methods* (Chapman and Hall, 1964)

[Is66] E. Isaacson and H. Keller, *Analysis of Numerical Methods*, pp. 501-512 (John Wiley, 1966)

[Ka74] M. H. Kalos, D. Levesque and Verlet, Phys. Rev. A9, 2178 (1974)

[Ko84] S. E. Koonin, in *Proceedings of Nuclear Theory Summer Workshop, 1981* Ed., G. F. Bertsch, (World Scientific, Singapore, 1982)

[La77] L. D. Landau and E. M. Lifshitz, *Quantum Mechanics (Nonrelativistic Theory)* (Pergamon Press, London, 1977)

[Me53] N. Metropolis, A. W. Rosenbluth, A. M. Teller and E. Teller, J. Chem. Phys. 21, 2087 (1953)

[Pa80] G. L. Payne, J. L. Friar, B. F. Gibson and I. R. Afnar, Phys. Rev. C22, 823 (1980), G. L. Payne, B. F. Gibson and J. L. Friar, Phys. Rev. C22, 832 (1980)

[Pa81] G. L. Payne, in *Proc. of the Ninth Inter. Conf. on the Few Body Problems*, Ed. by F. S. Levin, p61 (North Holland, Amsterdam, 1981)

[Pa84] G. L. Payne, B. F. Gibson and J. L. Friar, *Annual Review of Nuclear Physics* (Academic Press, New York, 1984)

[Pa65] A. Papoulis, *Probability, Random Variables and Stochastic Process* (McGraw Hill, 1965)

[Po33] G. Poschl and E. Teller, Z. Physik 83, 143 (1933)

[Re82] P. J. Reynolds, D. M. Ceperly, B. J. Alder and W. A. Lester, Jr., J. Chem. Phys. 77, 5593 (1982)

[Se77] E. Segre, *Nuclei and Particles* (Benjamin/Cummings, Mass., 1977)

[Wa54] Nelson Wax, Ed., *Selected Papers on Noise and Stochastics Processes* (Dover, New York, 1954)

[Wi47] E. P. Wigner and L. Eisenbud, Phys. Rev. 72, 29 (1947)

[Ya67] O. A. Yakubovsky Sov. J. Nucl. Phys. 5, 937 (1967)

Table-1 (4 pages)

Comparison between exact Gaussian distribution, Gaussian distributed pseudo-random numbers generated on the computer and the distribution of the values of the energy in a Monte Carlo simulation. r is the distance from the mean in units of variance. The numbers tabulated against r are the fraction of the number of events within a distance of r from the mean. The second column is the theoretical value given by 2erf(r). The third column is for 5000 computer-generated Gaussian distributed pseudo-random numbers. The fourth column is for 5000 energy values where to take care of transients we have discarded 2000 initial iterations out of 7000. In the last column we list the standard error for the sample size of 5000.

ρ	Exact	Pseudo-random	Energy	St. error
0.05	0.03988	0.0390	0.0406	0.00277
0.10	0.07966	0.0722	0.0840	0.00383
0.15	0.11924	0.1132	0.1242	0.00458
0.20	0.15852	0.1486	0.1646	0.00517
0.25	0.17942	0.1950	0.2068	0.00543
0.30	0.23582	0.2320	0.2441	0.00600
0.35	0.27366	0.2774	0.2827	0.00631
0.40	0.31084	0.3146	0.3211	0.00655
0.45	0.34728	0.3552	0.3581	0.00673
0.50	0.38728	0.3874	0.3955	0.00689

Table-1 (continued)

ρ	Exact	Pseudo-random	Energy	St. error
0.55	0.41768	0.4230	0.4325	0.00690
0.60	0.45150	0.4570	0.4659	0.00704
0.65	0.48430	0.4902	0.4985	0.00707
0.70	0.51608	0.5194	0.5257	0.00707
0.75	0.54674	0.5448	0.5551	0.00704
0.80	0.57628	0.5744	0.5883	0.00699
0.85	0.60468	0.6012	0.6171	0.00691
0.90	0.63188	0.6328	0.6467	0.00682
0.95	0.65788	0.6616	0.6705	0.00671
1.00	0.68268	0.6856	0.6941	0.00658
1.05	0.70628	0.7088	0.7163	0.00644
1.10	0.72866	0.7292	0.7337	0.00629
1.15	0.74986	0.7504	0.7544	0.00612
1.20	0.76986	0.7706	0.7744	0.00595
1.25	0.78870	0.7924	0.7906	0.00577
1.30	0.80640	0.8084	0.8064	0.00559
1.35	0.82298	0.8210	0.8246	0.00540
1.40	0.83848	0.8388	0.8372	0.00520
1.45	0.85294	0.8530	0.8528	0.00501
1.50	0.86638	0.8638	0.8710	0.00481

Table-1 (continued)

ρ	Exact	Pseudo-random	Energy	St. error
1.55	0.87886	0.8820	0.8822	0.00461
1.60	0.89040	0.8932	0.8940	0.00442
1.65	0.90106	0.9040	0.9032	0.00422
1.70	0.91086	0.9134	0.9098	0.00403
1.75	0.91988	0.9214	0.9168	0.00384
1.80	0.92814	0.9304	0.9242	0.00365
1.85	0.93568	0.9352	0.9320	0.00347
1.90	0.94256	0.9428	0.9386	0.00329
1.95	0.94881	0.9490	0.9440	0.00312
2.00	0.95450	0.9540	0.9496	0.00295
2.05	0.95964	0.9590	0.9552	0.00278
2.10	0.96428	0.9634	0.9600	0.00262
2.15	0.96844	0.9688	0.9644	0.00247
2.20	0.97220	0.9718	0.9696	0.00232
2.25	0.97556	0.9742	0.9738	0.00218
2.30	0.97856	0.9776	0.9756	0.00205
2.35	0.98122	0.9796	0.9790	0.00192
2.40	0.98360	0.9826	0.9798	0.00180
2.45	0.98572	0.9842	0.9822	0.00168
2.50	0.98758	0.9856	0.9850	0.00157

Table-1 (continued)

ρ	Exact	Pseudo-random	Energy	St. error
2.55	0.98922	0.9864	0.9868	0.00146
2.60	0.99068	0.9886	0.9880	0.00136
2.65	0.99194	0.9912	0.9894	0.00126
2.70	0.99306	0.9922	0.9906	0.00117
2.75	0.99404	0.9934	0.9920	0.00109
2.80	0.99488	0.9946	0.9932	0.00101
2.85	0.99562	0.9950	0.9938	0.00093
2.90	0.99626	0.9962	0.9948	0.00086
2.95	0.99682	0.9964	0.9954	0.00080
3.00	0.99730	0.9972	0.9956	0.00073

Table-2 (3 pages)

The values of $\overline{m}_1$ for the Gaussian distributed random numbers were calculated by simulation, using computer-generated pseudo-random numbers (Gaussian distributed). 20,000 numbers were generated with the seed 53193710303.00 . For the sample size of 50, 400 samples were used using 50 consecutive random numbers. Following are the values of m_1 for these samples. The distribution of m_1 is Gaussian about the mean, $\overline{m}_1$, as is shown in Table-7. Without listing m_1 for other sample sizes, the results are summarized in Table-3.

34.20	38.64	26.09	31.15	25.70	31.72	30.14	23.47
25.91	26.71	33.74	32.64	34.59	30.66	24.54	32.96
29.99	30.12	21.87	27.41	35.42	20.93	34.37	41.44
38.21	22.78	30.34	19.86	29.16	29.60	23.50	31.79
29.81	37.70	31.62	23.71	24.52	35.28	30.57	23.18
33.25	34.46	33.21	34.24	29.41	27.92	31.06	33.52
31.60	21.93	22.02	34.76	35.11	33.70	29.23	34.15
30.21	23.70	32.40	30.72	30.65	38.37	34.90	29.72
25.10	20.59	40.17	27.74	27.45	23.41	28.13	32.36
36.07	30.18	34.80	36.01	26.06	30.08	38.74	31.41
33.75	32.38	30.16	33.46	32.53	37.94	31.20	33.72
30.10	35.20	27.34	30.38	33.75	32.83	27.99	28.98
38.22	29.50	27.51	32.89	30.38	28.90	34.93	29.13
36.65	29.91	29.13	31.29	35.67	34.31	31.53	29.26
36.31	38.29	29.30	33.78	28.05	25.84	30.34	33.59

Table-2 (continued)

31.22	30.09	23.99	31.55	27.03	35.63	31.79	33.11
30.96	33.37	31.93	32.83	37.35	40.25	29.72	22.60
28.31	30.40	33.70	31.08	31.02	22.31	30.46	27.01
25.98	29.21	26.79	34.18	22.71	34.19	22.02	36.26
37.20	28.55	32.39	35.10	16.12	38.69	34.19	31.82
33.36	35.47	31.71	34.67	33.93	30.92	21.96	29.51
21.57	22.84	24.03	34.05	35.28	29.49	21.46	28.65
32.30	36.10	33.92	35.25	33.28	31.87	30.90	29.83
30.02	25.27	29.13	22.04	37.25	37.13	33.70	22.41
35.39	32.38	37.37	27.06	31.81	34.88	32.26	24.89
37.20	32.03	32.34	34.26	27.30	25.51	34.34	16.80
36.56	36.56	33.13	36.10	30.22	33.70	21.88	35.43
37.89	36.46	32.26	36.83	30.39	37.57	31.22	30.97
29.96	27.74	32.74	37.57	30.33	28.62	39.88	32.36
28.39	35.22	24.70	32.47	28.74	35.12	31.88	30.32
27.43	28.70	32.67	33.46	33.98	39.25	28.12	26.85
33.06	28.91	35.23	23.12	37.69	34.45	39.89	36.14
29.79	31.58	33.68	29.12	37.60	27.24	27.84	34.29
30.95	34.33	22.04	31.66	36.90	24.84	29.45	31.79
29.08	33.85	32.20	29.71	35.50	33.49	25.56	33.81

Table-2 (continued)

33.04	34.66	35.36	27.21	27.65	32.07	29.71	29.58
21.72	42.23	34.31	34.31	37.14	26.32	27.09	36.26
37.64	32.84	33.12	34.82	21.21	34.24	39.16	26.45
30.09	23.42	34.92	36.28	26.99	29.11	30.40	31.79
27.86	35.67	32.61	29.90	28.84	22.77	19.20	33.10
32.02	35.91	31.76	29.48	35.67	34.34	31.93	28.06
33.36	33.64	25.27	34.02	32.78	21.60	28.20	23.68
21.85	23.31	28.36	32.34	37.35	35.43	28.08	33.27
33.86	28.11	34.50	33.06	23.11	36.12	23.24	23.67
24.44	34.20	29.06	38.59	22.56	35.92	34.22	34.61
37.94	26.56	22.87	33.72	31.51	30.00	24.72	23.62
21.95	32.52	34.28	27.98	22.39	27.50	22.99	30.58
35.59	37.95	34.97	32.55	35.23	38.19	34.84	28.34
35.94	31.91	30.36	29.42	30.57	35.49	35.65	32.86
37.45	38.65	22.10	34.49	24.76	38.26	26.99	26.66

Table-3 (2 pages)

A Monte Carlo simulation to calculate $\overline{m}_1$ for the Gaussian distributed pseudo-random numbers. 20,000 numbers were generated with the seed 5319371303.00. S samples with size N were selected from these numbers, taking N consecutive numbers in each of the samples. σ is the standard deviation for m_1. The standard error is calculated as $\sigma / S^{1/2}$.

N	S	$\overline{m}_1$	σ	st. error	$\overline{m}_1 / N$
50	400	31.00	4.77	0.239	0.62001
100	200	61.77	8.12	0.575	0.61775
150	133	94.16	11.55	1.002	0.62772
200	100	126.31	11.19	1.119	0.63157
250	80	155.38	12.44	1.390	0.62151
300	66	185.17	15.71	1.935	0.61721
350	57	215.34	17.71	2.345	0.61526
400	50	252.31	18.82	2.661	0.63076
450	44	275.49	17.45	2.630	0.61221
500	40	315.49	13.69	2.164	0.63098
550	36	347.18	23.16	3.859	0.63124
600	33	383.05	19.50	3.394	0.63841
650	30	412.28	25.50	4.654	0.63427
700	28	444.03	23.47	4.436	0.63433
750	26	479.49	27.42	5.377	0.63931

Table-3 (continued)

N	S	$\overline{m}_1$	σ	st. error	$\overline{m}_1 / N$
800	25	511.32	22.64	4.527	0.63915
850	23	539.12	23.88	4.978	0.63427
900	22	571.08	20.17	4.299	0.63453
950	21	611.64	28.83	6.291	0.64372
1000	20	641.64	24.52	5.480	0.64164

Table-4

Comparison between the exact (ex), Monte Carlo (MC) and variational (var) calculation of the energy E and phase shift δ for a one-dimensional scattering problem. The potential is Poschl-Teller defined in Eq. (4.3.3) of Section-4.4 for U_0=$-8MeV$andx_0=$2fermi$. The parameter R defines the "box" boundary where the wave function is forced to have a node. The exact phase shifts are calculated both by solving the Calogero equation (Ca67) and from the exact value of E using Eq. 4.4.4. The former values are the true values, while the latter ones (shown in the parentheses) will coincide with these only when $V(r)$ is negligible for $r>R$. This table is reproduced from (Al84).

R(fm)	5.0	7.5	10.0	20.0
E_{ex}(MeV)	5.3732	2.1236	1.1453	0.2991
E_{MC}(MeV)	5.3752 ±0.0054	2.1236 ±0.0073	1.1404 ±0.005	0.3011 ±0.004
E_{var}(MeV)	5.4993	2.3176	1.3410	0.3951
δ_{ex}(rad)	0.6014 (0.5962)	0.7416 (0.7414)	0.7912 (0.7913)	0.7390 (0.7395)
δ_{MC}(rad)	0.5959 ±0.0013	0.7426 ±0.0041	0.7964 ±0.0051	0.7310 ±0.016
δ_{var}(rad)	0.5665	0.6341	0.5984	0.381

Table-5 (2 pages)

The values of iteration at which the ensemble is updated are listed. The upper limit of 90 and lower limit of 110 were imposed on the ensemble. The ensemble was updated to 100 whenever the above bounds were crossed. The data below pertain to the case discussed in Section-4.3. From the table we may guess that the stationary point is reached between iterations 214 and 824.

Iteration	Interval	Updated from
16	16	90
45	39	90
215	170	90
824	609	110
1376	548	90
1724	348	90
2006	282	90
2115	146	90
2533	378	90
2673	140	90
3512	839	90
4741	1229	110
4909	168	110
4958	49	110
5252	294	110

(Table-5 continued)

Iteration	Interval	Updated from
5368	116	110
5400	32	110
5681	281	110
5731	50	90
6130	399	110
6270	140	90
6383	113	110
6829	446	89

Table-6

The table below is for the case discussed in Section-4.4 . The sampling interval is tabulated against the number of initial iterations discarded. From the table we conclude that the stationary point is reached after about 700 iterations.

Iterations discarded	Sampling interval
0	42 ±2
100	42 ±2
200	39 ±2
300	37 ±2
400	35 ±2
500	35 ±1
600	35 ±1
700	31 ±1
800	31 ±1
900	31 ±1
1000	31 ±1

Table-7 (3 pages)

The table below gives the values of $\overline{m}_1 / N$ for various sampling intervals for the example in Section-4.4 . The table is for Case-b in Figure-6 where the first 700 iterations have been discarded. The error in the last column is the standard error in $\overline{m}_1 / N$. The striking feature is the fluctuation in the value beyond the sampling interval of 31. The theoretical asymptotic value of $\overline{m}_1 / N$ as $N \to \infty$ is 0.6325 .

Sampling Interval	$\overline{m}_1 / N$	Error
11	0.26280	0.01107
12	0.32250	0.00943
13	0.37093	0.01875
14	0.40914	0.01026
15	0.43385	0.00852
16	0.47336	0.01457
17	0.48519	0.00907
18	0.50359	0.00979
19	0.52326	0.01162
20	0.53726	0.01335
21	0.55895	0.01294
22	0.56119	0.00938
23	0.55392	0.01654
24	0.58744	0.01343
25	0.60039	0.01283

Table-7 continued

Sampling Interval	$\overline{m}_1 / N$	Error
26	0.56880	0.01324
27	0.60336	0.00985
28	0.59846	0.01220
29	0.59435	0.00803
30	0.61015	0.00777
31	0.65100	0.00924
32	0.63205	0.00869
33	0.60602	0.01159
34	0.62215	0.01377
35	0.63808	0.00803
36	0.62174	0.01176
37	0.65721	0.01035
38	0.65637	0.00974
39	0.65141	0.00609
40	0.62639	0.01005
41	0.62214	0.00742
42	0.67225	0.00638
43	0.64066	0.01223
44	0.65096	0.00905
45	0.60969	0.01144

Table-7 continued

Sampling Interval	$\overline{m}_1 / N$	Error
46	0.64814	0.00885
47	0.64715	0.00914
48	0.63809	0.00782
49	0.64311	0.01182
50	0.65939	0.01153
51	0.61469	0.00970
52	0.63628	0.00880
53	0.63588	0.00858
54	0.60011	0.01044
55	0.65487	0.00675
56	0.61787	0.00909
57	0.63243	0.01101
58	0.64093	0.00994
59	0.66597	0.00808
60	0.67873	0.00858

Table-8a.

The values of m_1 for the sampling of a time series of energy. The initial 700 iterations are discarded so that the system has relaxed. The sampling interval, however, is taken as 120 iterations enabling us to obtain 120 different samples of size 50. This enables us to compare the distribution of m_1 for this series with that of the pseudo-random series, recorded in Table-2.

28.91	34.55	34.55	37.08	34.78	32.25	30.32	32.33
31.03	24.87	28.52	31.56	30.59	32.78	34.31	34.22
36.62	31.71	32.65	32.97	34.93	34.23	34.46	34.22
34.36	34.64	34.28	31.48	31.61	33.14	31.73	31.94
34.25	32.81	33.87	36.00	33.69	37.35	35.41	37.11
36.96	27.47	31.38	38.33	37.55	38.71	38.19	37.49
35.50	35.99	35.96	36.33	35.40	30.75	29.90	29.21
24.35	26.46	29.79	29.49	29.14	29.27	29.74	27.58
29.49	29.97	31.08	29.52	29.97	27.30	23.36	20.91
24.57	29.88	24.78	27.15	24.35	32.19	22.94	22.42
22.18	22.02	27.37	29.84	31.07	31.89	32.31	32.38
34.16	30.69	32.04	32.33	20.14	16.23	17.85	24.29
25.40	27.81	26.62	27.15	25.28	25.96	30.59	31.43
27.83	28.81	28.86	20.27	22.47	27.54	28.07	22.88
27.33	30.20	32.19	32.00	28.68	32.12	30.79	32.80

Table-8b

This table summarizes the comparison between Table-2 and Table-8a. In Table-9 the distribution is compared in more detail. Note the closeness of the variance σ.

	Gaussian Random Numbers	Energy Time Series
N	50	50
S	400	120
$\overline{m}_1$	31.00	30.41
σ	4.771	4.64
St. error	0.239	0.423
$\overline{m}_1 / N$	0.620	0.608
St. error/N	0.00477	0.0085

Table-9 (4 pages)

The table below compares the distribution for m_1 for a Gaussian pseudo-random series and the time series for the energy obtained in the Diffusion Monte Carlo for the example in Section-4.4 . ρ is the distance from the average in the units of variance . As in Table-1 the fraction of events within this distance is tabulated. The second column is the exact value for the Gaussian distribution. The third column is the distribution of m_1, listed in Table-1 , for the samples from the pseudo-random series. The last column is for the samples of energy values sampled at an interval of 120 for which values of m_1 are listed in Table-8a. While comparing we should note that, while the number of events considered for column three is 400, this value is 120 for column four.

ρ	Gauss.	$m_{1(random)}$	$m_{1(energy)}$
0.05	0.03988	0.0300	0.0333
0.10	0.07966	0.0500	0.0750
0.15	0.11924	0.0975	0.1417
0.20	0.15852	0.1550	0.1667
0.25	0.17942	0.1825	0.2083
0.30	0.23582	0.2300	0.2500
0.35	0.27366	0.2625	0.3000
0.40	0.31084	0.3075	0.3417
0.45	0.34728	0.3400	0.3917
0.50	0.38728	0.3700	0.4000

Table-9 continued

ρ	Gauss.	$m_{1(random)}$	$m_{1(energy)}$
0.55	0.41768	0.3875	0.4333
0.60	0.45150	0.4325	0.4667
0.65	0.48430	0.4700	0.4917
0.70	0.51608	0.5200	0.5167
0.75	0.54674	0.5500	0.5500
0.80	0.57628	0.5775	0.5500
0.85	0.60468	0.6100	0.6167
0.90	0.63188	0.6400	0.6583
0.95	0.65788	0.6675	0.6750
1.00	0.68268	0.6875	0.6917
1.05	0.70628	0.7000	0.6917
1.10	0.72866	0.7225	0.7167
1.15	0.74986	0.7400	0.7333
1.20	0.76986	0.7500	0.7417
1.25	0.78870	0.7625	0.7750
1.30	0.80640	0.7725	0.7917
1.35	0.82298	0.7950	0.8250
1.40	0.83848	0.8150	0.8250
1.45	0.85294	0.8225	0.8417
1.50	0.86638	0.8350	0.8500

Table-9 continued

ρ	Gauss.	$m_{1(random)}$	$m_{1(energy)}$
1.55	0.87886	0.8625	0.8833
1.60	0.89040	0.8750	0.8833
1.65	0.90106	0.8925	0.9000
1.70	0.91086	0.9000	0.9083
1.75	0.91988	0.9175	0.9333
1.80	0.92814	0.9225	0.9500
1.85	0.93568	0.9300	0.9583
1.90	0.94256	0.9525	0.9583
1.95	0.94881	0.9700	0.9583
2.00	0.95450	0.9750	0.9583
2.05	0.95964	0.9775	0.9583
2.10	0.96428	0.9800	0.9667
2.15	0.96844	0.9825	0.9667
2.20	0.97220	0.9875	0.9750
2.25	0.97556	0.9875	0.9833
2.30	0.97856	0.9875	0.9833
2.35	0.98122	0.9900	0.9833
2.40	0.98360	0.9925	0.9833
2.45	0.98572	0.9925	0.9833
2.50	0.98758	0.9950	0.9833

Table-9 continued

ρ	Gauss.	$m_{1(random)}$	$m_{1(energy)}$
2.55	0.98922	0.9950	0.9833
2.60	0.99068	0.9950	0.9833
2.65	0.99194	0.9950	0.9833
2.70	0.99306	0.9950	0.9833
2.75	0.99404	0.9950	0.9917
2.80	0.99488	0.9950	0.9917
2.85	0.99562	0.9950	0.9917
2.90	0.99626	0.9950	0.9917
2.95	0.99682	0.9950	0.9917
3.00	0.99730	0.9975	0.9917

Table-10a

This table gives results of runs with various parameters for the problem defined in Section-4.4. Each run is 7000 iterations long with an integration step $\delta\tau = 0.001x10^{-23}sec$. In the fourth case the system was found to be destabilized every time the ensemble was restored to a nominal value of 100. Except for the last two cases the seed for the random number generator is the same. The last two cases, however, are the same as the first case with the seed for the random number generator changed.

N_U	N_0	N_L	N_E	N_R	N_S	S	E (MeV)	δE (MeV)
105	100	95	20	401	29	228	5.40205	0.01093
110	100	90	20	701	32	175	5.37471	0.01290
115	100	85	20	1301	35	163	5.39177	0.01476
120	100	80	20	....	...	...	.....	.....
205	200	195	20	801	27	229	5.37172	0.00873
210	200	190	20	401	35	189	5.38246	0.00947
220	200	180	20	801	36	172	5.37480	0.00972
105	100	95	10	401	30	220	5.38640	0.01254
105	100	95	25	401	37	178	5.38762	0.01093
105	100	95	30	401	83	80	5.38949	0.01995
105	100	95	35	401	65	102	5.39194	0.01806
105	100	95	40	401	35	189	5.39882	0.01349
105	100	95	20	401	29	227	5.38649	0.01233
105	100	95	20	401	31	213	5.37804	0.01286

Table-10b

The table below gives results of runs with different integration steps. The physical problem is the same as the one for Table-10a. The cases with the same integration steps were calculated with different seeds. Extrapolating by the linear least-square fit, $E(\delta\tau)=a+b\,\delta\tau$, we get $E(0)=5.37403-+0.0061$ MeV.

$\delta\tau$	L	N_E	N_R	N_S	S	E	δE
$(10-23 Sec)$	(10^3)					(MeV)	(MeV)
0.00100	7	20	401	32	175	5.41989	0.01707
0.00100	14	20	401	38	357	5.38759	0.00937
0.00075	10	20	401	48	200	5.37993	0.01406
0.00050	10	30	601	88	107	5.37471	0.01290
0.00050	10	40	801	87	105	5.40599	0.01829
0.000125	10	20	401	49	195	5.37981	0.01231

Table-11

This table gives the two-body binding energy, e, and the range of the potential, d, between the fragments for the three-body system. The system is one-dimensional and all the particles are of mass m. The interaction between the particles is square-well of depth V_0 and width a_0. We define d as the distance at which the effective interaction, defined in Section-5.2, reduces to $0.01V_0$. The mass of the particles is in units of m_p, the proton mass. In the last column we tabulate V_1, the depth at which the second energy level appears ($V_1=\frac{1}{m}[\frac{\pi\hbar}{2a}]^2$). For the last case, since there are two two-body bound states, we have given both the levels.

a_0 (fm)	m (m_p)	V_0 (MeV)	e (MeV)	d (fm)	V_1 (MeV)
1.0	1.0	10.0	-1.84162	5.37	102.323
2.0	1.0	10.0	-4.45825	5.56	25.5808
1.0	2.0	10.0	-3.00922	3.72	51.1615
1.0	1.0	20.0	-6.01844	3.72	102.323
2.0	2.0	10.0	-5.96385	4.53	12.7904
2.0	3.0	8.00	-5.06995	4.34	8.52693
2.0	3.0	20.0	-15.8387	3.72	8.52693
			-4.91347		

Table-12a

The result of the problem in Appendix-4 by relaxation. The boundary is defined by R_α=5.0 fm. Figure-6 shows the region in the XY-coordinate system defined in Appendix-1. The masses of all three particles are taken to be m_p. The potential is taken to be square-well with width 2.0 fm. The linear least-square fit, $E(\delta\tau)=a+b\,\delta\tau$, gives $E(0)=a=-3.11312$ MeV. The quadratic least-square fit, $E(\delta\tau)=a+b\,\delta\tau+c\,\delta\tau^2$ gives, $E(0)=a=-3.09789$ MeV. The energy for the two-particle fragment is -1.23553 MeV and therefore the system is in a bound state.

N_x	δX (fm)	$\delta\tau$ ($10^{-23}Sec$)	E (MeV)
40	0.25	0.0090	-2.32318
100	0.10	0.0015	-2.80544
200	0.05	0.00035	-2.95653
300	0.0333	0.00015	-3.00215

Table-12b

The Monte Carlo results corresponding to the relaxation results given in Table-12a. The linear least-square fit, $E(\delta\tau)=a+b\,\delta\tau$ gives, $E(0)=a=-3.06766\pm0.0329$ MeV.

$\delta\tau$ ($10^{-23}Sec$)	S	E (MeV)	δE (MeV)
0.0005	258	-3.14975	0.04803
0.0004	161	-3.05887	0.05730
0.0003	203	-3.10416	0.05357
0.0002	114	-3.11234	0.06885

Table-13

The results of the Monte Carlo simulation of the two-body approximation of the three-body problem. The problem is equivalent to the scattering of a particle of mass $M=2m/3$ and, as defined in Section-5.2 and shown in Fig.-7, by the effective potential $V(R)$. The direct result of the simulation gives the kinetic energy E_k, while total energy $E=E_k+e$ is tabulated below. The formula 5.2.3 gives the phase shift. The parameters are: $m=3m_p$, a_0=2 fm and $V_0=8.0MeV$ which gives $e=-5.06995$ MeV.

Case	a (fm)	$\delta\tau$ ($10^{-23}Sec$)	S	E (MeV)	δE (MeV)
1a	10.0	0.0020	181	-3.54046	0.01301
1b	10.0	0.0015	172	-3.52655	0.01162
1c	10.0	0.0010	88	-3.53457	0.01953
1d	10.0	0.0008	56	-3.50631	0.02703
1e	10.0	0.0006	30	-3.51066	0.02820
2	9.00	0.0010	82	-3.10346	0.02290
3	8.00	0.0010	87	-2.42564	0.02472
4a	7.00	0.0010	40	-1.36071	0.04586
4b	7.00	0.0010	53	-1.40955	0.03864
4c	7.00	0.0010	41	-1.37604	0.04276
5	6.50	0.0008	80	-0.62432	0.03977
6	6.30	0.0010	79	-0.28464	0.04045
7	6.25	0.0008	55	-0.12432	0.04932
8	6.20	0.0010	67	-0.07912	0.04328
9	6.15	0.0010	109	00.08417	0.03640
10	6.10	0.0010	105	00.04244	0.03826

Table-14

The results for the three-body problem defined in Section-5.2. The interaction between the pair 1-3 is a square-well of depth 8 MeV and the interaction between pairs, 2-1 and 2-3 is a square-barrier of height 8 MeV. The width of both the interactions is 4.0 fm. All three particles are of mass, $m=3m_p$ The kinetic energy E_k is given by $E_k=E-e$ and the phase shift is given by Eq.-5.2.4. The binding energy for the two-body bound state is e =5.06995 MeV.

Case	a	$\delta\tau$	S	E	δE
	(fm)	$(10^{-23}Sec)$		(MeV)	(MeV)
1a	10.0	0.0020	200	-3.71712	0.03300
1b	10.0	0.0015	155	-3.75545	0.03921
1c	10.0	0.0010	110	-3.69135	0.04701
1d	10.0	0.0008	68	-3.57813	0.05573
1e	10.0	0.0006	47	-3.77828	0.06588
2	9.00	0.0010	111	-3.29117	0.04593
3	8.00	0.0010	80	-2.57219	0.05469
4a	7.00	0.0020	82	-1.89203	0.06787
4b	7.00	0.0020	103	-2.00297	0.05297
4c	7.00	0.0015	47	-2.35525	0.04782
4d	7.00	0.0010	51	-1.80777	0.08414
4e	7.00	0.0008	75	-1.96906	0.06483
5a	6.50	0.0010	41	-1.22658	0.08476
5b	6.50	0.0008	131	-1.14399	0.05177
5c	6.50	0.0006	46	-1.18013	0.11218
6	6.00	0.0010	60	-0.52691	0.09209

Table-15

The comparison between the results of two-body approximation and the three-body Monte Carlo results. We tabulate the values of energy against the parameter a. E_2, the same as E of Table-13, is the result of the two-body approximation while E_3, the same as E in Table-14, is the Monte Carlo result for the three-body. We tabulate the results for $\delta\tau$=0.001 and the results obtained by extrapolation to $\delta\tau$=0, which are identified by * in the column for $\delta\tau$.

a	$\delta\tau$	E_2	E_3	δ_{ph2}	δ_{ph3}
(fm)	($10^{-23}Sec$)	(MeV)	(MeV)	(Rad.)	(Rad.)
10.0	0.001	-3.53457	-3.69135	-0.70672	-0.50495
		±0.01953	±0.04701	±0.0245	±0.0622
10.0	*	-3.50774	-3.6614	-0.74698	-0.66696
		±0.00838	±0.02365	±0.0104	±0.0299
9.00	0.001	-3.10346	-3.29117	-0.77809	-0.58632
		±0.02290	±0.04593	±0.0228	±0.0299
8.00	0.001	-2.42564	-2.57129	-0.89867	-0.78582
		±0.02472	±0.05469	±0.0189	±0.0430
7.00	0.001	-1.38210	-1.80777	-1.03332	-0.78992
		±0.04276	±0.06787	±0.0242	±0.0404
7.00	*		-1.204961		-0.63655
			±0.03073		±0.0192
6.50	0.001	-0.62432	-1.16013	-1.11481	-0.85008
		±0.03864	±0.11218	±0.0185	±0.0573
6.50	*		-1.02995		-0.91599
			±0.05595		±0.0281

Table-16

The table below gives results for the case with two two-body bound states. The pair (1,3) have negative potential while the other two pairs have positive potential. The parameters are: V_0 = 20 MeV, a_0=2 fm and $m=3m_p$. Referring to Table-11, two-body bound states are at -15.8387 MeV and -4.91347 MeV. L is the number of iterations carried out.

case	a	$\delta\tau$	L	S	E	δE
	(fm)	(10^{-23}Sec)			(Mev)	(MeV)
1	10.0	0.0005	7000	57	-14.5178	0.1186
2	6.00	0.0002	7000	47	-9.95226	0.1906
3a	5.00	0.0002	7000	54	-6.9584	0.1722
3b	5.00	0.0001	3000	25	-6.5214	0.3345
4a	4.50	0.0002	7000	*	Unstable	
4b	4.50	0.0001	1000	*	Unstable	
5a	4.75	0.00015	1000	*	Unstable	
5b	4.75	0.0001	1000	*	Unstable	
6	4.80	0.0001	1000	*	unstable	
7	4.90	0.0001	1000	*	Unstable	

Table-17

The results of the problem-C defined in Section-5.3. The interaction between the pair (1,3) is a square-barrier. And the interaction of the pairs (1,2) and (2,3) is the square-well. The height of the barrier and the depth of the well are chosen to be 10 MeV and all the interactions have width 4fm. All three particles are of mass $m=2m_p$. The kinetic energy is given by $E_k=E-e$ and the phase shift, δ_{ph} is then given by Eq.-5.3.5. The internal energy of the two-body bound state is $e=-5.96385$ MeV. Here the particles 1 and 3 are considered indistinguishable. We also restrict to the antisymmetric incoming channel.

Case	a	$\delta\tau$	E	δE	S	δ_{ph}
	(fm)	($10^{-23}Sec$)	(MeV)	(MeV)		(Rad.)
1	11.0	0.0010	-5.44696	0.17531	49	1.1361±0.34
2	10.0	0.0008	-4.99266	0.11012	55	0.6425±0.14
3	9.00	0.0005	-4.51007	0.10862	47	0.3898±0.10
4	8.00	0.0005	-4.13943	0.14227	31	0.4015±0.11
5	7.50	0.0005	-3.64872	0.06204	112	0.2478±0.05
6	5.50	0.0005	-1.52482	0.14700	57	0.2031±0.05

Table-18

The table gives the results of the simulation of Case-D. The particles 1 and 3 repel while the other two pairs of particles attract. The particles 1 and 3 are considered distinguishable. Further, we consider only the antisymmetric combination of the two channels in the incoming mode. Therefore, there are two channels. By superposition of two channels, however, we get Case-C and obtain the phase shift. The phase shift given here is to be compared with the value in Table-17.

Case		1	2	3
a	(fm)	9.0	8.0	7.0
b	(fm)	6.0	6.0	5.0
$\delta\tau$	(10^{-23}Sec)	0.0005	0.0005	0.0005
S		89	61	50
E	(MeV)	-4.8459	-4.32598	-3.47844
δE	(MeV)	0.0705	0.0823	0.1025
$D_{1,1}$	(fm)	-3.59	-4.01	-2.432
$\delta D_{1,1}$	(fm)	0.31	0.25	0.13
$D_{1,2}$	(fm)	-8.376	-7.054	-4.54
$\delta D_{1,2}$	(fm)	3.18	0.82	0.42
δ_{ph}	(Rad.)	1.231	0.924	0.398
$\delta\delta_{ph}$	(Rad.)	0.11	0.06	0.07

Table-19

The table gives the results of the simulation of Case-E. The particles 1 and 3 repel while the other two pairs of particles attract. The width of interaction is 4 fm and the depth is 10 Mev. The particles 1 and 3 are considered indistinguishable. Therefore, two modes of fragmentation are also indistinguishable. Therefore, there are two channels. The number of iterations is 7500 of which the initial 500 were discarded. The internal energy of the two-body bound state is e = -5.96386 MeV.

Case		1	2	3
a	(fm)	-4.75	-5.0	-5.25
b	(fm)	4.5	4.5	4.5
$\delta\tau$	(10^{-23}Sec)	0.0002	0.0002	0.0002
S		140	175	140
E	(MeV)	-5.13044±.0672	-5.3086±.0708	-5.56046±.0757
k	$\frac{1}{\text{fm}}$	.23150±0.0093	.20527±0.0111	.16106±0.152
$D_{1,1}$	(fm)	2.77225±.3672	1.941884±.4943	-.002918±.9432
$D_{\bar{1},1}$	(fm)	-6.11588±.2337	-6.3916±.1412	-6.5460±.5749
$S_{1,1}$				
Real:		-.11537±.0070	-.17553±.0066	-.05243±.0033
Imaginary:		-.16922±.0460	-.11457±.0492	.00641±.0102
$S_{\bar{1},1}$				
Real:		-.80873±.0687	-.53445±.0865	.12124±.2705
Imaginary:		.55136±.1128	.81880±.0964	.99121±.0770

Table-20

The table gives the results of the simulation of Case-F. The particles 1 and 3 repel while the other two pairs of particles attract. The width of interaction is 4 fm and the depth is 10 Mev. The particles 1 and 3 are considered distinguishable. Therefore, two modes of fragmentation are also distinguishable. Therefore, there are four channels. The number of iterations is 14000 of which the initial 500 were discarded. The internal energy of the two-body bound state is e = -5.96386 MeV.

a	(fm)	-5.0
b	(fm)	4.5
$\delta\tau$	(10^{-23}Sec)	0.0002
S		280
E	(MeV)	-5.28547±0.0857
k	$\frac{1}{\text{fm}}$	.20886±0.0100
$D_{1,1}$	(fm)	2.72746±.4995
$D_{\bar{1},1}$	(fm)	-5.46843±0.1615
$D_{3,1}$	(fm)	5.40002±0.1322
$S_{1,1}$		
Real:		-0.44645±0.0814
Imaginary:		0.31977±.0102
$S_{\bar{1},1}$		
Real		0.22111±0.0508
Imaginary:		-.42479±.0164
$S_{3,1}$		
Real:		0.20458±0.0898
Imaginary:		-0.43897±.0870

Figure-1.

Plot of $C_{N,n}$ and $P(\omega)$ for a sample of pseudo-random (Gaussian) numbers. $C_{N,n}$ and $P(\omega)$ are defined by Eqs.- 4.2.3 and 4.2.4, respectively. The sample, of size 200, was generated from the seed value 53193710303. Violent behavior of $C_{N,n}$ for large n and low values of $P(\omega)$ beyond the frequency of 100 is to be noted.

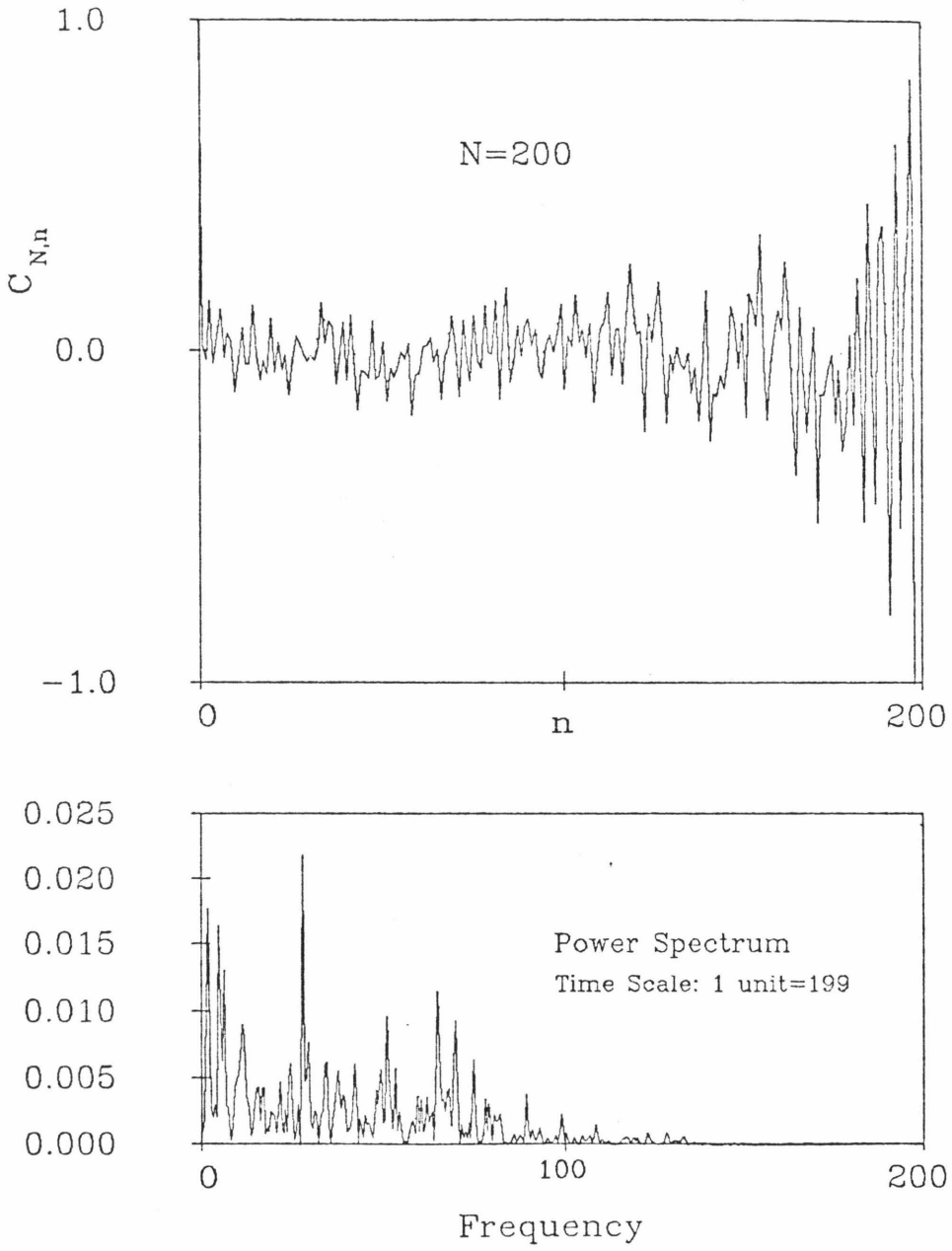
1.0
N=200
$C_{N,n}$
0.0
−1.0
0
n
200
0.025
0.020
0.015
0.010
0.005
0.000
Power Spectrum
Time Scale: 1 unit=199
0
100
200
Frequency

Figure-1

Figure-2.

Comparison of $C_{N,n}$ between energy sampled at an interval of 30 iterations (for the example in Section-4.4), and pseudo-random numbers (Gaussian). The plots a, b and c are for the samples of pseudo-random numbers and the plot d is for the energy sample. All samples are of size 200.

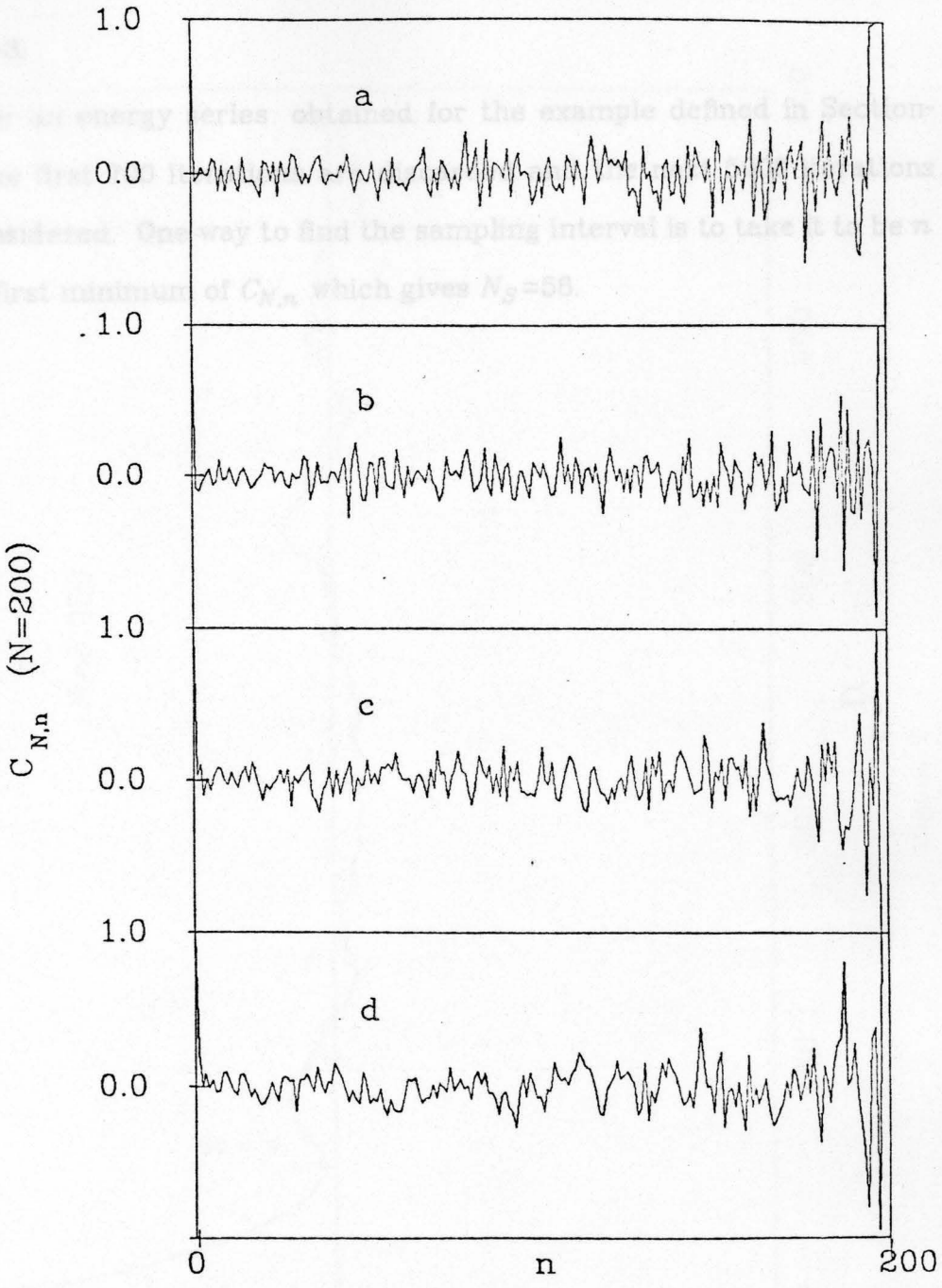

Figure-2

Figure-3.

$C_{N,n}$ for an energy series obtained for the example defined in Section-4.4. The first 700 iterations are discarded and the next 5000 iterations are considered. One way to find the sampling interval is to take it to be n at the first minimum of $C_{N,n}$ which gives N_S=56.

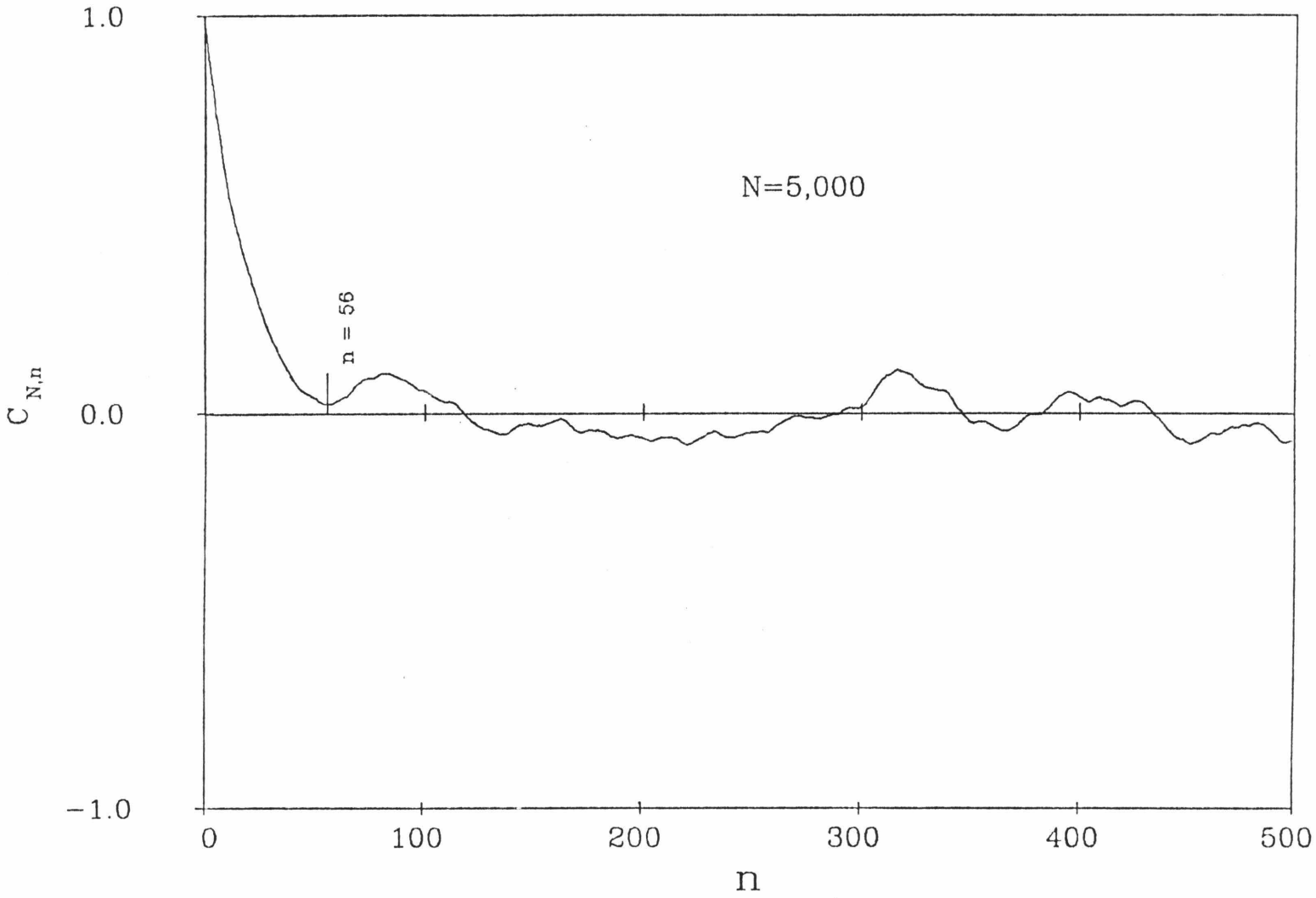

Figure-3

Figure-4

The power spectrum, defined by Eq.-4.2.3, for the energy series obtained from Monte Carlo. The physical example is the problem defined in Section-4.4. The duration of iterations is scaled to unity.

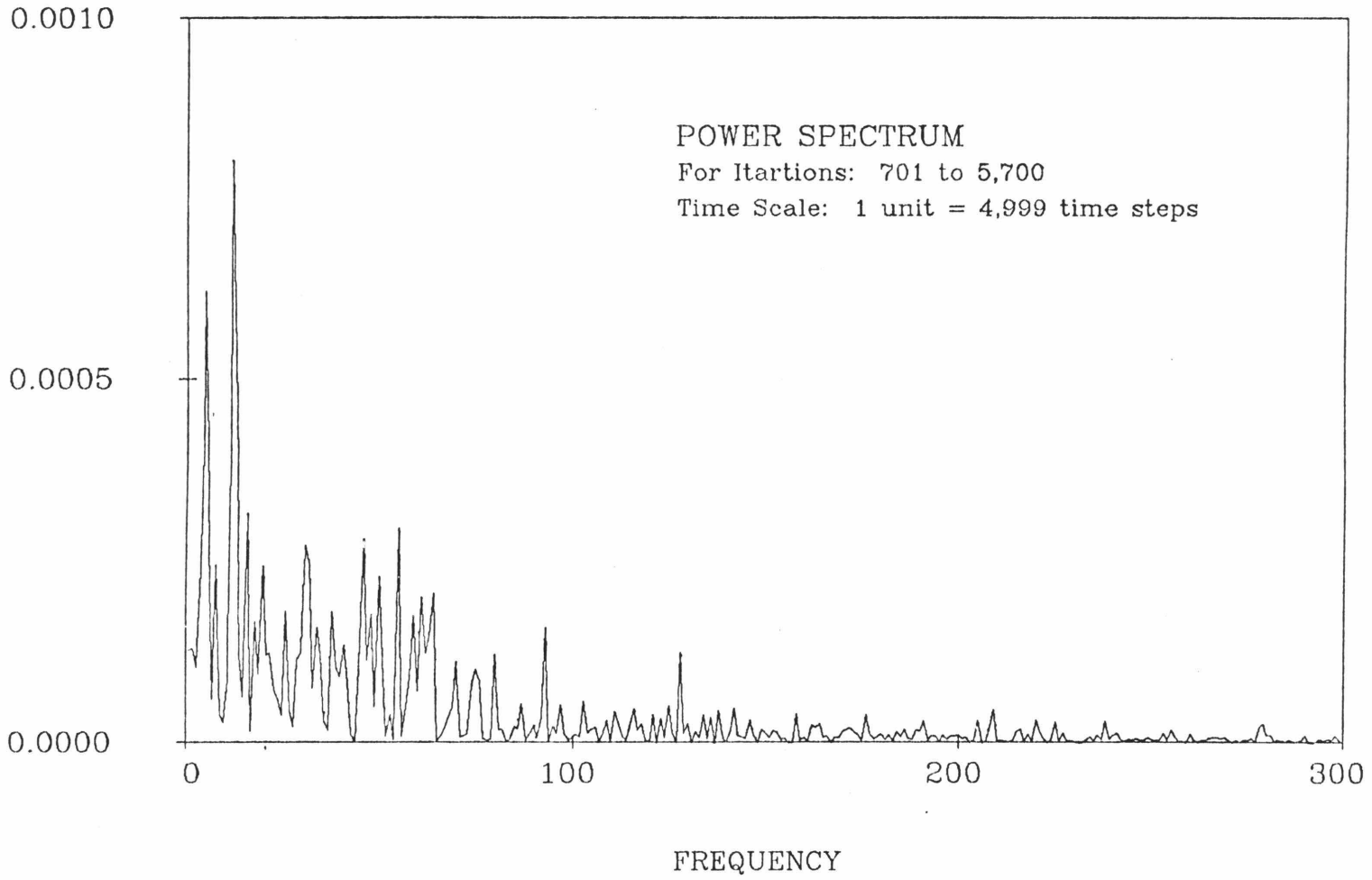
0.0010
0.0005
0.0000
POWER SPECTRUM
For Itartions: 701 to 5,700
Time Scale: 1 unit = 4,999 time steps
0
100
200
300
FREQUENCY

Figure-4

Figure-5

The plot of $\frac{\overline{m}_1}{N}$ against the sampling interval N_S. $\frac{\overline{m}_1}{N}$ is calculated using 5000 consecutive iterations. For the plots *a*, *b* and *c* the number of initial iterations discarded is, respectively, 0, 700 and 1000. The horizontal line corresponds to $\overline{m}_1 / N = 0.60$.

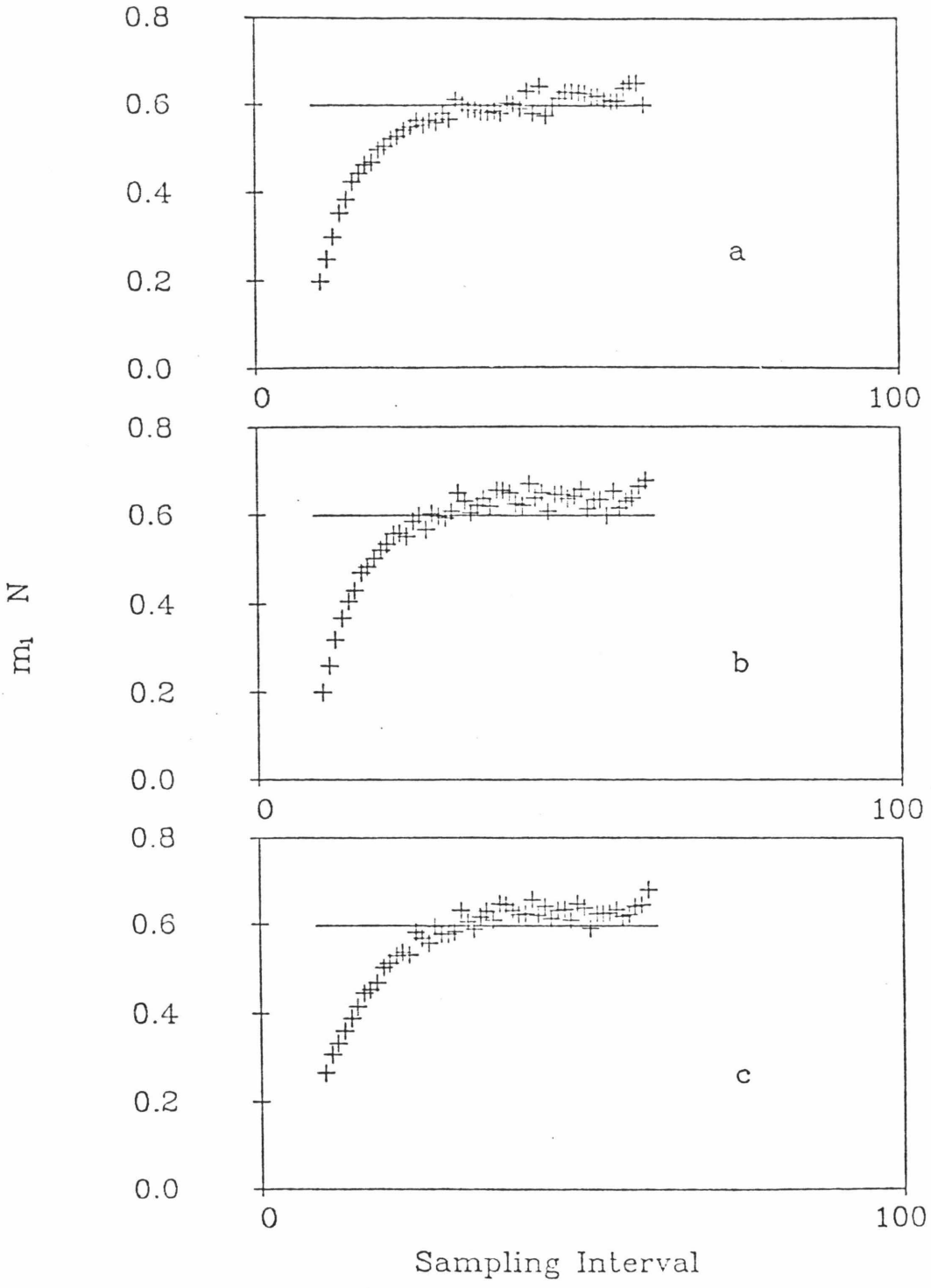

Figure-5

Figure-6

The bounded region $r_i \leq R$ in the X-Y coordinate system defined in Appendix-1. The region for $r_i \leq R_i$, which is also hexagonal, can be obtained by moving the boundary lines parallel to themselves. If $X=r_1$ and $Y=r_2$, the boundary lines at 45 degrees are due to the condition $r_3 \leq R_3$.

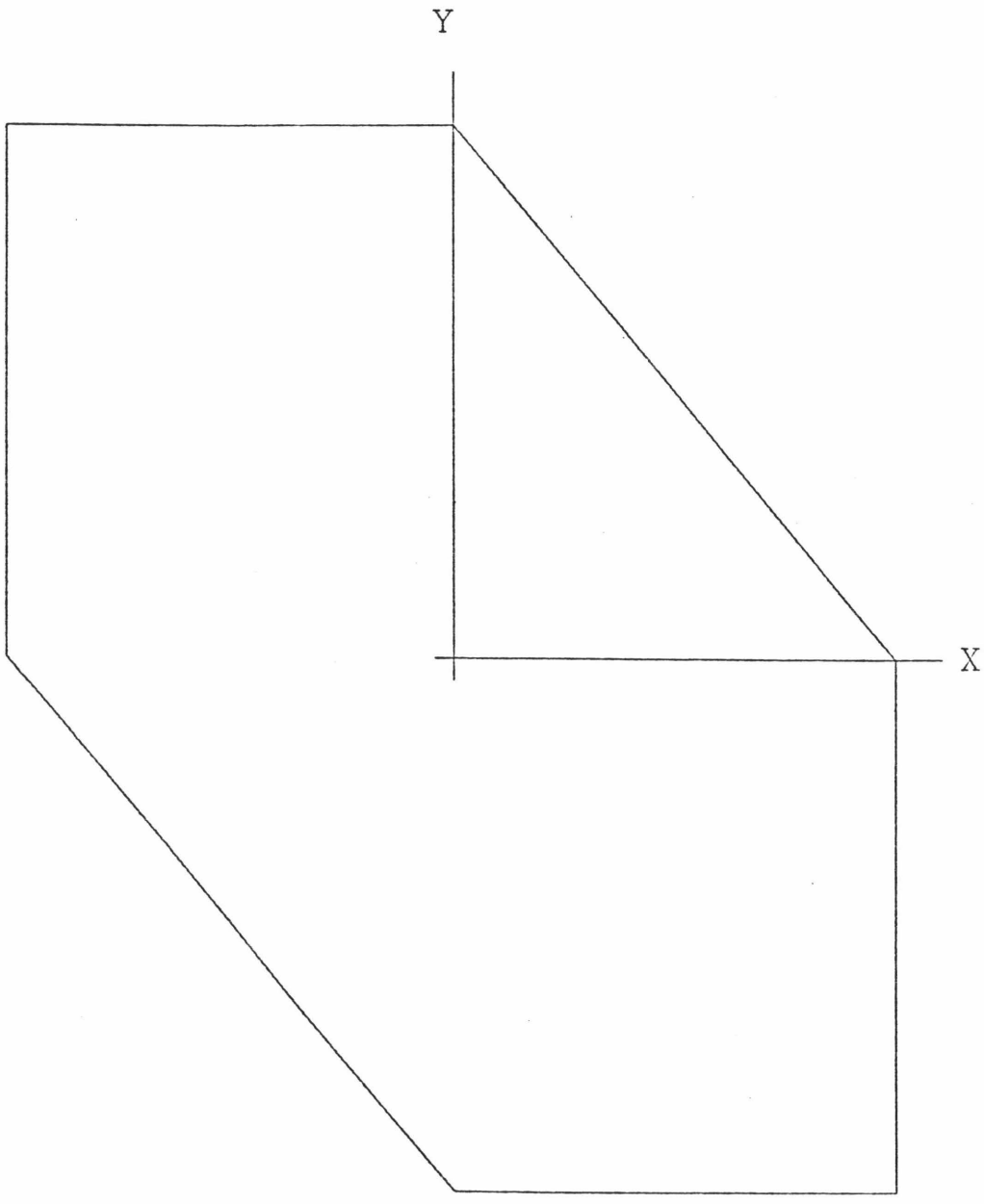

Figure-6

Figure-7

The effective potential, V(R), defined by Eq.-5.2.1. Interaction between particles 1 and 3 is a square-well while the other two pairs interact with a square-barrier. All three particles have equal mass, m.

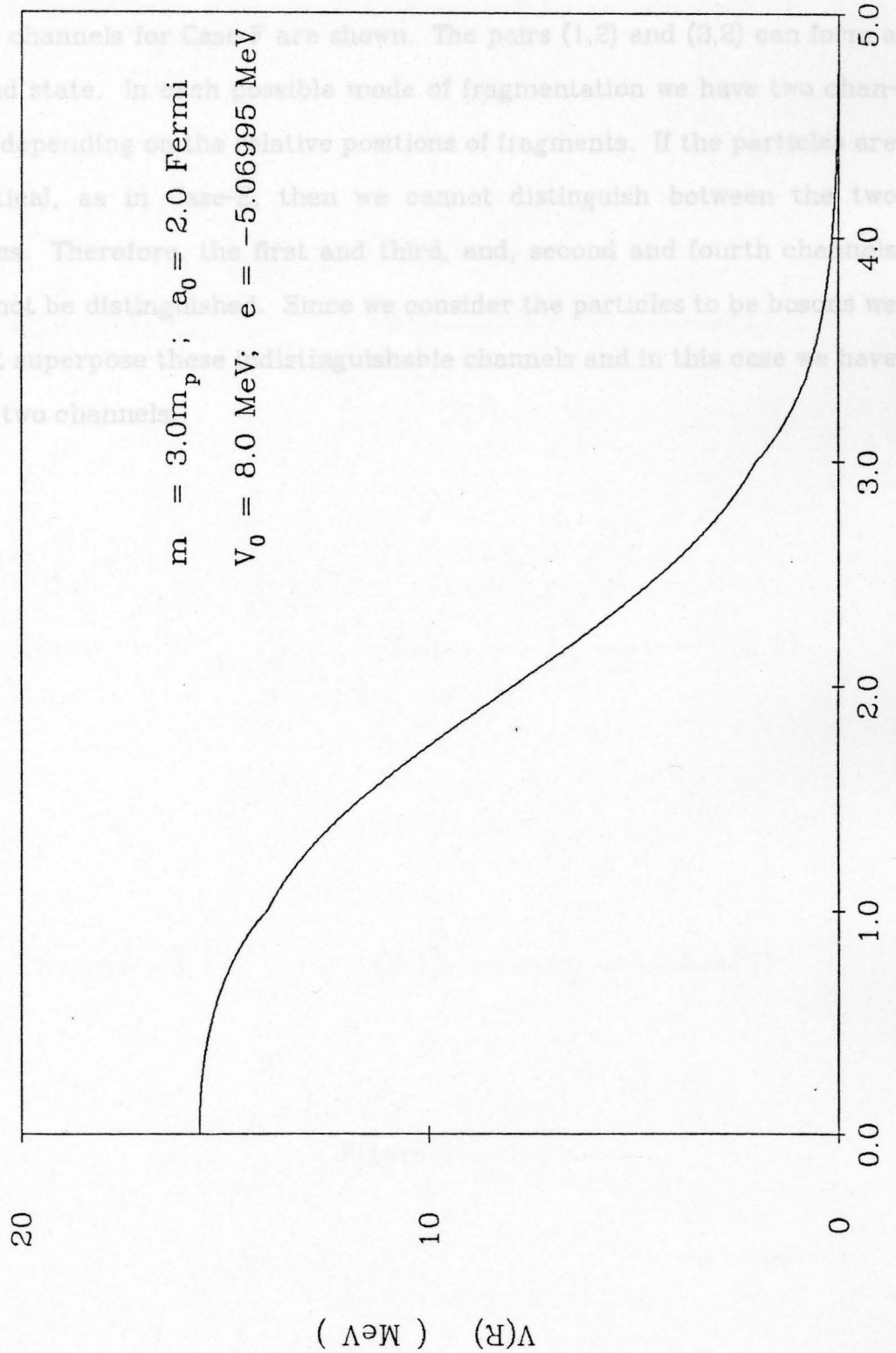
m = 3.0m$_p$; a$_0$ = 2.0 Fermi
V$_0$ = 8.0 MeV; e = −5.06995 MeV
V(R) (MeV)
R (Fermi)
0
10
20
0.0
1.0
2.0
3.0
4.0
5.0

Figure-7

Figure-8

Four channels for Case-F are shown. The pairs (1,2) and (3,2) can form a bound state. In each possible mode of fragmentation we have two channels depending on the relative positions of fragments. If the particles are identical, as in Case-E, then we cannot distinguish between the two modes. Therefore, the first and third, and, second and fourth channels can not be distinguished. Since we consider the particles to be bosons we must superpose these indistinguishable channels and in this case we have only two channels.

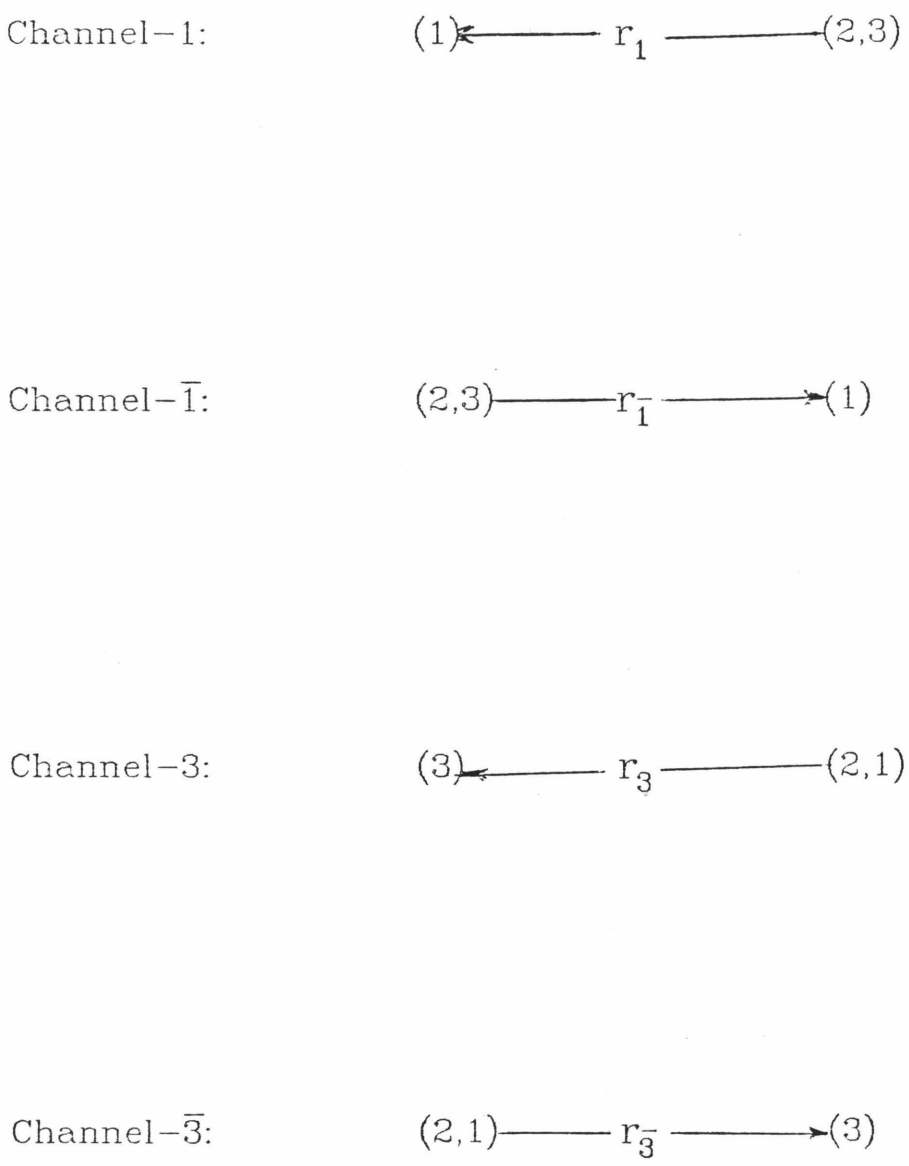
Channel-1:
(1)
r_1
(2,3)
Channel-$\bar{1}$:
(2,3)
$r_{\bar{1}}$
(1)
Channel-3:
(3)
r_3
(2,1)
Channel-$\bar{3}$:
(2,1)
$r_{\bar{3}}$
(3)

Figure-8